SPINS OF THE 5.03 Mev AND 2.14 Mev STATES IN B^{11} FROM ANGULAR CORRELATION MEASUREMENTS IN $B^{10}(dp)B^{11}$

by

BRIAN AUSTIN WHALEN

B.Sc, The University of Washington, 1959
M.Sc, The University of British Columbia, 1962

A THESIS SUBMITTED IN PARTIAL FULFILMENT OF

THE REQUIREMENTS FOR THE DEGREE OF

DOCTOR OF PHILOSOPHY

in the Department of

PHYSICS

We accept this thesis as conforming to the

required standard

THE UNIVERSITY OF BRITISH COLUMBIA

November 1965

In presenting this thesis in partial fulfilment of the requirements for an advanced degree at the University of British Columbia, I agree that the Library shall make it freely available for reference and study. I further agree that permission for extensive copying of this thesis for scholarly purposes may be granted by the Head of my Department or by his representatives. It is understood that copying or publication of this thesis for financial gain shall not be allowed without my written permission.

Department of PHYSICS

The University of British Columbia
Vancouver 8, Canada

Date DEC 4 1965

The University of British Columbia

FACULTY OF GRADUATE STUDIES

PROGRAMME OF THE

FINAL ORAL EXAMINATION

FOR THE DEGREE OF

DOCTOR OF PHILOSOPHY

of

BRIAN AUSTIN WHALEN

B.Sc.(Hons.)The University of Washington, 1959

M.Sc., The University of British Columbia, 1962

FRIDAY, DECEMBER 3, 1965, AT 3:30 P.M.

IN ROOM 304, HENNINGS BUILDING

COMMITTEE IN CHARGE

Chairman: Dr. B. N. Moyls

F. K. Bowers
K. L. Erdman
M. K. Craddock
G. Jones
B. L. White

Research Supervisor: B. L. White

External Examiner: A. E. Litherland

A.E.C.L.

Chalk River, Ontario.

SPINS OF THE 5.03 MeV. AND 2.14 MeV STATES IN B^{11} FROM ANGULAR CORRELATION MEASUREMENTS IN B^{10} (dp) B^{11}

ABSTRACT

An experimental investigation of the spins of the 2.14 (J_I) and 5.03 (J) Mev Levels in B^{11} has been made using the B^{10} (dp)B^{11} reaction to populate the 5.03 Mev level in B^{11} and then studying p γ and p γ γ angular correlations to determine the values of J and J_I. The theoretical analysis of the angular correlation data is based on a method in which the dp reaction mechanism is represented by a relatively small number of experimentally determined parameters and therefore the resulting spin assignments are not open to the usual criticisms of the use of (sometimes doubtful) nuclear reaction theories for the positive determination of nuclear spins.

Using the information gained from this experiment and previous experimental information on the statistical distribution of M1 to E2 multipole mixing ratios it was possible to assign an overwhelming statistical probability in favour of the $J = \frac{3}{2}, J_I = \frac{1}{2}$ spin assignment. These spin assignments are in agreement with previous tentative ones and with the theoretical shell model calculations of Cohen and Kurath.

The parameters, determined by this experiment, describing the dp reaction are compared with those calculated using stripping theory and are shown to be in disagreement with both the Butler Plane Wave and Distorted Wave Born approximation calculations.

GRADUATE STUDIES

Field of Study: Nuclear Physics

Electromagnetic Theory	G. M. Volkoff
Theory of Measurements	J. Prescott
Nuclear Physics	J. B. Warren
Elementary Quantum Mechanics	W. Opechowski
Group Theory	W. Opechowski
Nuclear Reactions	B. L. White
Theory of Solids	R. Barrie
Waves	P. Savage
Theory of Relativity	P. Rastall

Related Studies:

Electromagnetic Theory	G. B. Walker
Electronic Instrumentation	F. K. Bowers

PUBLICATIONS

E. Almqvist, D.A. Bromley, J.A. Kuehner and B. Whalen. "Alpha Particles From $C^{12}(C^{12},\alpha)$ Ne^{20}" Proc. Int. Conf. on Nuclear Structure, Kingston (1960)

J.A. Kuehner, B. Whalen, E. Almqvist and D.A. Bromley. "Quasi-Molecular Resonances in C^{12} + C^{12}"
Proc. Int. Conf. on Nuclear Structure, Kingston (1960)

E. Almqvist, D.A. Bromley, J.A. Kuehner and B. Whalen. "Spins and Partial Widths of Quasimolecular Resonances in C^{12} + C^{12} Interactions" Phys. Rev. 130, 1140 (1963)

B. Whalen and B.L. White.
"Spins of the 2.14 and 5.03 Mev States in B^{11} From Angular Correlation Measurements in $B^{10}(dp)$ B^{11}"
Bull. Can. Phys. Soc. Vol.2 (1965)

ABSTRACT

An experimental investigation of the spins of the 2.14 (J_I) and 5.03 (J) Mev levels in B^{11} has been made using the $B^{10}(dp)B^{11}$ reaction to populate the 5.03 Mev level in B^{11} and then studying $p\gamma$ and $p\gamma\gamma$ angular correlations to determine the values of J and J_I. The theoretical analysis of the angular correlation data is based on a method in which the dp reaction mechanism is represented by a relatively small number of experimentally determined parameters and therefore the resulting spin assignments are not open to the usual criticisms of the use of (sometimes doubtful) nuclear reaction theories for the positive determination of nuclear spins.

Using the information gained from this experiment and previous experimental information on the statistical distribution of M1 to E2 multipole mixing ratios it was possible to assign an overwhelming statistical probability in favour of the $J = \frac{3}{2}$, $J_I = \frac{1}{2}$ spin assignment. These spin assignments are in agreement with previous tentative ones and with the theoretical shell model calculations of Cohen and Kurath.

The parameters, determined by this experiment, describing the dp reaction are compared with those calculated using stripping theory and are shown to be in disagreement with both the Butler Plane Wave and Distorted Wave Born approximation calculations.

TABLE OF CONTENTS

LIST OF FIGURES.

LIST OF TABLES

ACKNOWLEDGEMENTS

The author wishes to express his gratitude to Dr. B.L. White for his many helpful suggestions on both the experimental methods and theoretical analysis used in this report. He also wishes to thank Messrs. E.W. Blackmore and A.J. Kestelman for their assistance with the experimental measurements and Dr. G. Jones for his suggestions on the design of the electronics used during these measurements.

The author is also indebted to the National Research Council for the scholarships received during the course of the experiment.

He also wishes to thank Mrs. Kelly O'Malley for her many hours of toil spent typing this thesis .

CHAPTER I

INTRODUCTION

A major part of the effort made in theoretical low energy nuclear physics has been directed toward the production of models which approximate the many-body nuclear systems. The accuracy and usefulness of these models is then investigated by comparing the predicted characteristics of the nuclear states with those derived from experiment. The characteristics most easily determined by experiment are the spectroscopic quantities of the nuclear states such as total angular momentum, parity, energy and ground state magnetic moments. It has been of primary interest to experimental nuclear physicists to make reliable measurements of these nuclear properties since they may be calculated using various nuclear models.

The existence of the very large body of spectroscopic information about the low lying energy levels of light nuclei would seem to suggest that for all but a few unimportant exceptions, the characteristic quantum numbers of all of these states have been determined. However, a closer investigation of the experimental methods used to determine the spin assignments of the excited states of various nuclei reveals that the existing assignments are not all completely conclusive. In a typical spectroscopic experiment measurements are made of branching ratios, lifetimes, angular distributions and angular correlations. The first two types of measurement have relied for their spectroscopic interpretation upon the use of specific nuclear models and arguments based on the relationship between gamma multipolarity and lifetimes which are at the same time imprecise and in many cases circuital in nature. Any spin assignments wich are based primarily on such arguments must be regarded as tentative only. The second two types of measurement can provide conclusive spin assignments but in many instances where the spin assignments are of particular importance in a critical analysis of the theory they have been

based on the first class of experiments rather than the second. This thesis describes measurements made in an attempt to provide the first conclusive spin assignments to the first and third excited states of B^{11}.

The low lying excited states of B^{11} have been studied extensively by previous workers for a variety of reasons:

1.) Reliable spectroscopic information on the states of B^{11} is essential since this nucleus is in the middle of the 1p shell in the independent particle model and as Cohen and Kurath 1.) have shown is therefore a particularly good nucleus on which to test that model.

2.) The $B^{10}(dp)B^{11}$ reaction leading to the first excited state in B^{11} shows a typical $\ell = 1$ stripping angular distribution. (Evans et al 2.) That is, the proton angular distribution measured with respect to the incident deuteron beam shows a strong forward peaking, the shape of which is quite accurately predicted using stripping theory. Since B^{10} has a J^{π} of 3^+, the $\ell = 1$ stripping pattern would indicate that this state has negative parity and a spin value in the range $\frac{3}{2} \leq J \leq \frac{9}{2}$. However, other independent investigations of the first excited state such as the measurements of $B^{10}(dp\gamma)B^{11}$ angular correlation (Gorodetzky et al 3.) lifetime (Metzger et al 4.) and branching ratios (Donovan et al 5.) all suggest a spin assignment of $\frac{1}{2}$. To explain the discrepancy in the spin assignment derived from these and the stripping measurement, the mechanism of "irregular" stripping was introduced (Wilkinson 6.). A positive determination of the spin of this level would confirm the experimental evidence that such a mechanism must indeed exist.

3.) The concept of charge independence of nuclear forces was originally established by comparing the corresponding states in mirror nuclei, including C^{11} and B^{11}. (A study of the states in C^{11} was conducted recently in this laboratory by A.S. Rupaal 7.) in which the spins of the low lying

levels in C^{11} were assigned.) This concept is of such fundamental importance to the theory of nuclear interactions, and to the theory of elementary particles, that the basic experimental results concerned in demonstrating its validity must be established with the utmost rigour. For this reason it is essential to determine the spectroscopic properties of the low lying states of B^{11} with certainty.

On the basis of experimental evidence limited almost exclusively to branching ratio measurements such as those of Gove et al 8.) and the above described measurements the following tentative J assignments have been made for the low lying levels in B^{11}

5.03	$3/2^-$
4.46	$5/2^-$
2.13	$1/2^-$
G.S.	$3/2^-$

As has been indicated a more conclusive method of determining the spins of these levels especially the 1st excited state was required. Since, in general, gamma correlation measurements are only dependent on the angular momenta of the particles involved in a transition and the multipolarity of the gamma ray transitions, correlation measurements provide such a method. There are a number of correlation measurements that could be made on the B^{11} excited states. In the past particle-gamma correlations have been measured in such reactions as $B^{10}(dp\gamma)B^{11}$ (Gorodetzky 3.) and $B^{11}(p_1p'\gamma)B^{11}$ Blair et al 9.), however, to interpret these results nuclear reaction theory had to be introduced and since the validity of the theory itself is doubtful, the spin assignments which resulted were inconclusive. Therefore measurements, in the interpretation of which nuclear models or reaction theories play no role or are represented by a small number of experimentally determined para-

meters were required if the correlation measurements on the $B^{10}(dp)B^{11}$ reaction were to be used for definite spin assignments. A convenient method developed recently and outlined by Litherland and Ferguson 11.) has the required characteristics. They show that the $(dp\gamma)$ double and $(dp\gamma\gamma)$ triple correlation can be expressed as a function of the spins of the states of the daughter nucleus and a limited number N_I of parameters, called statistical tensors, representing the B^{11} excited states formed by the dp reaction. The number of parameters required is shown to be further limited to $N_2 \leq N_1$ if the state populated in B^{11} is formed in a cylindrically symmetric fashion. If enough information is gained from the experiment, these parameters along with the spins of the levels in the daughter nucleus involved in the transitions can not only be determined but possibly overdetermined.

As an indication of the amount of information that can be derived from double and triple correlation measurements consider the ground, first and third excited states of B^{11}. It is known from Donovan et al 5.) that the 5.03 Mev state decays by gamma cascade through the first excited state to the ground state or by gamma emission directly to the ground state

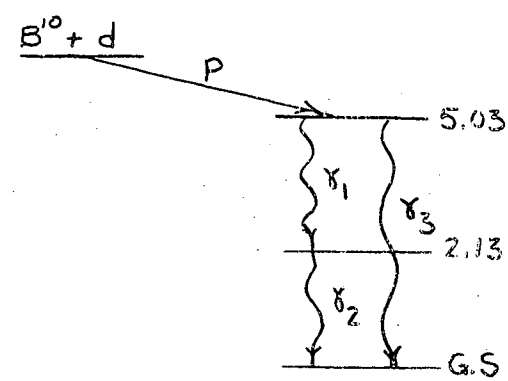

If the $(p\gamma_1)$, $(p\gamma_2)$ and $(p\gamma_3)$ angular correlations are measured, the results are usually fitted to a sum of Legendre Polynomials P_i and seldom are terms higher than P_4 necessary to fit the results. e.g.

$$W(\Theta) = \sum_i a_i P_i(\cos\Theta)$$

If no interference between intermediate states is considered only even

orders will occur. Usually only the ratios of the coefficients $\frac{a_i}{a_0}$ are significant, so as a result of each of the measurements two ratios have been determined, making a total of six. If the triple correlation $(p\gamma_1\gamma_2)$ is measured, the results are fitted to functions of three angles, the angles γ_1 and γ_2 make with a fixed axis (in this experiment this axis corresponded to the incident deuteron beam direction) and the azimuthal angle between γ_1 and γ_2. e.g.

$$W_{p\gamma_1\gamma_2}(\theta_1\theta_2\phi) = \sum_{KMN} A_{KMN} P_K^N(\cos\theta_1)\, P_M^N(\cos\theta_2)\cos N\phi$$

Under the same conditions which required terms up to P_4 to be used in the double correlation, nineteen coefficients (A_{KMN}) are required for the expansion of above. With these coefficients eighteen ratios $\frac{A_{KMN}}{A_{000}}$ can be determined from the triple correlation and including the six from the double correlation we have a total of twenty-four. All of these ratios, however, are not independent and when normalization is allowed for it is found that there are left only eighteen independent ratios. The number of adjustable theoretical parameters (spin values, statistical tensor elements, and multipole mixing ratios) available to fit these experimental ratios is dependent on the spin of the initial (5.03 Mev state) but usually will be no more than ten, therefore the determination of these parameters, and in particular the spins of the nuclear states should be assured.

The statistical tensor elements determined as described in the preceeding paragraph are directly related to the population parameters of the various magnetic substates of the initial state formed by the dp reaction. These population parameters can also be calculated using dp reaction theory. By comparing the calculated with the experimentally determined parameters, it was possible to investigate the validity of the use of dp reaction theory to describe the reaction investigated in this experiment.

An outline of the theory of correlation measurements of radiations

from axially symmetric aligned nuclei appears in Chapter II. The experimental arrangement and apparatus for the correlation measurement are described in Chapter III and the results of these measurements appear in Chapter IV. In Chapter V the correlation results are analysed in terms of the theory outlined in Chapter II and the most probable value of spin assignment made. The parameters determined by the correlation measurement are then in Chapter VI compared with those predicted by nuclear models and reaction theory.

CHAPTER II

RADIATION FROM ALIGNED NUCLEI

A.) INTRODUCTION

This chapter describes the theoretical interpretation of correlation measurements made between protons populating levels in B^{11} in the reaction $B^{10}(dp)B^{11}$ and gamma rays resulting from the decay of these states. The theoretical treatment of angular correlations of particles and gamma rays resulting from nuclear reactions will be discussed using the procedure developed by Fano 12.) and reviewed by Biedenharn and Rose 13.) and Blatt and Biedenharn 14.) The theoretical background and interpretation of this experiment is most clearly defined by Litherland and Ferguson 11.)

In the past various forms of nuclear reaction theory have been employed in an attempt to describe the dp stripping reaction and its effect on pγ correlations. As was pointed out in Chapter I, the use of this type of reaction theory in the determination of nuclear spins should be avoided if possible since the applicability of the theory itself is often in doubt. In the following, no unjustifiable assumptions are made concerning the dp reaction, (such assumptions are made when using the usual stripping formalism), only arguments based on symmetries present in the dp reaction will be used.

The density matrix and statistical tensor formalism is introduced in Part B.) of this chapter to facilitate the incorporation of these symmetries into the angular correlation theory. As will be shown this formalism presents a convenient parameterization of the states of B^{11} formed by the dp reaction and simplifies the process of reducing the number of parameters needed to describe the state by appealing to the rotational properties of the statistical tensors. In the remaining portion of the chapter the correlation between protons populating the 5.03 Mev level in B^{11} and gamma rays resulting from the de-excitation of these levels is calculated in terms of the parameters describ-

ing the formation of the levels. The correlation functions will be used in Chapter IV in the interpretation of $(p\gamma)$ and $(p\gamma\gamma)$ correlation measurements made in the reaction $B^{10}(dp\gamma)B^{11}$ and $B^{10}(dp\gamma\gamma)B^{11}$.

B.) THE DENSITY MATRIX AND STATISTICAL TENSORS

The notation used in this section closely follows that of Litherland et al 11.). Let ψ be the wavefunction representing a pure (i.e. fully determined) state. In the following ψ represents the wavefunction of the state formed in B^{11}(5.03 Mev level) and is in general a time dependent wavefunction. Since ψ represents the initial state in the decay scheme investigated it is convenient to define the time (t) at which the state is formed by dp reaction as t = 0. ψ at time t = 0 (ψ_o) may be expanded in terms of a complete orthonormal set of stationary states U_k.

$$\psi_o = \sum_k A_k U_k.$$

In this representation the density matrix $\rho_{kk'}$ is defined as:

$$\rho_{kk'} = A_k \bar{A}_{k'} \qquad \bar{A}_{k'} = \text{complex conjugate of } A_{k'}$$

It is easily shown Beidenharn et al 13.) that if Q is an observable the expectation value of Q is:

$$\langle Q \rangle = TR(\rho Q)$$

It may be noted that all the information on the state ψ_o is contained in the elements $\rho_{kk'}$.

The states considered in this report are eigenfunctions of total angular momentum J and are expanded in terms of the set of states $\psi(Jm)$ which are eigenfunctions of J and J_Z, the projection of J on the quantization (Z) axis. That is:

$$\psi_o(J) = \sum_m A_m \psi_o(Jm)$$

The density matrix is then written as:

$$\rho^{m\ m'}_{J\ J} = A_m \bar{A}_{m'}$$

It is useful to enquire what restrictions if any can be placed on the elements of ρ if various rotational symmetry properties are imposed on the states. However ρ transforms under rotations as a product representation $\vec{J} \times \vec{J}$ (Reference 13) and the effect on ρ of demanding various rotational symmetry properties is not obvious. This difficulty is overcome if the statistical tensor $R(kq : JJ)$ is introduced, where R is defined as:

$$R(kq : JJ) = \sum_{mm'} (-1)^{J-m'} (JJm-m' | kq) \; \rho^{m\,m'}_{J\,J}$$

$(JJm-m' | kq)$ the Clebsch-Gordon Coefficient.

It can be shown (e.g. W.T. Sharpe 24) that the R's are tensors of rank k and have all the usual rotational properties of any tensor, that is, in particular that the R(kq)'s transform under rotations as the spherical harmonics Y(lm) (Defined in Condon and Shortley 36). From the definition of the R's it can be seen that k takes values $0 \leqslant k \leqslant 2J$ and that q, the component of the tensor, takes values $-k \leqslant q \leqslant k$. Therefore, the total number of elements in the statistical tensors is $(2J+1)^2$. The term "tensor parameters" is usually used for these elements and will be used in this chapter. If normalization is included there will be in general $(2J+1)^2 - 1$ independent parameters. The inverse of the above expression is easily found to be, (using the orthogonality conditions of the Clebsch-Gordon coefficient):

$$\rho^{m\,m'}_{J\,J} = \sum_{kq} (-1)^{J-m'} (JJm-m' | kq) R(kq : JJ)$$

Any rotational symmetry properties are now readily handled by appealing to the well known rotational properties of the tensors $R(kq : JJ)$. In particular if the state is axially symmetric and this axis is chosen as the Z axis, Litherland 11) shows that this symmetry condition requires that only the $R(ko : JJ)$'s are non-zero. Further, if the state has definite parity

and reflections through the origin are considered (in this case this is equivalent to considering rotations of 180° about the Y axis) it is shown that only the R(ko : JJ)'s with even k are non-zero. The number of tensor parameters needed to describe the state has been reduced by the condition of axial symmetry. In summary, the axial symmetry of the state when applied to the statistical tensors representing the state requires:

$$R(kq : JJ) = 0 \qquad q \neq 0$$

$$R(ko : JJ) = 0 \qquad k \text{ not even.}$$

The equivalent requirements on the density matrix are

$$\rho^{m\,m'}_{J\,J} = \rho^{m\,m}_{J\,J}\,\delta_{mm'}$$

$$\rho^{m\,m}_{J\,J} = \rho^{-m-m}_{J\,J}$$

It is now possible to define the orientation, alignment, and polarization of a state in terms of these tensor parameters representing the state. Steenland and Tolhoek 15.) show that for a random orientation all the $\rho^{m\,m'}_{J\,J}$'s are equal and the only non-zero tensor parameter is R(OO:JJ). If all the $\rho^{m\,m'}_{J\,J}$'s are not equal then the system is said to be oriented. Further if the state is symmetric about a quantization (Z) axis the only non-zero tensor parameters will be the ones with q = 0 (as pointed out previously) i.e.:

$$R(kq : JJ) = 0 \qquad q \neq 0$$

Then when $R(ko : JJ) = 0$ for $k \neq 0$ we have:

1. alignment if k = even
2. polarization if k = odd.

C.) ALIGNMENT RESULTING FROM NUCLEAR REACTIONS

As an example of how alignment can result from nuclear reactions consider the case where a spinless particle is incident on a spinless nucleus and only spinless particles from the reaction are detected by a counter at

0° to the incident beam. If the incident particle direction is defined as the Z axis (axis of quantization) only states with zero projection of total angular momentum ($m = 0$) can be populated in the residual nucleus, which must have non-zero spin for this to be a meaningful statement. This is clear since the only angular momentum carried by the incident and emergent particles is in the form of orbital angular momentum which for a plane wave has by definition $m = 0$. Since there can be no change in total magnetic quantum number during this reaction, only $m = 0$ states in the residual nucleus will be populated. Any radiation from the residual nucleus in coincidence with the particles detected at zero degrees to the incident beam will have an angular distribution characteristic of the decay of an $m \neq 0$ state. Also the density matrix for states of the residual nucleus formed in this manner will have only one non-zero element, which correspond to a high degree of alignment. If we consider instead an initial nucleus and bombarding particle both having non-zero spins, it is possible for $m = 0$ states to be populated. However, the population of the magnetic substates of the residual nucleus will be affected by the non-random distribution of the orbital angular momenta ℓ of the incoming and outgoing particles ($m_\ell \neq 0$) and a non-isotropic alignment of the residual nucleus may result. For a more detailed discussion of these effects see Litherland et al 11.).

It was pointed out in the previous paragraph that for the $B^{10}(dp)B^{11}$ reaction, since all the particles involved in the reaction have non-zero spins, no definite statements as to the value of the magnetic substate populations of the residual B^{11} nucleus can be made on the basis of these simple arguments. If however, the deuteron beam and B^{10} target are unpolarized and the protons from the reaction are detected by a non-polarization sensitive counter in an axially symmetric way, the axis of symmetry (Z axis) being the incident beam direction, the B^{11} states will be formed in an axially symmetric fashion. In

this situation the conditions on the statistical tensors representing a cylindrically symmetric state outlined in Part B.) may be applied to the states in B^{11}. To retain the axial symmetry the protons were detected by a circular semiconductor counter whose face was centered at 0° to the beam. Any gamma rays detected in coincidence with these protons will then have an angular distribution characteristic of the decay of a cylindrically symmetric state. The calculation of these angular distributions is outlined in Part D.) for both ($p\gamma$) and ($p\gamma\gamma$) coincidence measurements.

D.) ANGULAR DISTRIBUTION OF GAMMA RAYS FROM CYLINDRICALLY SYMMETRIC STATES

i.) DOUBLE ANGULAR CORRELATION.

The term double angular correlation will refer to the measurement of the coincidence count rates between protons populating a nuclear state of spin J and gamma rays from the decay of this state, as a function of the angle θ between the γ rays and the Z axis. The Z axis is the axis of symmetry and as pointed out in Part C.) corresponds to both the deuteron beam direction and the direction of the average momentum of the protons detected by the solid state counter fixed at 0° to the beam. The figure below shows an energy level diagram of the reaction studied in this experiment.

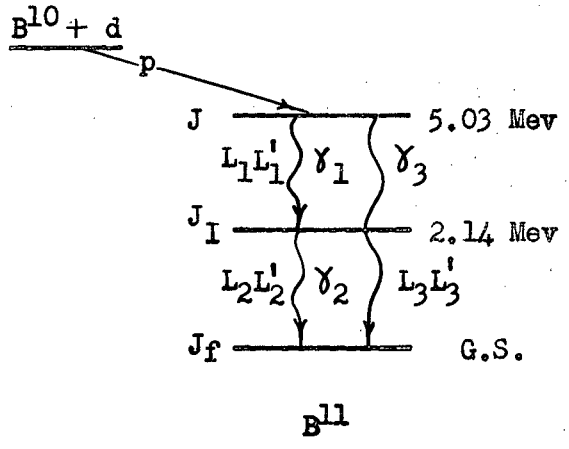

The correlation function W can be expressed in terms of the tensor parameters R (k0:JJ) for the 5.03 Mev level formed by the dp reaction

(Litherland 11.).

$$W_{\gamma_i}(\theta) = \sum_{kL_iL_i'p} R(k0 : JJ)\, A_k(JJ_iL_iL_i')x_i^p\, P_k(\cos\theta)$$

i take values 1 or 3

J_i = total angular momentum of the final state involved in the γ_i transition.

L_iL_i' = the multipolarities of the γ_i transition

x_i = multipole mixing ratios between L_i and L_i'

i.e.

$$x_i = \frac{\langle J_i \| L_i + 1 \| J\rangle}{\langle J_i \| L_i \| J\rangle}$$

p takes the values of 0, 1, 2 for dipole, interference and quadrupole terms in the correlation:

$$A_k(JJ_iL_iL_i') = \mathrm{Re}(i^{-L_i+\pi\ -L_i'\ -\pi'\ -2k+2+2J_i\ -\ 2J})$$
$$\hat{J}\hat{L}_i\hat{L}_i'(L_iL_i' - 11|k0)W(JL_i'JL_i;J_ik)$$

$\hat{a}$ = $(2a+1)^{\frac{1}{2}}$

π = parity of the radiation

$(L_iL_i' - 11|k0)$ = Clebsh - Gordon Coefficient

W = Racah Coefficient as defined in W.T. Sharp 24.) and tabulated by Sharp et al 37.)

A convenient tabulation of the A_k may be found in Kaye et al 32.)

If the excited state represented in the correlation function by the R(k0 : JJ)'s (the 5.03 Mev level) decays through the intermediate state of spin J_I by the emission of gamma ray (γ_1), then J_I decays to the final state of spin J_f by emission of γ_2 and only the γ_2 angular distribution is recorded, the ($p\gamma_2$) distribution may be calculated (Litherland 11.) and takes the form:

$$W_{\gamma_2}(\theta) = \sum_{kL_1L_2L_2'p} R(k0 : JJ)C_k(JJ_IJ_fL_1L_2L_2')\, x_2^p\, P_k(\cos\theta)$$

$$C_k = (-1)^{1-J_f-p-k/2-J}\,\hat{k}\,\hat{L}_1(L_1L_1-11|00)W(JJ_IJJ_I:L_1k)$$
$$Z_1(L_2J_IL_2'J_I:J_fk)$$

Z_1 is the coefficient defined by Blatt and Biedeharn 14) and tabulated in Reference 37.)

ii.) TRIPLE ANGULAR CORRELATION.

The triple angular correlation measurement will refer to the triple coincidence measurement made between the protons populating the 5.03 Mev. level in the manner outlined in Part C.) and the two cascade gamma rays γ_1 and γ_2 (See previous figure). The triple correlation function will depend on the angles θ_1 and θ_2 that gamma rays γ_1 and γ_2 make with the Z axis, and on the azimuthal angle ϕ between γ_1 and γ_2. Writing the triple correlation function $W(\theta_1\theta_2\phi)$ using the same notation as Kaye et al 32),

$$W(\theta_1\theta_2\phi) = \sum R(k0\ JJ)A^N_{KM}(JJ_IJ_fL_1L_1'L_2L_2'k)x_1^{p1}\ x_2^{p2}\ X^N_{KM}(\theta_1\theta_2\phi)$$

The summation is over $KMNL_1L_1'L_2L_2'$ and k. The A^N_{KM} are tabulated by Kaye et al 32) and are defined as:

$$A^N_{KM}(JJ_IJ_fL_1L_1'L_2L_2'k) = (-1)^{J_I-J_f-p_2-\frac{k}{2}}\ \underset{\hat{K}\ \hat{M}}{2^N\ J}\ (k\text{-}MON\ KN)$$

$$G\begin{pmatrix} J & L_1 & J_I \\ k & K & M \\ J & L_1' & J_I \end{pmatrix} \qquad Z_1(L_2J_IL_2'J_I;J\ M)$$

G and Z_1 are coefficients defined and tabulated by Ferguson and Rutledge 38)

$$X^N_{KM}(\theta_1\theta_2\phi) = \left[\frac{(2K+1)(K-N)!\ \ (2M+1)(M-N)!}{(K+N)!\ \ (M+N)!}\right]^{\frac{1}{2}} P^N_K(\cos\theta_1)\ P^N_M(\cos\theta_2)\ \cos N\phi.$$

x_1 and x_2 are the multipole mixing ratios of γ_1 and γ_2 as defined in D.) i.)

E.) RESTRICTIONS ON MULTIPOLE MIXING

In Chapter I evidence was presented which set the parity of all three states under consideration as negative, therefore the gamma ray transitions γ_1, γ_2 and γ_3 must be of the type M1, E2, M3 and E4 or some mixture of these.

The transition probabilities (which are proportional to the radiation widths Γ) for each type of decay were estimated (assuming on average gamma ray energy $E_\gamma = 3$ Mev) using the Weisskopf extreme single particle model (Wilkinson 16.) and on this basis a restriction was set as to the extent of multipole mixing.

$$\Gamma_W(M1) = 0.6 \text{ ev}$$
$$\Gamma_W(E2) = 4\ 10^{-4} \text{ ev}$$
$$\Gamma_W(M3) = 3.5\ 10^{-10} \text{ ev}$$
$$\Gamma_W(E4) = 4\ 10^{-14} \text{ ev}$$

It is seen that the lowest multipolarity L allowed by the rule $J_i + J_f \geqslant L \geqslant J_i + J_f$ where $\vec{J}_i$ and $\vec{J}_f$ are the angular momenta of the initial and final states, should also be the dominant component of the transition - i.e.

$$L = J_i - J_f \qquad \text{for } J_i - J_f = 0$$
$$L = 1 \qquad \text{for } J_i - J_f = 0 \ , \ J_i = 0$$

Experimentally it has been found that $\Gamma E2$ is enhanced over the Weisskop estimate (Wilkinson 16.) in many instances and the multipole mixture x(where $x^2 = \frac{\Gamma E2}{\Gamma M1}$) can become non-negligible (x's up to 0.2 or 0.3). There have been no experimental measurements of mixing ratios $\frac{\Gamma ME}{\Gamma E2}$ or $\frac{\Gamma E4}{\Gamma M3}$ which however are not expected to be much greater than the values predicted by the Weisskopf lifetimes (i.e. $\frac{M3}{E2} \cong 10^{-6}$, $\frac{E4}{M3} \cong 10^{-4}$ with resulting x's of 10^{-3} and 10^{-2}). Multipole mixing of this amount would have a negligible effect on the angular correlation, therefore only $\frac{E2}{M1}$ mixing was included in the correlation formalism. That is, it was assumed that

$$L = J_i - J_f \qquad \text{for } J_i - J_f \geqslant 2$$
$$L = 1 \text{ and } 2 \qquad \text{for } J_i - J_f = 1 \text{ or } 0$$

F.) PRELIMINARY RESTRICTIONS ON SPIN ASSIGNMENTS FROM PREVIOUS MEASUREMENTS.

The number of possible spin assignments for J and J_I (spins of 5.03 and 2.14 Mev states in B^{11}) that would have to be allowed in the calculation

of angular distributions would be very large indeed if no previous knowledge were available on these states. However as has been pointed out a large body of data is available in the literature from which preliminary restrictions on the possible range of spin values for J and J_I may be made. The restrictions made in the following are based on lifetime measurements and are compared for consistency with restrictions that may be made on other less conclusive measurements. Note that the lifetime measurements are being used only to rule out certain multipolarities; they are not being used to choose a single multipole assignment from several nearly equally probable assignments.

i.) LIFETIME MEASUREMENTS.

The lifetime of the first excited state (2.14 Mev) has been measured by Wilkinson 6.) and Metzger 4.), and was found to be approximately 5 10^{-15} sec. This value may be compared with the Weisskopf extreme single-particle lifetime estimate to put a limit on the maximum multipolarity of the γ decay to the ground state. If L is the angular momentum of the multipole radiation emitted, the Weisskopf estimate of the lifetime T_{EL} of this state if it decays by electric multipole (EL) is (Reference 16.)

$$T_{E1} = 2.4\ 10^{-16} \text{ sec.}$$

$$T_{E2} = 1.2\ 10^{-11} \text{ sec.}$$

$$T_{E3} = 1.2\ 10^{-6} \text{ sec.}$$

$$T_{E4} = 0.17 \text{ sec.}$$

The statistical factor(S) in Reference 16.) whose magnitude is for all cases of the order of unity, has been taken to be unity for this estimate.

Wilkinson 16.) shows that the extreme single particle estimate is quite often out by a factor of 10^3 - 10^4 from the experimentally determined lifetime and in some extreme cases the estimate deviates from the measured value by a factor of approximately 10^5. Therefore if it is assumed that the Weisskopf estimate is not wrong by factors exceeding 10^5, E3 and E4 transi-

tions may be ruled out with certainty for γ_2(2.14 Mev state to ground state decay gamma ray). It is unlikely that γ_2 is an E2 transition but L = 2 transitions cannot be definitely ruled out by the lifetime measurement. On this basis a limit on the possible range of spins for the 2.14 Mev state (J_I) may be set since

$$\vec{J}_I = \vec{J}_F + \vec{L}$$

where J_F = spin of ground state = $\frac{3}{2}$

$\vec{L}$ = maximum allowed L value for the γ_2 transition = 2.

That is

$$\frac{1}{2} \leqslant J_I \leqslant \frac{7}{2}$$

No measurements on the lifetime T of the 5.03 Mev level has been found in the literature by the author, however an upper limit was set in this experiment of $T \leqslant 10^{-7}$ sec. by using a fast coincidence (~10ns resolution time) circuit (Refer to Chapter IV Part B.). It is known (Donovan et al 5.) that this state decays mostly (~90%) by gamma emission directly to the ground state. The single particle lifetime estimate for an E4 transition from this state to the ground state is found to be (Reference 10.)

$$T_{E4} \cong 0.1 \text{ sec.}$$

Therefore, using the same reasoning as before L=4 transitions may be ruled out and the range of allowed spin values of J(spin of 5.03 Mev state) is:

$$\frac{1}{2} \leqslant J \leqslant \frac{9}{2}$$

ii.) STRIPPING.

The angular distributions of the protons from the $B^{10}(dp)B^{11}$ reaction leading to the first three excited states has been studied extensively (e.g. N. Evans et al 2.) and all the proton groups exhibit $\ell = 1$ stripping patterns. If

the reaction follows the regular stripping mechanism J and J_I should have values which satisfy:

$$\vec{J},\vec{J}_I = \vec{J}_{B10} + \vec{J}_{\frac{3}{2}}$$

or, since $J_{B10} = 3$

$$\frac{3}{2} \leqslant J, J_I \leqslant \frac{9}{2}$$

However, as pointed out in the Introduction (Chapter I.) there is strong evidence in the literature that $J_I = \frac{1}{2}$. This spin value can be reached by the stripping process if the "spin flip" mechanism (Wilkinson 6.) is introduced. A spin of $\frac{1}{2}$ therefore should not be excluded on the basis of the stripping data and the range of spin values should be extended to include $\frac{1}{2}$. That is

$$\frac{1}{2} \leqslant J, J_I \leqslant \frac{9}{2}$$

This range of values for J and J_I, derived from the stripping data, is consistent with that derived from lifetime measurements i.)

iii.) BRANCHING RATIO MEASUREMENTS.

The branching ratios for the gamma ray de-excitation of the first three excited states of B^{11} has been measured by Donovan et al 5.). Using the rather imprecise arguments usually necessary for the interpretation of such measurements the spin assignments $J = \frac{3}{2}$, $J_I = \frac{1}{2}$ were made. Obviously these values lie in the range of spins allowed by the lifetime measurements.

In summary the range of values for the first and third excited states in B^{11}, allowed by lifetime measurements is

$$\frac{1}{2} \leqslant J_I \leqslant \frac{7}{2} \qquad\qquad \frac{1}{2} \leqslant J \leqslant \frac{9}{2}$$

This range of values is consistent with that predicted from stripping data and from gamma branching ratio measurements. It was assumed therefore in the calculation of the correlation functions that only those values of spins which lie in this range need be considered.

G.) ANGULAR CORRELATION TABLES

The theoretical $p\gamma_1$ and $p\gamma_3$ angular correlation functions $W_{\gamma_1}(\theta)$ and $W_{\gamma_3}(\theta)$ were calculated for all the possible choices of J and J_I consistent with the restrictions imposed in Part E.) and F.) of this chapter and the results of this calculation appears in Table 1. Listed here are the values of $B_k(\gamma_i)$ for each choice of initial and final state spins (J, J_i) of the γ_i decay, where the B_k's are the theoretically calculated coefficients in the expansion.

$$W_{\gamma_i}(\theta) = \sum_k a_k B_k(\gamma_i J J_i) P_k(\cos\theta)$$

The a_k's are the tensor parameters

$$a_k = R(k0;JJ)$$

and appear in all the calculated correlation functions.

Similarly Table 2. displays the results of evaluating the double correlation function $W_{\gamma_2}(\theta)$ defined in D.) i.). Listed here are the values of $C_k(\gamma_2)$ for each choice of spin of the 5.03 Mev state (J) and 2.14 Mev state (J_I) where the $C_k(\gamma_2)$'s are the coefficients in the expansion.

$$W_{\gamma_2}(\theta) = \sum_k a_k C_k(J J_I) P_k(\cos\theta)$$

The theoretical triple correlation function $W(\theta_1\theta_2\phi)$ was calculated for the six possible choices of spin assignment which were found in Chapter V to be consistent with the three double correlation measurements. The values of the multipole mixture parameters x_i determined from the double correlation measurements (See Chapter V) have been substituted into the triple correlation function. Table 3. lists the theoretical values of the triple correlation function for the five points at which the correlation was measured.

TABLE 1.

DOUBLE CORRELATION TABLE ($P_3\gamma_1$ and $P_3\gamma_3$)

$J\ J_i$	k = 0	k = 2	k = 4	k = 6
$\frac{1}{2}\ J_i$	1			
$\frac{3}{2}\ \frac{1}{2}$	$(1 + x_i^2)$	$(0.5000 + 1.7360x_i - 0.5000x_i^2)$		
$\frac{3}{2}\ \frac{3}{2}$	$(1 + x_i^2)$	$(-0.4000 + 1.5491x_i)$		
$\frac{3}{2}\ \frac{5}{2}$	$(1 + x_i^2)$	$(0.1000 - 1.1833x_i + 0.3571x_i^2)$		
$\frac{3}{2}\ \frac{7}{2}$	1	$- 0.1429$		
$\frac{5}{2}\ \frac{1}{2}$	1	$- 0.0534$	-0.6171	
$\frac{5}{2}\ \frac{3}{2}$	$(1 + x_i^2)$	$(0.3741 + 1.8972x_i - 0.1910x_i^2)$	$0.7053x_i^2$	
$\frac{5}{2}\ \frac{5}{2}$	$(1 + x_i^2)$	$(-0.4275 + 1.0142x_i + 0.1910x_i^2)$	$-0.4951x_i^2$	
$\frac{5}{2}\ \frac{7}{2}$	$(1 + x_i^2)$	$(0.1337 - 1.3887x_i + 0.3244x_i^2)$	$0.1176x_i^2$	
$\frac{7}{2}\ \frac{1}{2}$	1	0.1237	-0.1066	-0.0151
$\frac{7}{2}\ \frac{3}{2}$	1	-0.4686	-0.3582	
$\frac{7}{2}\ \frac{5}{2}$	$(1 + x_i^2)$	$(0.3274 + 1.8899x_i - 0.0780x_i^2)$	0.6366	
$\frac{7}{2}\ \frac{7}{2}$	$(1 + x_i^2)$	$(-0.4365 + 0.7560x_i + 0.2493x_i^2)$	$-0.3560x_i^2$	
$\frac{9}{2}\ \frac{3}{2}$	1	-0.2522	0.1281	0.0031
$\frac{9}{2}\ \frac{5}{2}$	1	-0.4324	-0.2685	
$\frac{9}{2}\ \frac{7}{2}$	$(1 + x_i^2)$	$(0.3027 + 1.8709x + 0.0197x^2)$	$0.4365x^2$	

TABLE 2.

DOUBLE ANGULAR CORRELATION TABLE ($R_{\gamma\gamma}$)

$J\ J_I$	k = 0	k = 2	k = 4
$J\ \frac{1}{2}$	1		
$\frac{3}{2}\ \frac{3}{2}$	$(1 + x_2^2)$	$(-0.0800 + 0.3099x_2)$	
$\frac{3}{2}\ \frac{5}{2}$	$(1 + x_2^2)$	$(0.2799 + 1.4199x_2 - 0.1429x_2^2)$	
$\frac{3}{2}\ \frac{7}{2}$	1	$- 0.3061$	
$\frac{5}{2}\ \frac{3}{2}$	$(1 + x_2^2)$	$(- 0.2994 + 1.1594x_2)$	
$\frac{5}{2}\ \frac{5}{2}$	$(1 + x_2^2)$	$(0.2460 + 1.2468x_2 - 0.1254x_2^2)$	$-0.1008x_2^2$
$\frac{5}{2}\ \frac{7}{2}$	1	$- 0.4090$	-0.2079
$\frac{7}{2}\ \frac{3}{2}$	$(1 + x_2^2)$	$(- 0.2618 + 1.0142x_2)$	
$\frac{7}{2}\ \frac{5}{2}$	$(1 + x_2^2)$	$(0.3274 + 1.6598x_2 + 0.1659x_2^2)$	$0.4092x_2^2$
$\frac{7}{2}\ \frac{7}{2}$	1	$- 0.3785$	-0.1308
$\frac{9}{2}\ \frac{3}{2}$	$(1 + x_2^2)$	$(-0.0121 + 1.5223x_2 + 0.3011x_2^2)$	
$\frac{9}{2}\ \frac{5}{2}$	$(1 + x_2^2)$	$(0.3028 + 1.5352x_2 - 0.1545x_2^2)$	$0.3069x_2^2$
$\frac{9}{2}\ \frac{7}{2}$	1	$- 0.4324$	-0.2685

TABLE 3.

TRIPLE CORRELATION TABLE

θ_1 θ_2 ϕ \ JJ_I	$\frac{3}{2}\frac{1}{2}$	$\frac{3}{2}\frac{3}{2}$	$\frac{3}{2}\frac{5}{2}$	$\frac{5}{2}\frac{3}{2}$	$\frac{5}{2}\frac{5}{2}$
90 90 0	$0.891a_0$	$0.846a_0a_2$ $-0.359a_2^2$ $0.515a_0^2$	$0.700a_0a_2$ $-0.571a_0^2$ $-0.0286a_2^2$	$0.894a_0a_2$ $-0.048a_0^2$ $-0.036a_2^2$	$0.733a_0a_2$ $-0.143a_0^2$
90 90 45	$0.891a_0$	$1.329a_0a_2$ $-0.479a_2^2$ $0.399a_0^2$	$0.836a_0a_2$ $0.113a_0^2$ $-0.028a_2^2$	$0.768a_0a_2$ $0.024a_0^2$ $0.018a_2^2$	$0.850a_0a_2$ $-0.035a_0^2$
90 90 90	$0.891a_0$	$0.973a_0^2$ $0.973a_0a_2$ $-0.198a_2^2$	$0.972a_0a_2$ $0.797a_0^2$ $-0.028a_2^2$	$0.462a_0a_2$ $0.096a_0^2$ $0.072a_2^2$	$0.967a_0a_2$ $0.073a_0^2$
90 0 0	$0.891a_0$	$0.283a_2^2$ $0.892a_0a_2$ $-0.160a_2^2$	$0.836a_0a_2$ $0.113a_0^2$ $-0.014a_2^2$	$0.893a_0a_2$ $-0.047a_0^2$ $-0.036a_2^2$	$0.731a_0a_2$ $0.071a_0^2$
0 90 0	$1.220a_0$	$-0.077a_0^2$ $1.143a_0a_2$ $-0.077a_0^2$	$1.064a_0a_2$ $0.113a_0^2$ $-0.014a_2^2$	$1.463a_0a_2$ $-0.047a_0^2$ $-0.036a_2^2$	$1.301a_0a_2$ $0.071a_0^2$

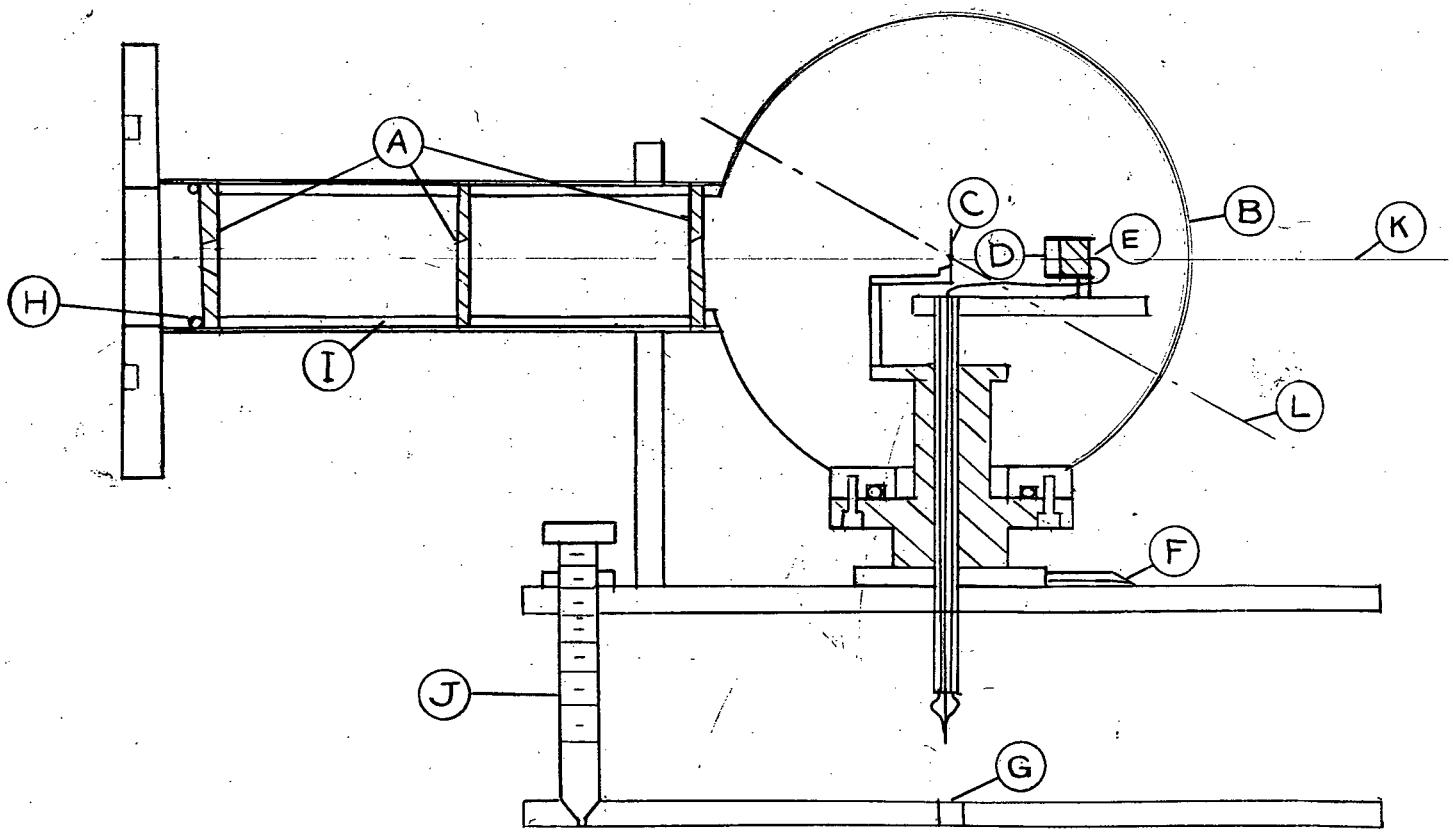

FIGURE 1. TARGET CHAMBER

CHAPTER III

EXPERIMENTAL ARRANGEMENT FOR THE CORRELATION MEASUREMENTS

The schematic diagram below shows the placement of the target, collimators, gamma counters and solid state counter with respect to the incident deuteron beam direction. The angles θ_1, θ_2 and ϕ, defined in Chapter II Part D ii.) are also indicated in this figure.

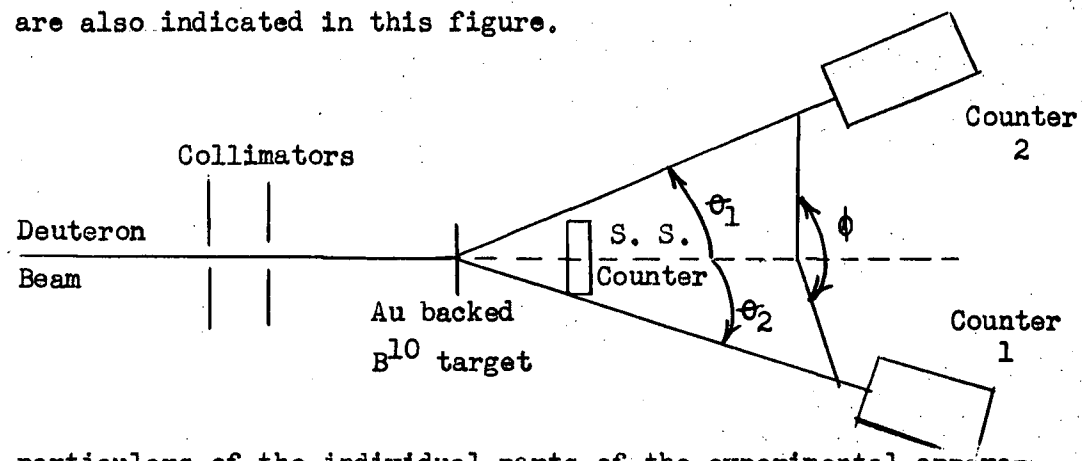

The particulars of the individual parts of the experimental apparatus are discussed in the following Chapter, including the design and construction specifications of the electronics and mechanical components. Also included is a description of the alignment and operation of the mechanical components.

A.) TARGET CHAMBER AND TARGET.

The target chamber including the placement of the solid state counter (E) and beam collimators (A) is shown in Figure 1. Considerable effort was made during the design and construction of this chamber to ensure that the arrangement of collimators, target (C) and solid state counter was symmetric about the Z axis (K). Also, the mass of gamma absorber in the region between the source (B^{10} target) and the gamma counters was kept to a minimum. Referring to Figure 1. this is the region above the plane which passes through the line (L) and is perpendicular to the plane in which the crossection of the target box was taken. To this end the sphere (B) forming the majority of the target box enclosure was made of aluminium and the mass of the solid state

counter mount in the above region was kept to a minimum. As a check on the effect produced by gamma absorption in the target chamber, the intensity of gammas from a Co^{60} source placed at the target point, with the chamber removed, was recorded over the half sphere described previously. The gamma intensity was then recorded with the source in the same position but with the target chamber and solid state counter in place. It was found that to within experimental error ($\pm 1\%$) no fluctuation in gamma intensity was introduced by the target chamber and solid state counter.

The effect due to gamma ray absorption in the Au target backing was calculated using the known shape of the backing and was found to be negligible ($< 0.1\%$).

The isotopically pure (99% purity) B^{10} targets, 500 micrograms per cm^2 in thickness, were obtained from A.E.R.E. Harwell. Gold was chosen for the target backing because of its low (dp) reaction crossection. A backing thickness of 0.0005 inches was selected which just stopped the 1.5 Mev. incident deuterons, but did not introduce a large amount of energy straggle in the reaction protons which passed through the foil. This target was supported by a brass ring of 0.004 inch thickness and 0.010 inch width which produced negligible gamma absorption.

B.) COUNTERS

i.) SOLID STATE COUNTER.

The Q value for the $B^{10}(dp)B^{11}$ reaction is 9.24 Mev, therefore the solid state counter used to detect the protons from this reaction had to stop approximately 10 Mev. protons in its active region to ensure that the response of the counter was linear for all the protons resulting from the reaction. For this reason a deep depletion depth (~1mm) Nuclear Diodes (PH 8-25-10) counter was chosen. The response of this counter to a thin Am^{241} alpha

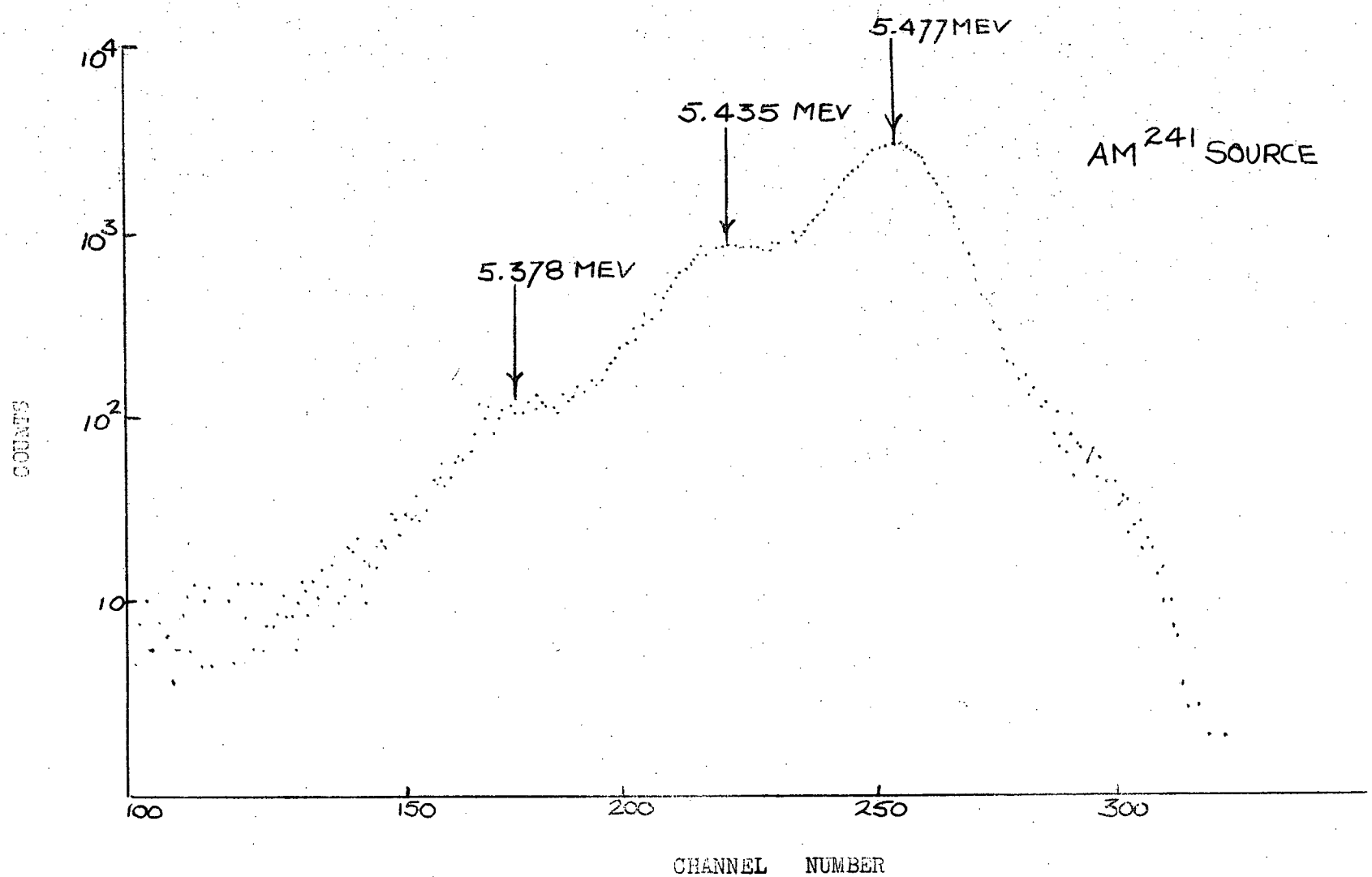

FIGURE 2. SOLID STATE COUNTER RESPONSE

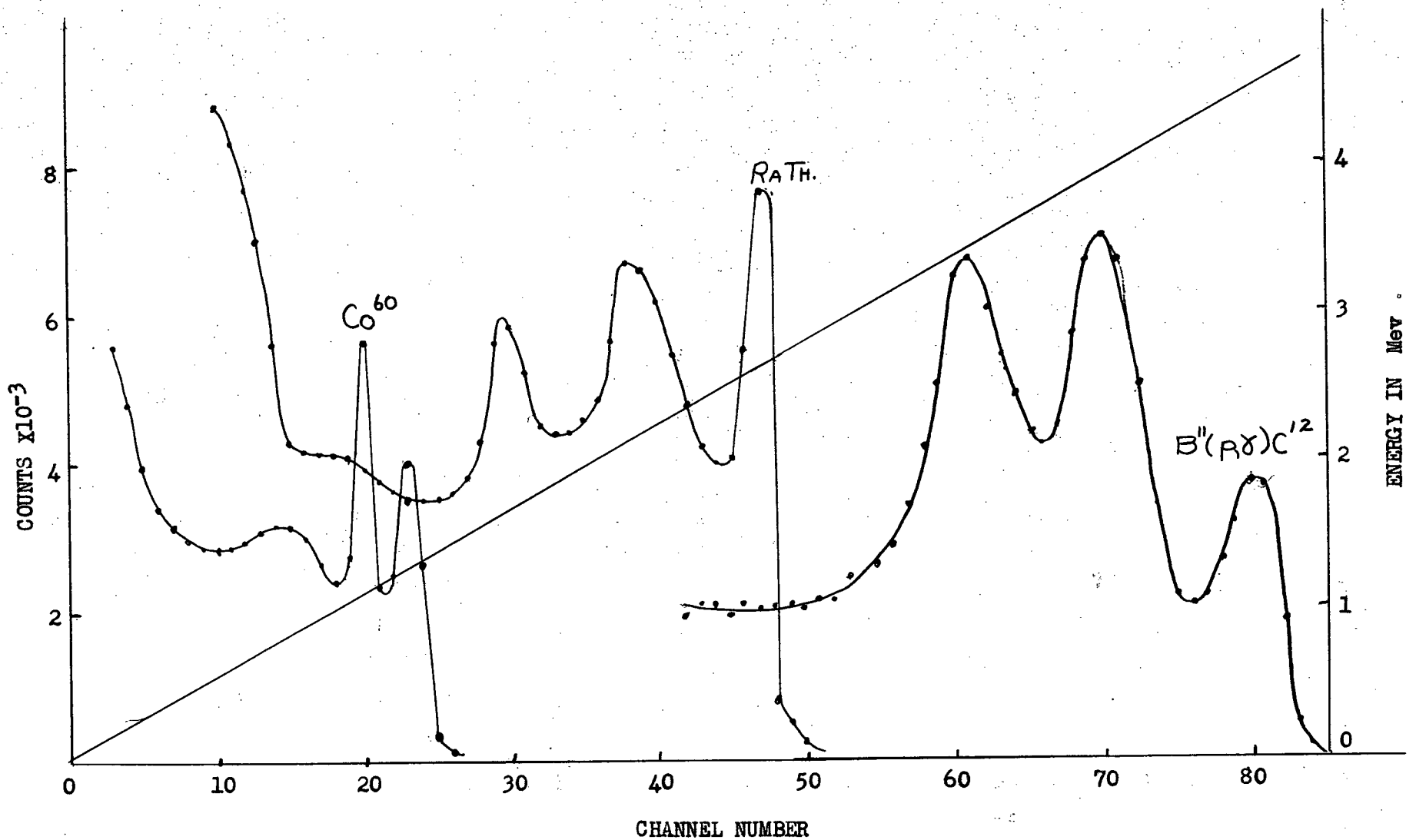

FIGURE 3. RESPONSE OF 2" x 2" NaI CRYSTAL

source is shown in Figure 2. This spectrum was obtained using the ORTEC. Low Noise Preamp. Model #101 and Ortec. Low Noise Biased Amp. (total electronic Noise ~6 Kev).

Indicated on this curve are the alpha energies corresponding to each peak. The resolution of this counter at 300 volts applied bias was found to be approximately 30 Kev.

During the angular correlation measurements it was found that deuterons scattered from the beam were reaching the solid state counter. To prevent this from happening an aluminum foil thick enough to stop deuterons of the beam energy (approximately 0.0008 inches) was placed directly in front of the solid state counter. Referring to Figure 1., the foil (D) is indicated. Also, during these measurements it was found that after 10^9 to 10^{10} proton counts of average energy 5 Mev., the resolution of the counter decreased and the leakage current increased rapidly with increasing counts. This counter degeneration was consistent with the normal lifetime of solid state counters as outlined by Dearnaley and Northrop 35.)

ii.) GAMMA COUNTERS.

Harshaw 2" x 2" NaI (Tl) crystals mounted on 6810A photomultipliers were used for the gamma detectors. The 6810A photomultiplier was chosen because of its fast response, high resolution, and low delay time between anode pulses arising from electrons emitted simultaneously at different points on the photocathode. This low delay time is desireable for use with the fast coincidence circuit. The response of this system to various gamma ray calibration sources is shown in Figure 3. Indicated in this figure are the spectra from two radioactive sources Co^{60} (2 gammas 1.33 Mev. and 1.17 Mev.) and Rath (2.61 Mev.). To determine the response of the gamma counter to higher energy gammas an isotopically pure B^{11} target was bombarded with a 163 Kev proton beam from the U.B.C. low energy accelerator. The 4.43 Mev.

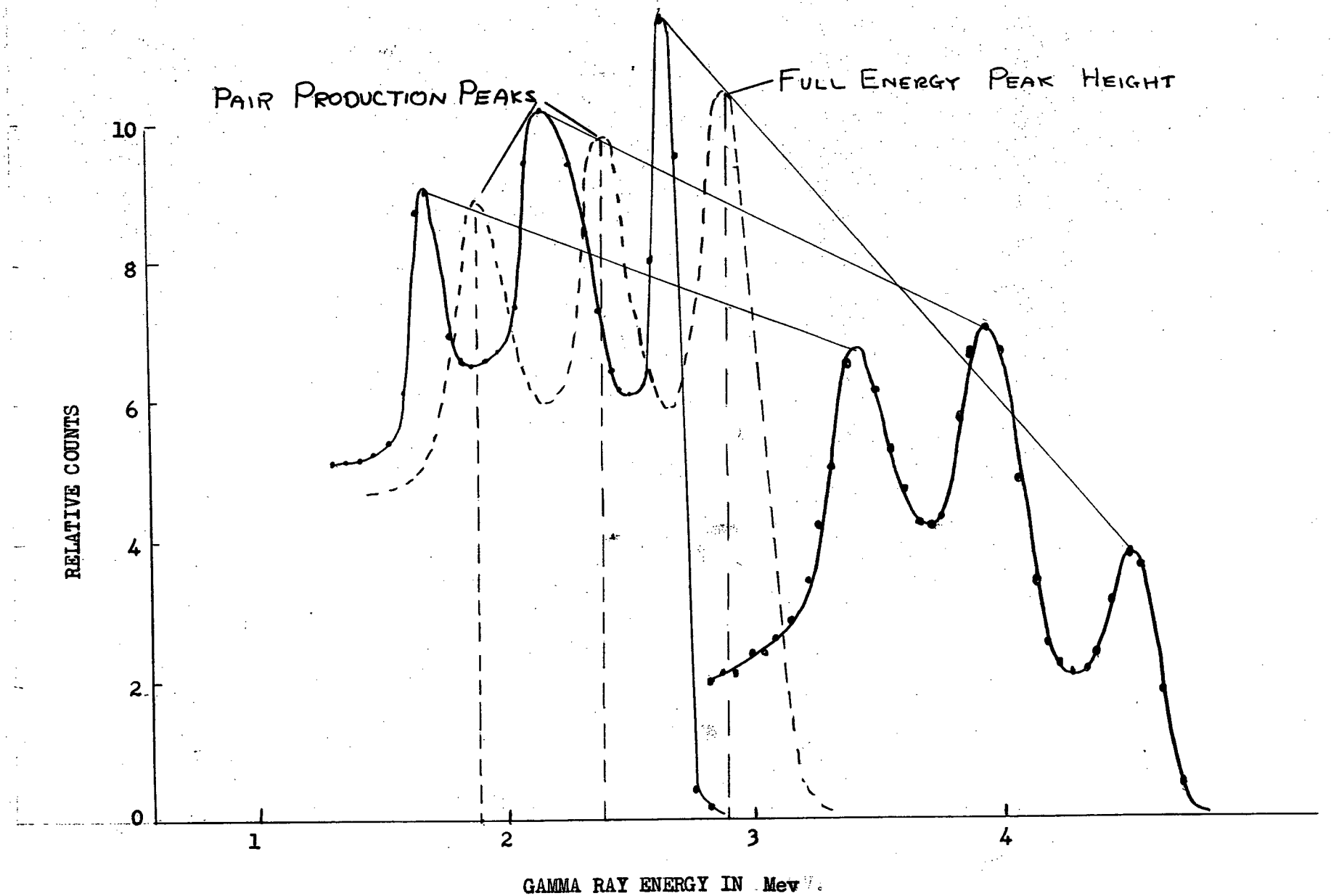

FIGURE 4. INTERPOLATED GAMMA RAY SPECTRUM

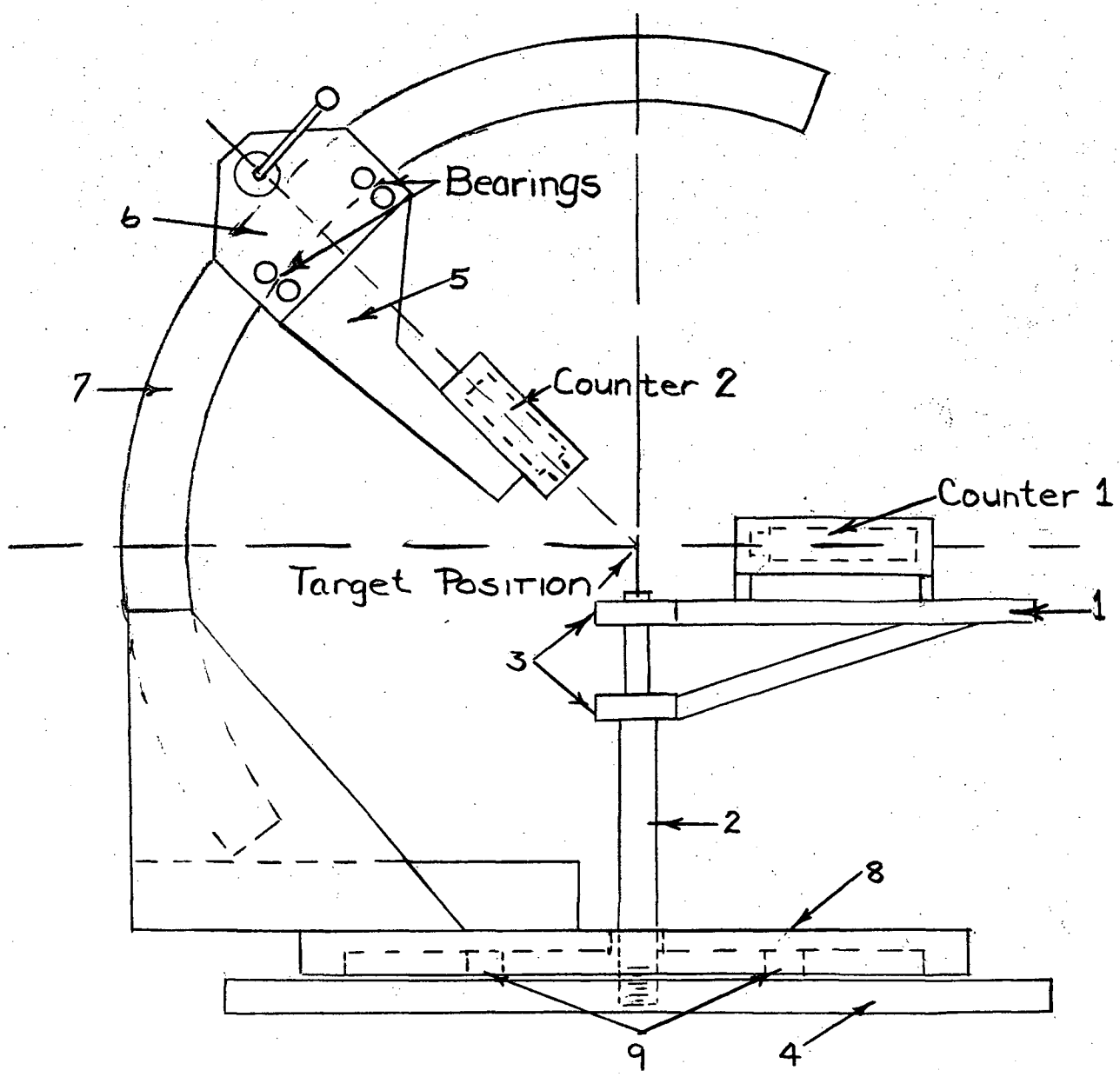

FIGURE 5. ANGULAR DISTRIBUTION TABLE

gamma component from the $B^{11}(p\,\gamma)C^{12}$ reaction is displayed in Figure 3.

To interpret the gamma spectra obtained from the $B^{10}(dp)B^{11}$ reaction it is necessary to know the response of this counter to 2.89 Mev. gamma rays. The relative heights of the three peaks, the full energy and the one and two photon escape peaks, were obtained by linear interpolation between the 4.43 Mev. and the 2.61 Mev. peaks. Figure 4. displays the interpolation method. The relative peak heights of the full energy peaks were determined from efficiency curves and peak-to-total ratios, (References 17 and 18) for a 2" x 2" NaI crystal. The heights of the peaks in the spectra were assumed to change linearly from 2.61 Mev. to 4.43 Mev. gamma energies. Since the interpolation is only carried over a small energy interval (approximately 300 Kev) above the 2.61 Mev. gamma, no large errors in spectrum shape should be introduced by this procedure. The same procedure was used in approximating the valley depths and other features of the spectrum. The outline of the expected 2.89 Mev. gamma spectrum shape resulting from this linear interpolation is indicated in Figure 4. by the dashed line.

C.) THE ANGULAR DISTRIBUTION TABLE

The requirements on the table were that the distance between the target point and both gamma counter faces would be held fixed, independent of the position of the counters and that the faces of both counters would be held perpendicular to a line joining the target point and the geometric centre of the counter face. A drawing of the table is shown in Figure 5. Gamma counter number 1 is mounted on a T beam arm (1) which is fixed by means of two MJ2 R & M roller bearings 3 to a 3" diameter steel shaft (2) tapered at the top to fit the bearings. The shaft was tapped at the lower end and screwed into the gun mount base (4). This structure allowed gamma counter 1 to be moved in the horizontal plane at a fixed distance from the target point which lay on the centre line of the shaft. Gamma counter 2 was mounted on an alum-

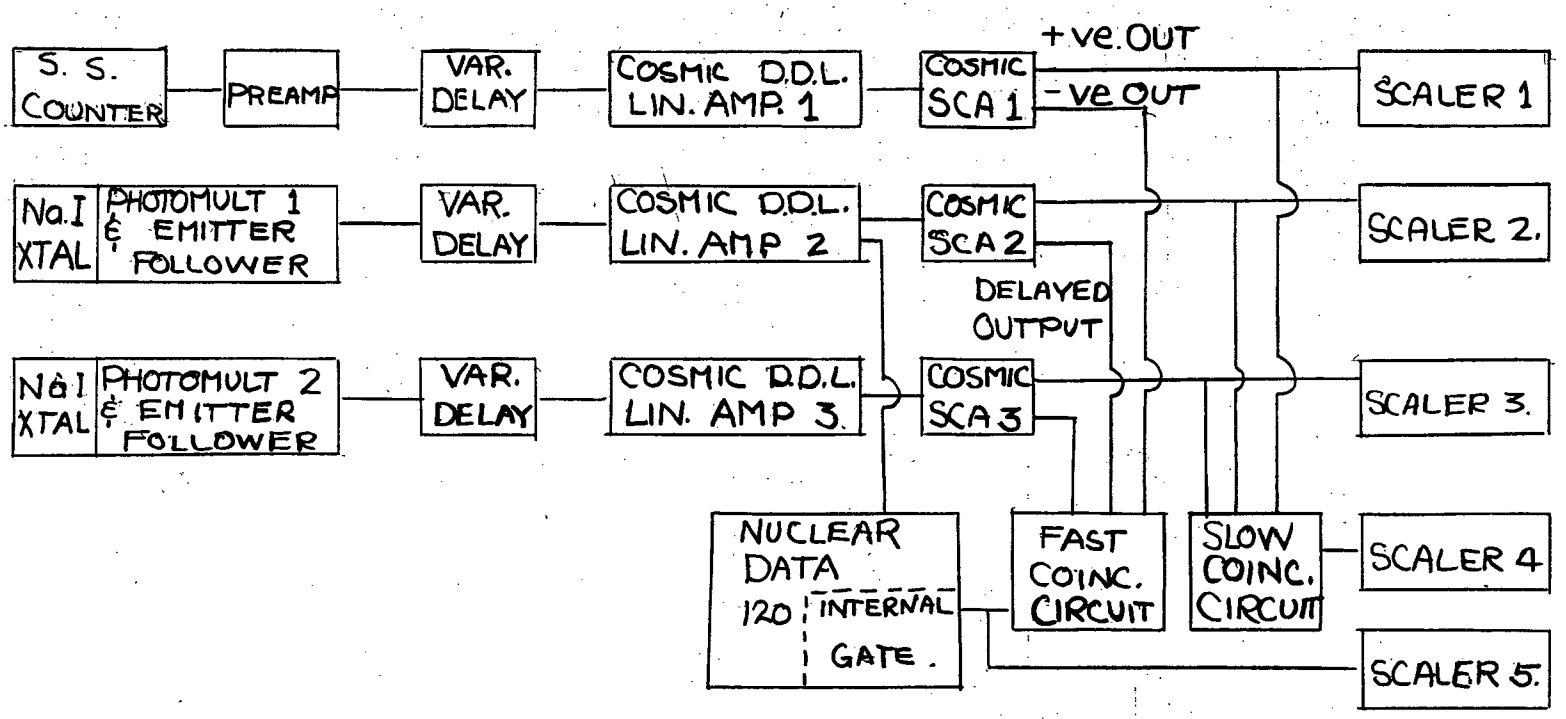

FIGURE 6. CIRCUIT DIAGRAM

inium arm (5) attached to a cart (6) which moved along an arc described by the curved 6" steel I beam (7). The I beam was fixed to the gun mount table (8) which rotates in the horizontal plane on the gun mount bearing (9). By moving the cart and the gun mount table, it was possible to locate gamma counter 2 on any point of a half sphere centered at the target point. This system was designed such that a load of 300 pounds of shielding, when placed at the extremities of either of the two arms of mounts (1) and (5), would cause less than a $\frac{1}{16}$" deflection of the arm ends from the no load position. This characteristic was checked under load - no load conditions and found to be satisfied.

The centres of rotation of both gamma counter mounts were aligned such that they coincided with the target point which was set at 44½" above the floor of the Van de Graaff laboratory. This is approximately the distance that a horizontal particle beam from the Van de Graaff emerges from the beam selector box. The alignment was carried out by mounting pointed brass rods from the centre of, and perpendicular to, the positions of the gamma counter faces on each counter mount. The mounts were then adjusted such that the ends of both brass pointers coincided with the target position, independent of the position of either mount. The target chamber was then set in place and the proton counter, target and collimators were centered visually by sighting down the Van de Graaff beam direction with a WILD T2 theodolite. All three components were centered to within an estimated $\frac{1}{64}$".

D.) ELECTRONICS

A schematic diagram of the circuitry used for the correlation measurements is shown in Figure 6. A current pulse generated in the solid state counter by an impinging charged particle was fed into the solid state preamplifier and a pulse proportional to the time integral of the current from the counter appeared at the preamplifier output. This pulse passed through a

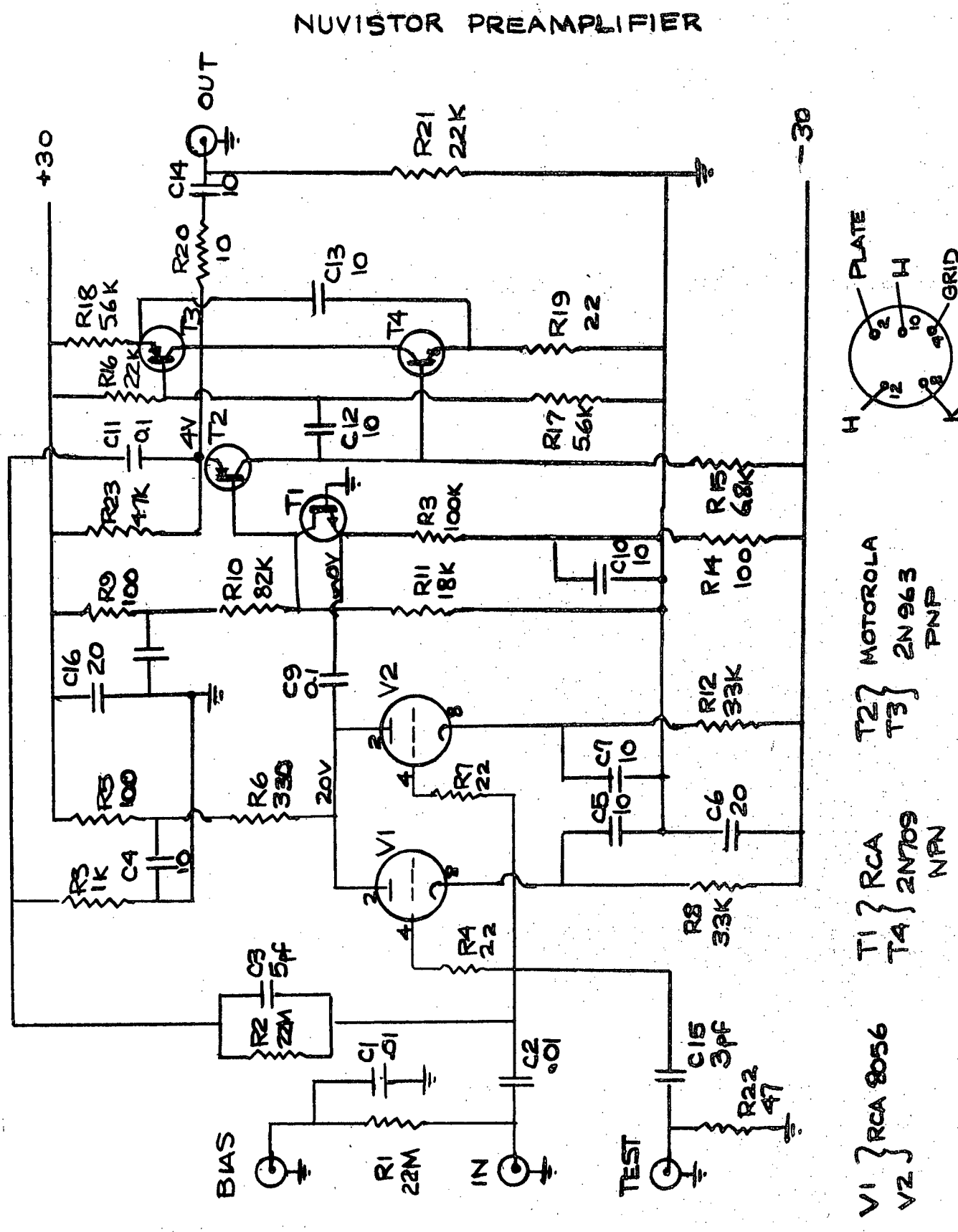

FIGURE 7. Nuvistor Preamplifier Circuit

500 nano second variable delay and was amplified by a COSMIC DOUBLE DELAY LINE LINEAR AMPLIFIER 1 (DDL LIN. AMP 1). The amplified and shaped pulse was fed into COSMIC SINGLE CHANNEL ANALYSER 1 (S.C.A. 1) and if the pulse was of the amplitude range selected by the analyser, a pulse was generated at both outputs when the delay line shaped pulse passed through the zero crossover point. The pulse from the positive output went to SCALER 1 and the slow coincidence circuit. The pulse from the negative output went directly to the fast coincidence circuit. A similar process was followed by pulses from the two NaI - photomultiplier - emitter follower combinations which were recording gamma rays. When a coincidence event occurred in the fast coincidence circuit, a pulse was generated, opening the internal gate in the NUCLEAR DATA 120 KICKSORTER (K.S.) allowing the coincident gamma ray pulse from the delayed output of the amplifier to be analysed by the kicksorter. As indicated in the diagram scalers4 and 5 recorded the number of fast and slow coincidence events which occurred during each run.

i.) NUVISTOR PREAMPLIFIER.

The circuit diagram of the nuvistor preamplifier appears in Figure 7. The circuit design, basically that of Alexander 33.) was modified by Dr. G. Jones 34.) for use in this experiment. The two nuvistors served as a high gain amplifier and the output was fed back through capacitor C3(5pf), making the system a current integrator. A pulse proportional to the total charge injected at the input by the solid state counter appeared at the emitter of transistor (T2). The combination of T_2, T_3 and T_4 served as a low output impedance emitter follower. This amplifier combined the desireable characteristics of low noise (approximately 25 Kev) and fast risetime (approximately 15 ns). (These values of noise and risetime refer to the case of zero input capacitance.) The combination of R_2 and C_3 was chosen to give the required pulse decay time (100 ns) compatible with the Cosmic amplifiers.

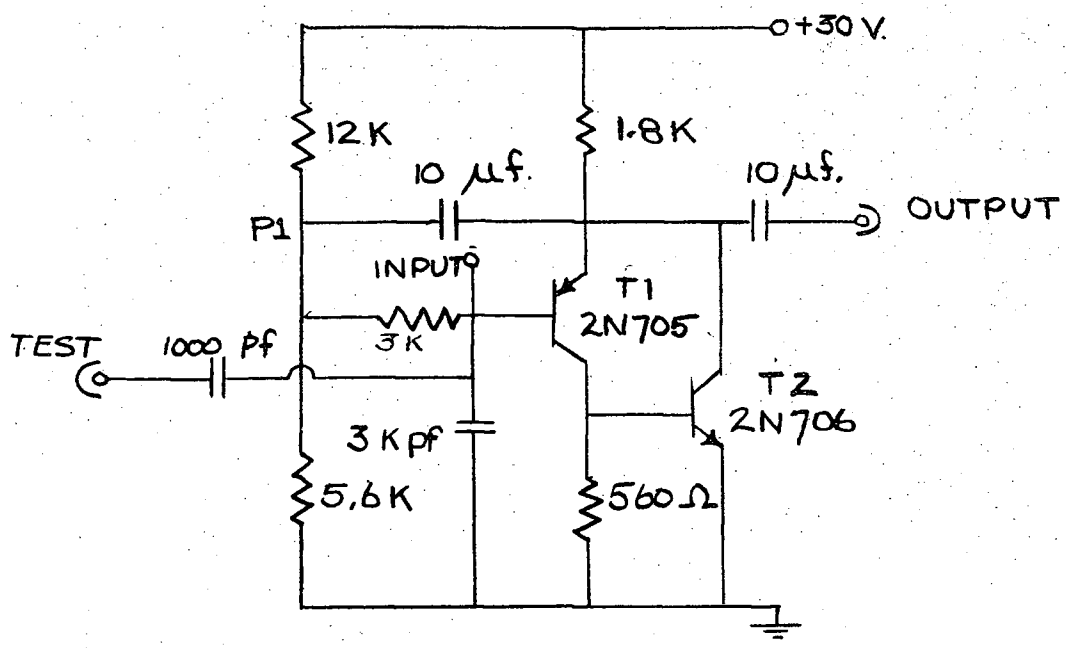

FIGURE 8. PHOTOMULTIPLIER EMITTER FOLLOWER

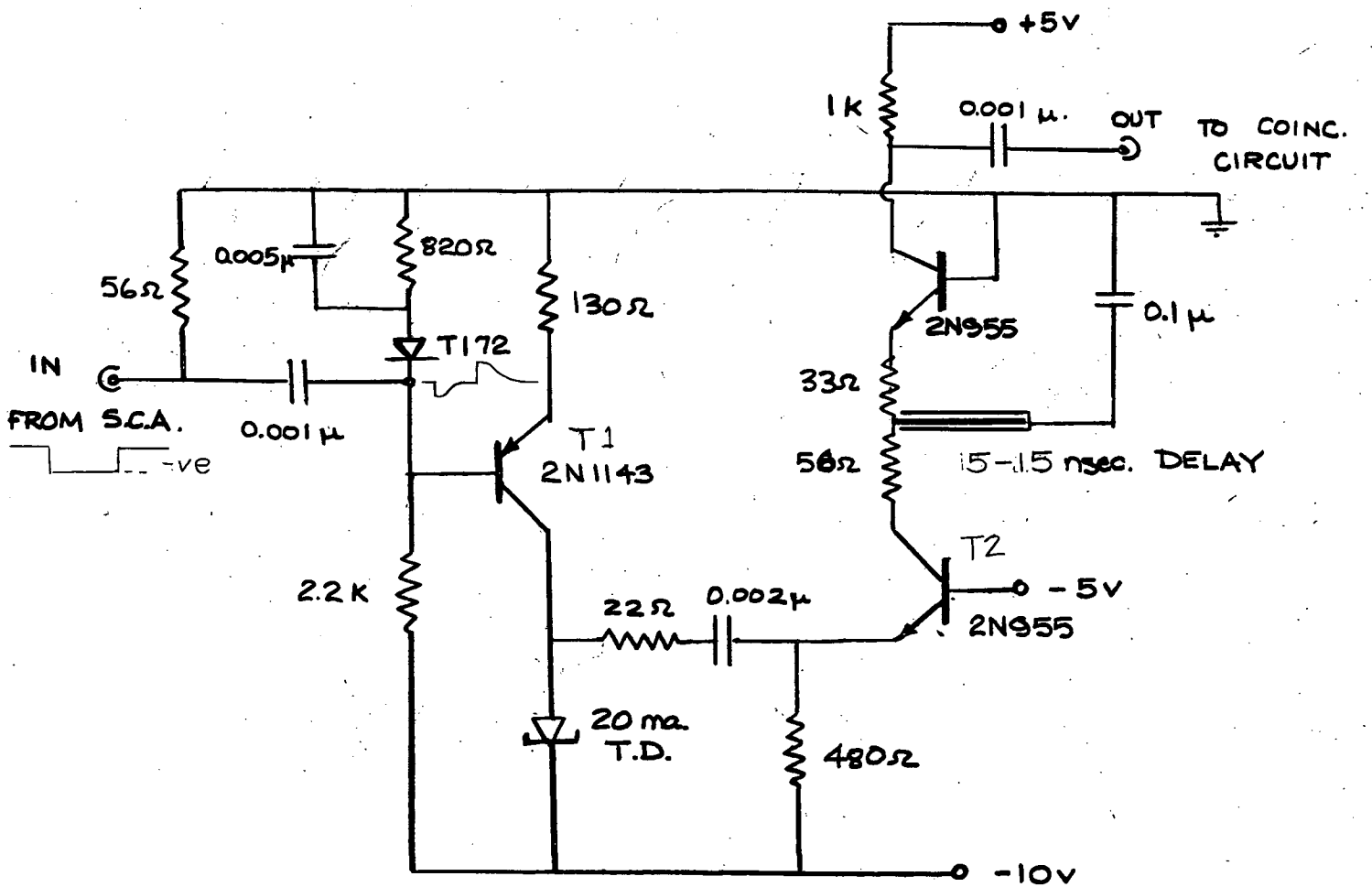

FIGURE 9. PULSE GENERATOR

ii.) PHOTOMULTIPLIER EMITTER FOLLOWER.

An emitter follower was used in conjunction with the output of the 6810A. photomultiplier and the circuit diagram is given in Figure 8. A negative current pulse from the anode of the photomultiplier was fed into the input (base of T1) of the emitter follower. This pulse turned on a small amount of current through T1 which turned T2 hard on. The pulse which appeared at the output of the emitter follower was proportional to the time integral of the current pulse (total charge) from the photomultiplier which was integrated on the 3000pf capacitor. The 10μf condensor between the emitter of T1 and point P1 "bootstraped" this point and had the desired effect of lengthening the decay time of the pulse to make it compatible with the Cosmic amplifiers.

iii.) FAST COINCIDENCE CIRCUIT.

The Fast Coincidence Circuit consisted of three 10ns wide pulse generators, triggered by the negative outputs of the Cosmic S.C.A. and a fast discriminator. The circuit diagram of the pulse generators appears in Figure 9. A negative 6 volt (20 ns risetime) pulse from the Cosmic S.C.A. appeared at the input of the pulse generator. This pulse was shaped by diode T1 72 such that the negative going portion of the pulse turned on enough current in transistor T1 to trigger the 20 ma tunnel diode. The positive going portion turned transistor T1 completely off and reset the tunnel diode. The fast rising pulse (approx. 3ns risetime) generated by the tunnel diode turned the 10 ma standing current in transistor T2 completely off. The resulting 10 ma pulse appeared at the collector of T2 where it was clipped by the shorted delay line to the required length (5 ns). This pulse then passed through transistor T3 to the output point. The net effect of this circuit was that a short ($\sim$5 ns in width) fast (3 ns rise and fall times) 5 ma pulse was generated at the output when a pulse from the S.C.A. arrived. A small negative pulse also appeared at the output caused by the resetting of the circuit.

FIGURE 10. Coincidence Circuit

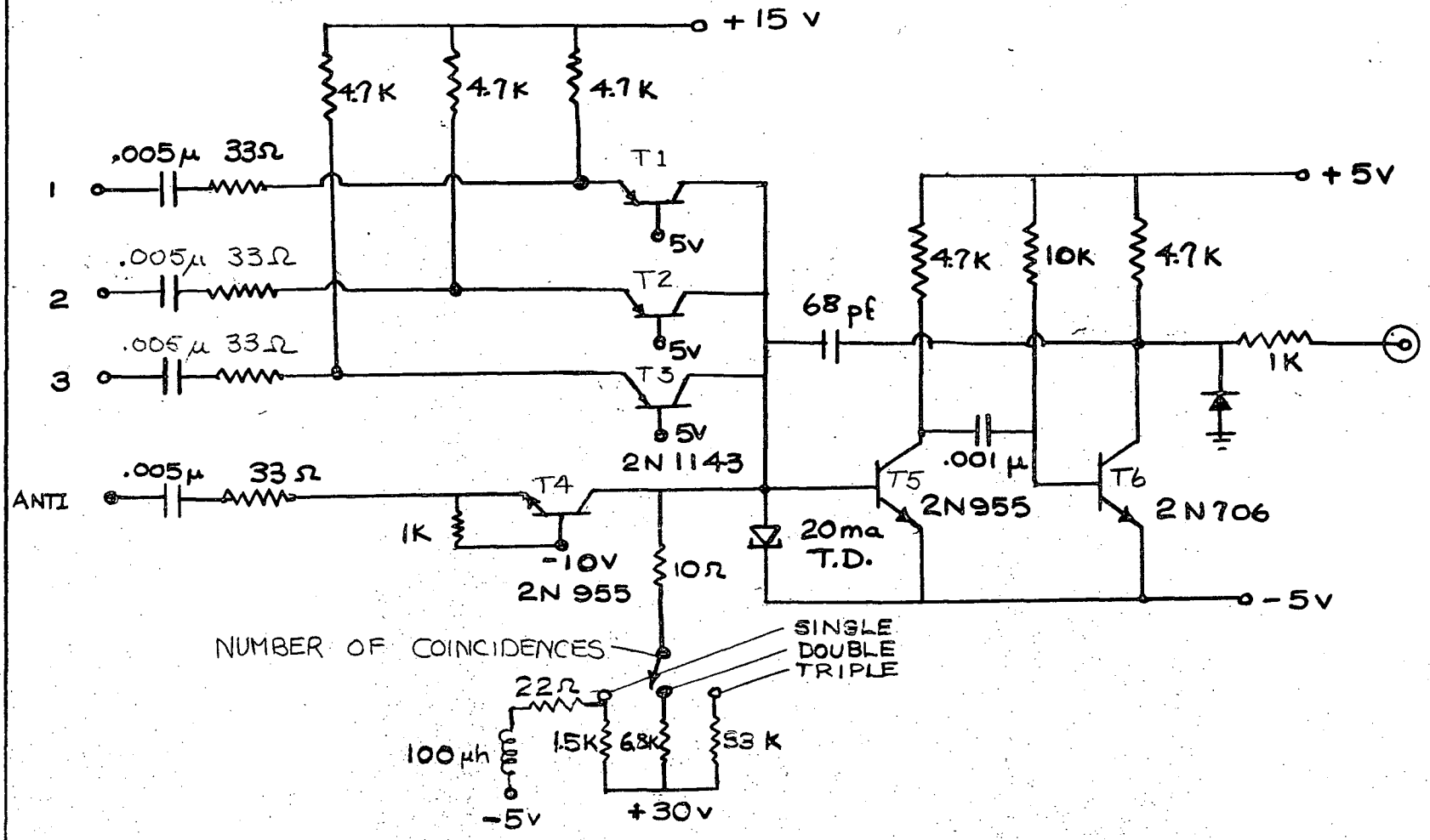

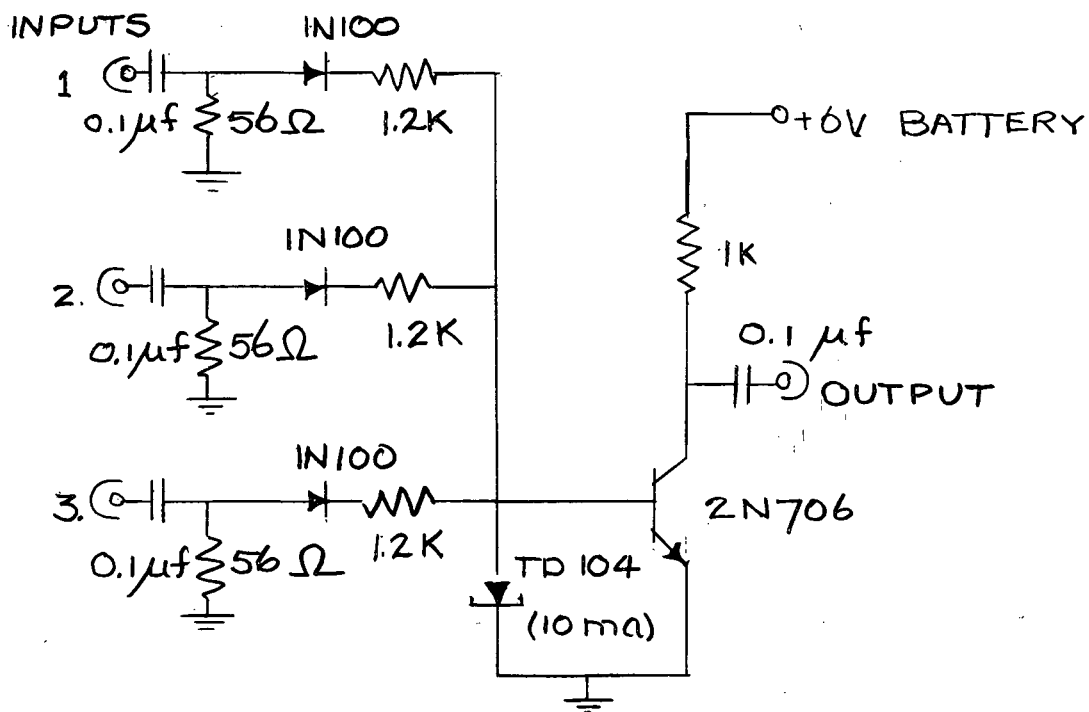

FIGURE 11. SLOW COINCIDENCE CIRCUIT

The coincidence circuit diagram appears in Figure 10. Pulses arriving from the pulse generators at the three inputs passed through transistors T1, T2 and T3 and then through a 20 ma tunnel diode. The amount of steady state current passing through the tunnel diode was controlled by the "NUMBER OF COINCIDENCES" switch. When the switch was in its "singles" mode, approximately 17 ma was flowing through the tunnel diode. Therefore if a pulse (5 ma) arrived at any of the three inputs the 20 ma TD switched into its high voltage state, turning on transistor T5. The voltage at the collector of T5 fell to approximately - 5 volts turning transistor T6 off for the length of time determined by resistance (R) and capacitance (C). After a time RC (approximately 2 μs) transistor T6 again came into conduction and its collector voltage fell to - 5 volts. The 68pf capacitor connected to the collector of T6 drew enough current at this time to reset the tunnel diode. The pulse generated was designed to open the kicksorter gate for 1 μs. The difference between kicksorter "ON" time (1 μs) and T6 off time (2 μs) resulted from the slow rise time (1 μs) of the gating pulse. By setting the "NUMBER OF COINCIDENCES" switch to "doubles" or "triples" mode a 12 ma or 7 ma standing current flowed through the tunnel diode. Thus when the switch was set to "doubles" (or "triples") two (or three) pulses had to arrive simultaneously (i.e. within twice the pulse width) at the inputs to cause the tunnel diode to trigger an output pulse.

iv.) SLOW COINCIDENCE (RANDOM COUNT RATE MONITOR) CIRCUIT.

During the Triple Coincidence measurement it was found that the correction for random coincidences was sufficiently large to require the continued monitoring of the triple random rate. Therefore a circuit to monitor the random coincidence rates was incorporated. A "Slow Coincidence Circuit" which duplicated the response of the fast triple coincidence circuit but which had a longer resolution time was built for this purpose and its circuit diagram is displayed in Figure 11. Pulses from the positive outputs of the S.C.A.'s arrived at the

three inputs and only when all three pulses arrived simultaneously (within 100 ns of each other) did the tunnel diode trigger into its high voltage state. This turned the transistor on producing a negative 6 volt pulse at the output.

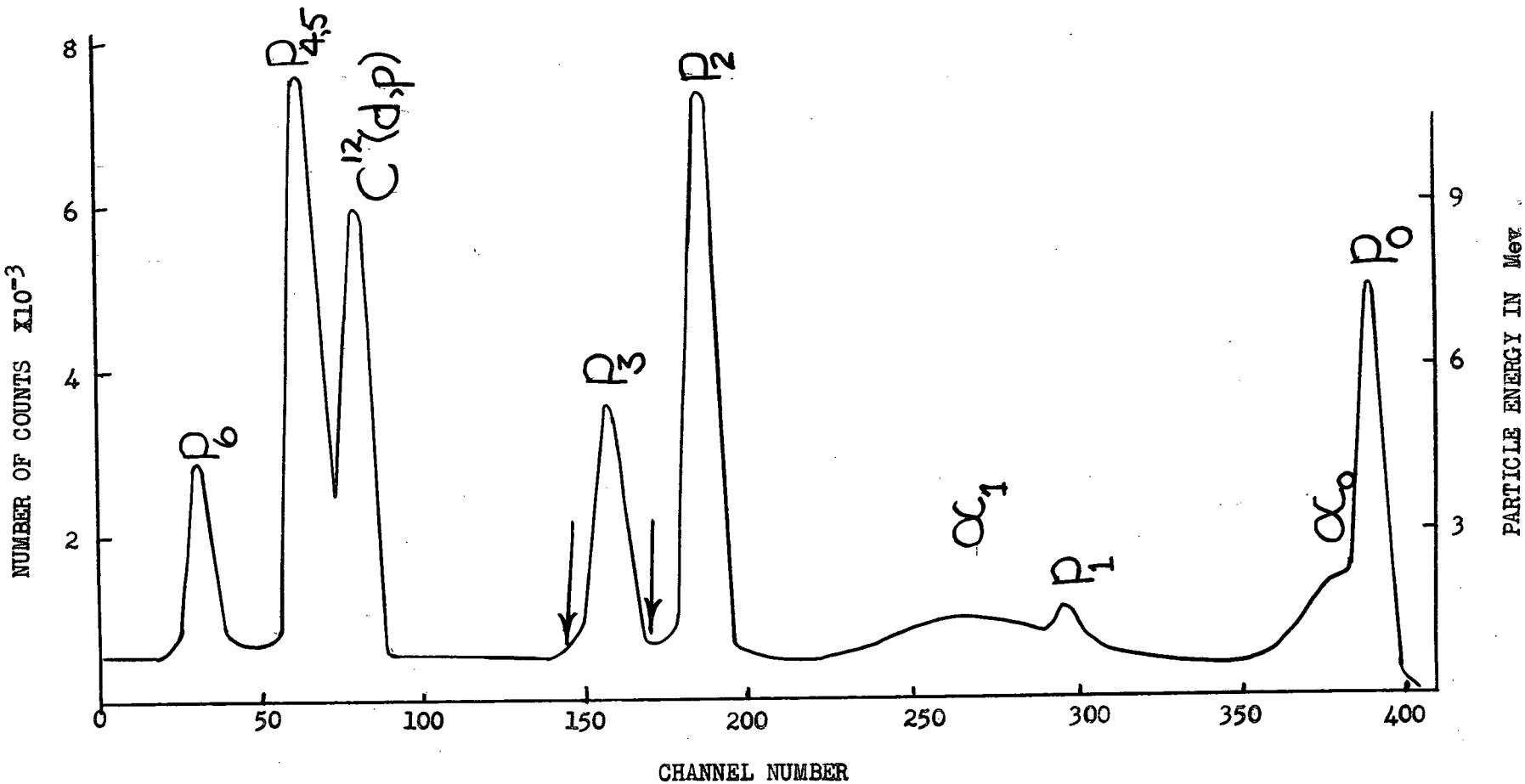

FIGURE 12. PARTICLE SPECTRUM

CHAPTER IV

ANGULAR CORRELATION MEASUREMENTS AND RESULTS

The B^{10} target, collimators and solid state counter were aligned as outlined in Chapter III Part C.) and a 1.5 Mev deuteron beam from the U.B.C. Van de Graaff accelerator was directed into the target system (refer to Figure 1.) along the collimation axis. The machine energy was maintained at 1.5 Mev to an accuracy of about 5 Kev throughout all the measurements made during the experiment. Particles from the B^{10} target emerging in a cone at an angle of less than 5° from the incident beam were detected by the solid state counter and this particle spectrum is displayed in Figure 12.). The sources of the various peaks in the spectrum are indicated above each peak along with their corresponding energies. Effects which produce most of the broadening of the proton peaks, along with an estimate of the magnitude of each effect for 5 Mev protons are:

a) B^{10} target thickness (25kv)

b) Straggling of protons in target, gold target backing, and aluminum foil in front of the proton counter. (50kv)

c) Varying length of travel of protons in backing and foil due to different angles of incidence of protons in foils. (20kv)

d) Kinematics, i.e. proton energy difference due to change of energy with angle of emission (50kv)

e) Electronic noise in counter and amplifier. (40kv).

The total peak broadening to be expected from the above mentioned effects is approximately 90 Kev which compares favourably with the measured value of 110 Kev. This small discrepancy can be accounted for in terms of the beam energy spread and the apparent increase in counter noise from the high flux of beta particles (see below).

Alpha particles from $B^{10}(d\alpha)Be^{8}$ leading to the ground and first

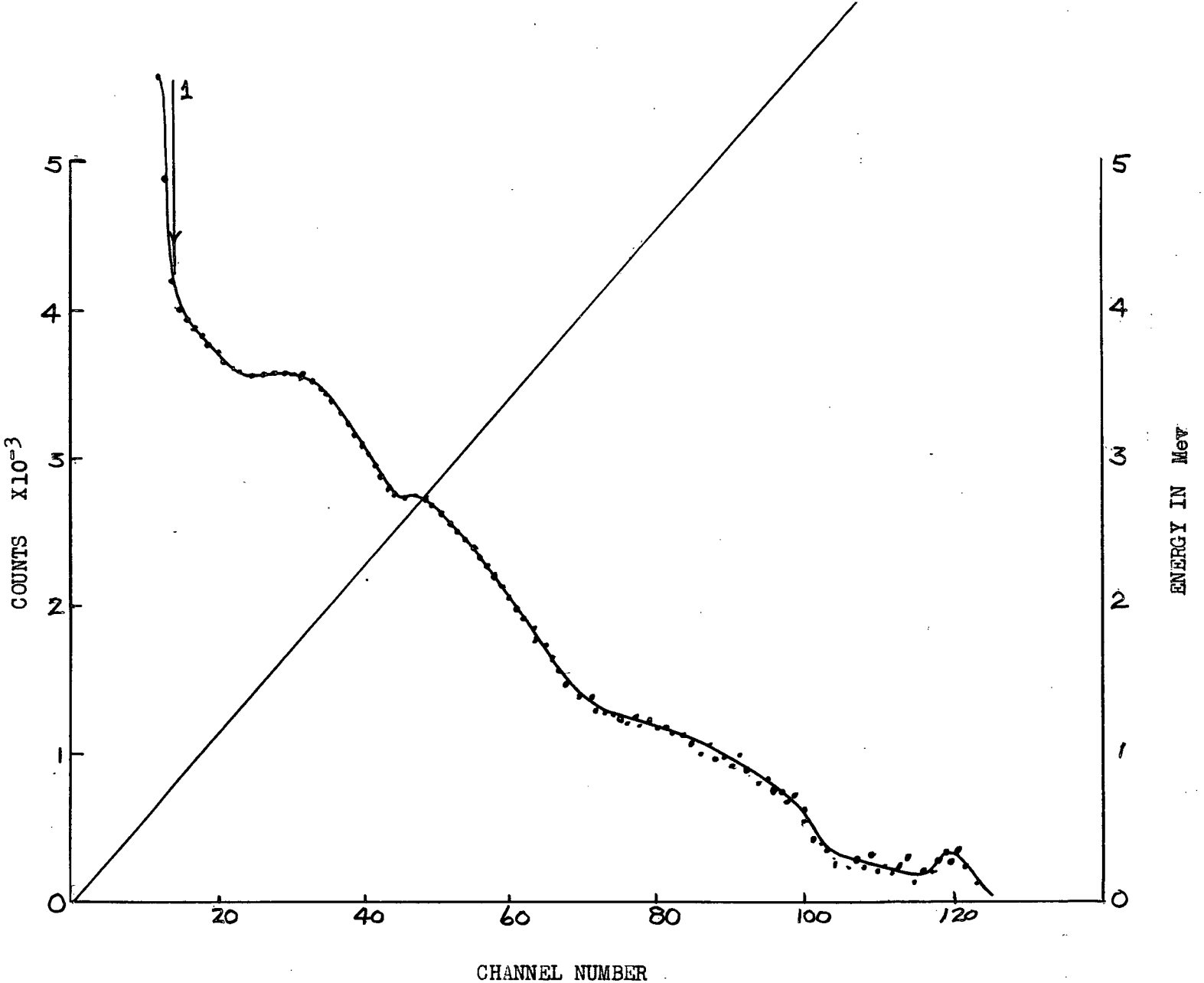

FIGURE 13. DEUTERON - EXCITED GAMMA SPECTRUM

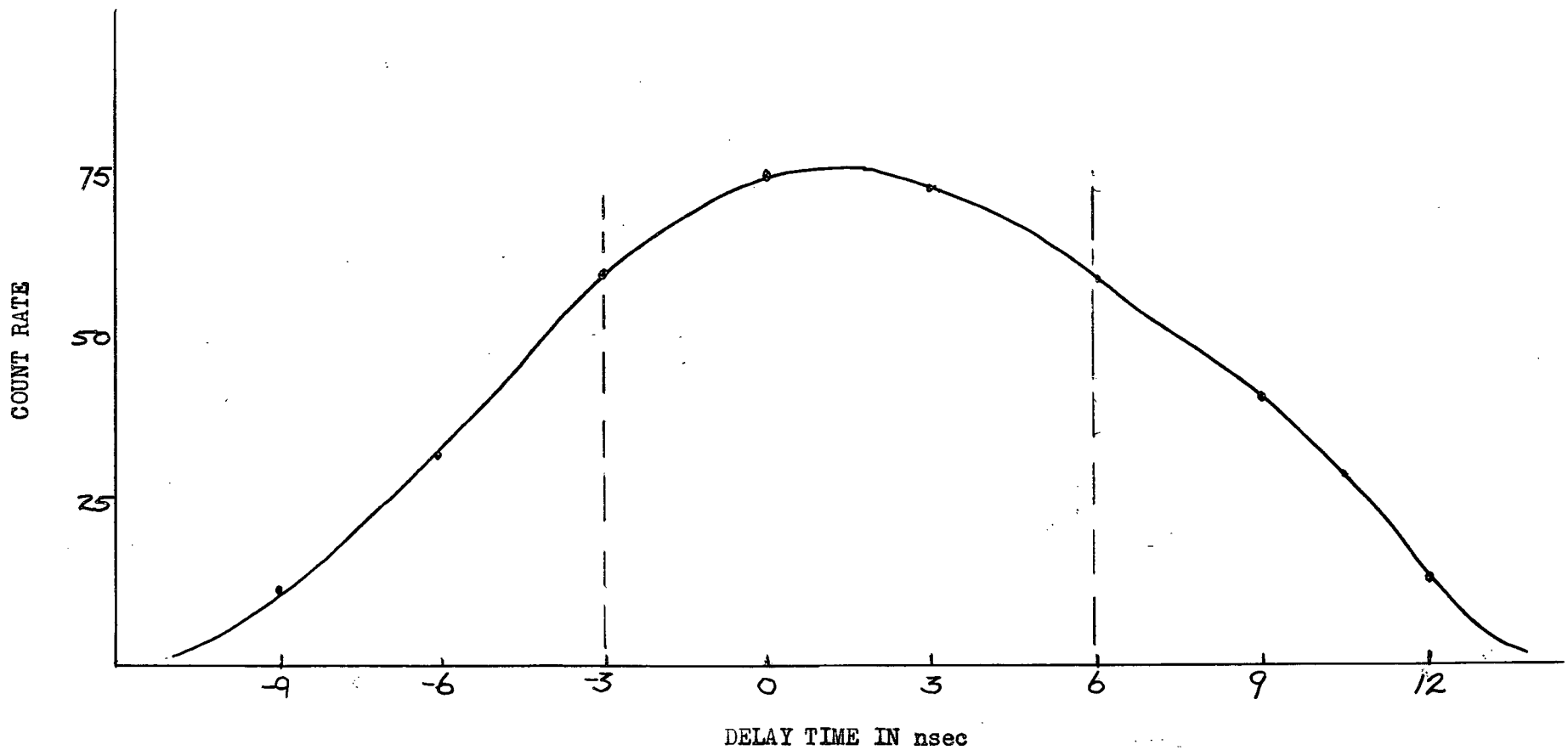

FIGURE 14. COINCIDENCE CIRCUIT RESPONSE

excited states also appear in Figure 12. The energy calibration for the alphas is not the same as that indicated for the protons, because of the much higher energy loss of the alphas in the gold and aluminum foils. Most of the alpha peak width is due to the large width of the states populated in the Be^8 nucleus.

The gamma spectrum induced by the deuteron beam is displayed in Figure 13. This spectrum is devoid of any prominant peaks because of the exceedingly large number of states populated by the (dp) and(dn) reactions with the target and surroundings. A sharp rise at the lower end of the spectrum (approx. channel 14) results from β^+ annihilation radiation from the reaction $B^{10}(dn)C^{11}(B^{11}\beta^+)$. That is the dn reaction on B^{10} produces C^{11} which has a β^+ half life of approximately 20 minutes. At the high energy end of the spectrum (approx. channel 120) an apparent peak results from the saturation of the Cosmic Linear Amplifier.

A.) PROTON, GAMMA COINCIDENCE MEASUREMENTS

To obtain measurements of $(p_3\gamma)$ coincidences the base line and window width of the Cosmic Single Channel Analyser (S.C.A. 1; see circuit diagram), Figure 6. was adjusted to select protons populating the 5.03 Mev level in B^{11}. Referring to Figure 12. this corresponded to selecting only those pulses whose heights lay between the two arrows on either side of p_3. S.C.A. 2 was set to select those gamma pulses whose height was above the point indicated in Figure 13. by the arrow marked 1. This corresponded to choosing only those gammas whose energy was greater than 0.7 Mev. The coincidence circuit was switched to the double coincidence mode and the timing adjusted by varying delays 1 and 2 (see circuit diagram) until a maximum coincidence count rate had been obtained. (For the relative delay time versus coincidence count rate curve see Figure 14.). In this figure the background random coincidence count rate has been subtracted. The region inside the two vertical dotted lines cor-

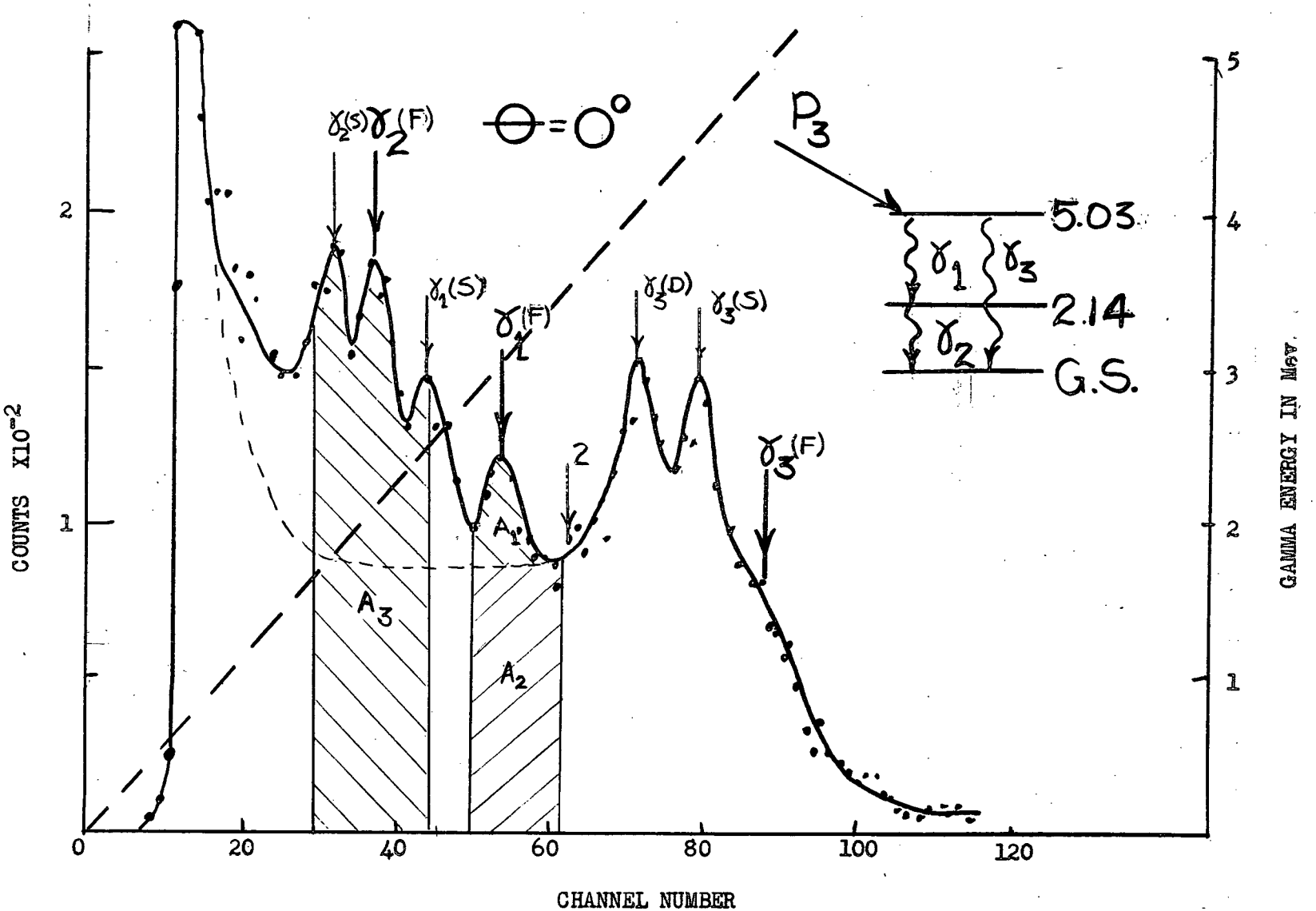

FIGURE 15. $p_3\gamma$ COINCIDENCE SPECTRUM

responds to the resolution time of the coincidence circuit. From this the efficiency of the coincidence network was estimated as being the ratio of the area inside the vertical lines to the total area. In this estimate it was assumed that all the "true" coincidences lay inside the region shown in Figure 14. and that the response of the coincidence circuit did not distort the shape of the actual time versus count rate curve. The efficiency was also calculated as the ratio of the observed coincidence count rate to the theoretical coincidence count rate calculated from the single count rates in the proton and gamma detectors (allowing for the counting efficiences of the proton and gamma counters), and was found to agree with this estimate. This loss in efficiency which arose from time "jitter" in the circuit, can be attributed almost exclusively to the Cosmic Single Channel Analysers, each of which has a time "jitter" of 8-9ns. This jitter results from the fact that different pulse heights from the Cosmic Amplifier cause the output pulses from the S.C.A. to be generated at times that vary by 8-9ns after the amplifier pulses pass through their zero crossover points.

With the timing set at the maximum count rate position, the pulses from the gamma counter were gated into the kicksorter when a coincidence event was recorded. The coincidence gamma ray spectrum ($p_3\gamma$) is shown in Figure 15. Indicated on this spectrum are the full energy $\gamma_1(F)$ and single and double escape $\gamma_1(S)$, $\gamma_1(D)$ peaks of the three gamma rays resulting from the two different decay schemes shown.

In the analysis of the 5.03 Mev level decay scheme it was necessary to know the shape of a 5 Mev gamma ray spectrum below the pair production peaks. An approximation to this spectrum was obtained by recording the coincidence gamma ray spectrum for the decay of the 4.46 Mev level which has been shown (Donovan et al 5.) to decay by gamma emission direct to the ground state only. This spectrum was obtained by adjusting S.C.A. 1 to select the protons

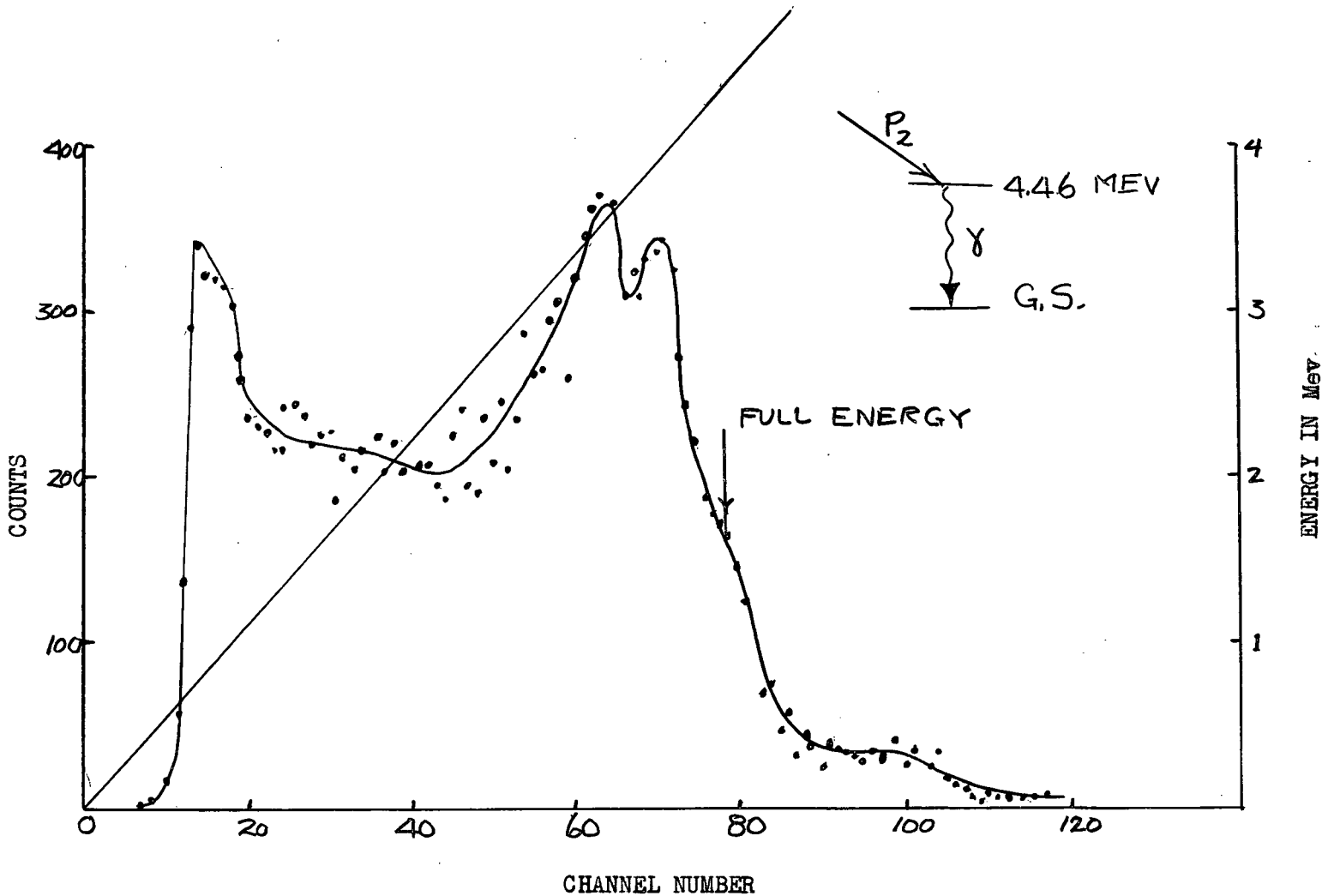

FIGURE 16. $p_2\gamma$ COINCIDENCE SPECTRUM

(p_2) populating the 4.46 Mev level and proceeding with the $p_2\gamma$ coincidence measurement as outlined for the $p_3\gamma$ measurement. Figure 16. shows the spectrum of the gamma rays depopulating the 4.46 Mev state.

i.) $p_3\gamma_3$ ANGULAR CORRELATION MEASUREMENT

The ($p_3\gamma_3$) correlation measurement was obtained by setting S.C.A. 1 so that protons populating the 5.03 Mev level (p_3) were selected as before. S.C.A. 2 was then adjusted to select only those gamma pulses whose height was above the point indicated in Figure 15. by the arrow marked 2. This corresponded to selecting gamma energies above 3.3 Mev. The coincidence count rate $p_3\gamma_3$ was then recorded for various angles θ, where θ is the angle between the incident beam and the gamma propagation direction, (see Table 4.). To ensure that no time dependent effects would introduce fluctuations in the angular distribution, the angle θ was chosen randomly and the count rate at each angle recorded numerous times. The number of coincidence counts at each point was normalised to the number of protons (p_3) recorded by scaler 1.

Throughout the double correlation measurement, readings of the random coincidence count rate were recorded. These were obtained by setting the proton circuit timing (delay 1) approximately 200 nano seconds off coincidence and recording the coincidence count rate. The angular distribution of random coincidences was found to be isotropic, and had an average magnitude of 28 counts at each angle listed below. The random coincidence rate was also calculated using the usual equation:

$$N_{rand} = 2N_p N_{\gamma_3} \tau$$

N_{rand} = random count rate

N_p = count rate at coincidence circuit input from proton counter

N_{γ_3} = count rate at coincidence circuit input from

γ_3 counter

τ = width at one half maximum of the pulses from the timing pulse generators = 5ns

The calculated and measured random count rates were found to agree very closely (within 10%).

TABLE 4.

$p_3\gamma_3$ ANGULAR DISTRIBUTION

θ	Coinc. Counts*	Fitted Curve**
0	184	183
10	171	183
20	181	185
30	208	189
40	200	194
50	186	201
60	199	209
70	218	217
80	221	223
90	234	225
100	232	223
110	211	217
120	219	209

* Coincidence Counts per 4 10^5 proton counts

**Defined and calculated in Chapter V

An upper limit on the lifetime of the 5.03 Mev state was measured during this measurement for the purpose outlined in Chapter II Part F.) This lifetime limit was determined by injecting timing pulses at the inputs to the solid state counter preamplifier and gamma counter emitter follower in time

coincidence (within 10 ns of each other) which closely approximated the actual pulses produced by these counters. The timing of the coincidence circuit was then adjusted to the maximum coincidence count rate position by varying the time delays for the two counters and the timing noted. The $p_3\gamma_3$ coincidence measurement was then made and the coincidence count rate optimised as described at the beginning of this section and the timing noted once again. The timing for the $p_3\gamma_3$ coincidence measurement was found to agree to within 10 ns with the timing found using the simulated pulses which represented a zero lifetime state (i.e. lifetime shorter than mesureable with the coincidence circuit.). Also the half width of the $p_3\gamma_3$ coincidence count rate versus time delay curve (refer to Figure 14.) was found to be approximately 15 ns. Therefore, an upper limit on the lifetime of the state may be set at approximately 35 ns and for the purpose of Chapter II Part F.) a limit of 100 ns may be set with certainty.

ii.) $p_3\gamma_1$ and $p_3\gamma_2$ ANGULAR CORRELATION MEASUREMENT.

Spectra similar to the one displayed in Figure 15.) were obtained for various angles θ using the method outlined previously and the $p_3\gamma_1$ and $p_3\gamma_2$ angular distributions were extracted from these spectra by a method of spectrum stripping. Spectrum stripping is applied to cases where it is necessary to determine the contribution of individual gamma rays in a spectrum which is the sum of the spectra of several different gamma rays. The spectra to be analysed are sum spectra of γ_1, γ_2 and γ_3 and the contributions of each of these spectra are determined by fitting the known shapes of the individual gamma ray spectra to the sum. The shape of the individual gamma ray spectra are usually derived from separate experiments and in this case the shapes of γ_1 and γ_2 were determined using sources (Chapter III Part B.) and the shape of γ_3 was approximated by the shape of the pure 4.46 Mev gamma ray from the $B^{10}(dp)B^{11}$ reaction. One advantage of using the 4.46 Mev ($p_2\gamma$) coincidence gamma rays from the $B^{10}(dp_2)B^{11}$ reaction is that the $p_2\gamma$ coincidence spectrum is recorded under the same conditions

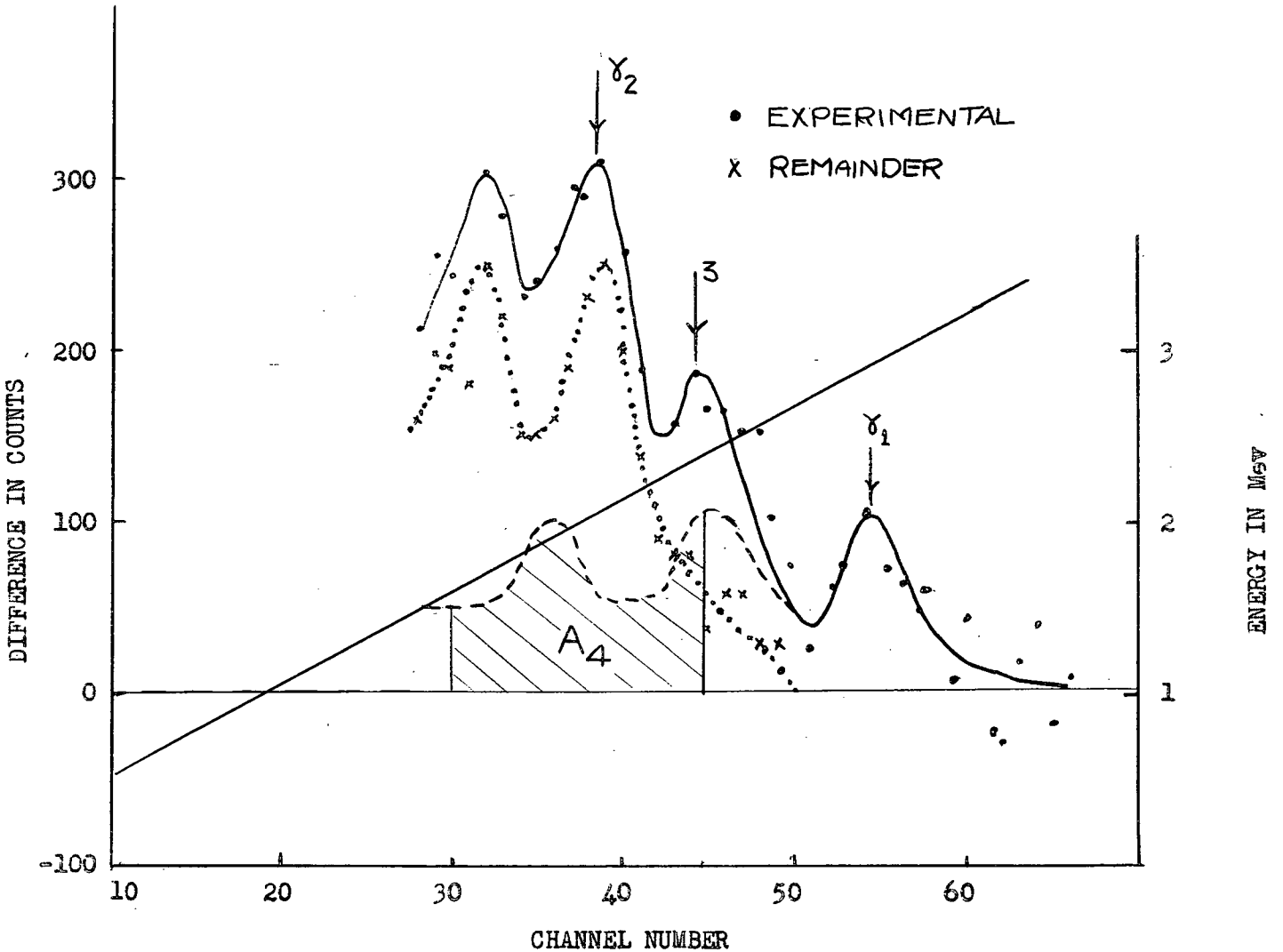

FIGURE 17. SUMMED $p_3\gamma_1$ AND $p_3\gamma_3$ SPECTRUM

as the $p_3\gamma$ spectrum, therefore the background (random coincidences) should be approximately the same for both spectra since they both took of the order of the same length of time to be recorded.

The particular method used in the analysis of the $p_3\gamma$ coincidence spectrum was first to strip the γ_3 portion of the spectrum (refer to Figure 15.) from the sum spectrum, the remainder was then analysed into its two components γ_1 and γ_2. The full energy and two pair production peaks of the 4.46 Mev gamma ray (Figure 16.) and γ_3 (Figure 15.) spectra were caused to fall in the same channels by shifting the whole $p_2\gamma$ spectrum up 9 channels. The $p_3\gamma$ spectrum was normalized to give the same total number of counts as the $p_2\gamma$ spectrum between channels 60 and 90. The shape of the 5.03 Mev (γ_3) spectrum below channel 60 as obtained by this process is displayed in Figure 15. as a dotted line. The shifted ($p_2\gamma$) spectrum was then subtracted from the normalised ($p_3\gamma$) spectrum leaving only the summed ($p_3\gamma_1$) and ($p_3\gamma_2$) spectrum. The $\theta = 0^\circ$ spectrum resulting from this subtraction is displayed in Figure 17. Three curves are indicated in this figure, the continuous line represents the sum of the γ_1 and γ_2 spectra. The dashed line starting at channel 28 represents the expected shape of the γ_1 spectrum in the region from channel 28 to channel 51 obtained by the method outlined in Chapter II. The dashed curve has been normalised to the experimental points by making the area under the curve between channels 51 and 60 equal to the total number of counts in these ten channels. The dotted curve is the remainder when the γ_1 spectrum (i.e. dashed curve) has been subtracted from the summed spectrum and should represent a pure γ_2 radiation. Referring to Figure 17. the total number of counts in the subtracted spectrum lying between channel 51 and 61 was recorded for each angle θ at which ($p_3\gamma$) coincidence spectra were taken and are listed in Table 5. in column 1. Also listed in this table in column 2 is the total number of counts in the remainder spectrum

TABLE 5.

$p_3\gamma_1$ AND $p_3\gamma_2$ ANGULAR DISTRIBUTION

θ	1.	2.	Norm. Factor	$p_3\gamma_1$ A.D.	$p_3\gamma_2$ A.D.
0	546	2002	1	546	2002
15	538	2470	1.01	543	2495
30	325	1576	1.03	335	1623
45	486	1713	1.08	525	1850
60	338	1828	1.15	389	2100
75	279	1208	1.21	338	1461
90	217	1869	1.23	267	2299

between channels 30 and 45.

As described in the preceeding paragraph the areas listed in Table 5. are normalised to give a constant number of counts in the $(p_3 \gamma_3)$ peaks so, to normalise the $(p_3 \gamma_1)$ and $(p_3 \gamma_2)$ spectra to a constant reaction rate, the $p_3 \gamma_3$ angular distribution must be removed. The $(p_3 \gamma_3)$ angular distribution is listed in Table 5., under the column marked 'Normalisation factor' and was taken directly from the fitted $p_3 \gamma_3$ angular distribution (Chapter V Part A.)i.) To obtain the normalised $(p_3 \gamma_1)$ and $(p_3 \gamma_2)$ angular distribution columns 1 and 2 in Table 5. were multiplied by the normalisation factor and the result is listed in the remaining two columns.

B.) TRIPLE COINCIDENCE MEASUREMENT

Cosmic Single Channel Analyser 1 was adjusted to select only the p_3 protons as outlined in Part A.) S.C.A. 2 and 3 were set to select only γ_1 and γ_2 respectively, when the coincidence circuit was operated in the triple coincidence mode. This was done by setting the baseline of S.C.A. 2 at a level which corresponded to selecting those gamma pulses which lay above the point indicated on Figure 17. by the arrow marked 3, (i.e. E_γ greater than 2.4. Mev). S.C.A. 3 was then set up to select gamma pulses below this level and above the β^+ annihilation radiation peak (above channel 15 in Figure 17). The triple coincidence count rate was maximised by adjusting delays 2 and 3 for maximum $p_3 \gamma$ double coincidence count rates. With the coincidence circuit set on the triple coincidence mode, five quantities were recorded by the scalers (see circuit diagram) for each particular angular configuration:

a) The total number of counts in each of the three counters.

b) The number of fast triple coincidence counts.

c) Slow coincidence (random coincidence monitor) counts.

A sampling of the random coincidence count rate was taken at intervals throughout the measurement by setting the p_3 timing (delay 1) approximately

TABLE 6.

TRIPLE CORRELATION RESULTS

θ_1 θ_2 ϕ	N_{coinc}	$N_p 10^{-7}$	$\frac{N_{coinc}}{N_p 10^{-5}}$
90 90 0	206	2.61	0.79
90 90 45	81	0.87	0.93
90 90 90	143	1.63	0.87
90 0 0	144	1.66	0.87
0 90 0	139	1.29	1.08

300 nano seconds off coincidence and recording the coincidence count rate. The random coincidence counts were subtracted from the measured triple coincidences and the result is displayed in the Table 6. (For a discussion of random rates and subtraction see Appendix I. The angles, defined in Chapter II Part D.) were chosen to give a maximum fluctuation in the triple coincidence count rate.

C.) DISCUSSION OF ERRORS

i.) ERRORS RELEVANT TO ALL ANGULAR DISTRIBUTION MEASUREMENTS.

(a) Counter Mounts

An attempt was made during the design of the target chamber and gamma counter mounts to ensure spherical symmetry about the target spot. It was found that the centre of rotation of both counters was coincident with the target spot to $\frac{1}{32}$ inch for all counter orientations, therefore the distance of the counter face (r_{ex}) to the target spot was fixed to this order of magnitude. A fluctuation in distance dr between counter and source at the target spot would introduce a fluctuation in the count rate due to the change in solid angle $d\Omega$

$$\Omega = \frac{dA}{r_{eff}^2}$$

r_{eff} = "effective distance" of source from detector (See J.L. Leigh 39.)

$r_{eff} = r_{ex} + e$ (e is > 0) depends on the gamma ray energy and crystal geometry.

From above it is found that

$$\frac{d\Omega}{\Omega} = -2\frac{dr_{eff}}{r_{eff}}$$

The experimental conditions are such that

$$e \ll r_{ex}$$

$$r_{ex} = 3.5 \text{ inch}$$

$$dr = \frac{1}{32}$$

Therefore

$$\left.\frac{d\Omega}{\Omega}\right)_{max.} = \frac{-2(\frac{1}{32})}{3.5} \cong 0.02.$$

That is, this would introduce a maximum apparent fluctuation in gamma intensity of about 2%.

(b) Target Box Absorption

The absorption of the target box was checked with a gamma source as outlined in Chapter II and was found to be spherically symmetric to within experimental error (approx. 2%). Therefore the maximum fluctuation introduced by geometrical and attenuation effects was less than 3%.

(c) Non Cylindrical Symmetry

It was pointed out in Chapter III that a great deal of care was taken in the construction and alignment of the target box and solid state counter mount to ensure that the condition of axial symmetry about the deuteron beam axis was satisfied. As an experimental check on how well this condition was satisfied a reading of the $p_3\gamma$ coincidence count rate was recorded in both the plane of the beam (as a function of θ) and in the plane perpendicular to the beam and passing through the target point (as a function of ϕ). It was found that the coincidence count rate:

1.) varied by approximately 10% in the θ plane and was symmetric about the $\theta = 0^\circ$ point ($\theta = 0^\circ$ being the deuteron beam direction) and

2.) was isotropic in the ϕ plane to within experimental accuracy ($\sim 1\%$).

Although this was not an absolute test it does give a strong indication that the condition of axial symmetry was satisfied to the degree required for the experiment.

ii.) ERRORS RELEVANT TO INDIVIDUAL DOUBLE ANGULAR CORRELATION MEASUREMENT

(a) $p_3\gamma_3$ Angular Distribution

Care was taken during this measurement to ensure that no time dependent effects would introduce fluctuations in the angular distribution. Also the amount of background due to random coincidences that had to be subtracted from the angular distribution was small, and adds very little to the statistical error. Therefore, most of the error, outside the statistical error, should arise from those effects outlined in i.)

(b) $p_3\gamma_1$ and $p_3\gamma_2$ Angular Distributions

1) Normalization.

As outlined in Part B.) ii.) of this chapter these two angular distributions were normalized to the $p_3\gamma_3$ angular distribution and since there is an uncertainty in the $p_3\gamma_3$ distribution, this will introduce a corresponding error in the $p_3\gamma_1$ and $p_3\gamma_2$ angular distributions. The angular distributions $p_3\gamma_i$ were fitted to functions of the form $W_{\gamma_i}(\theta)=\sum_n b_n(\gamma_i)P_n(\cos\theta_i)$ (See Chapter V Part A.) and the statistical errors on the coefficients $b_n(\gamma_3)$ in the normalized (i.e. $b_0=1$) $p_3\gamma_3$ angular distribution were found to be:

$$b_2(\gamma_3)_{\text{error}} = \pm 0.04$$
$$b_4(\gamma_3)_{\text{error}} = \pm 0.05$$

This will introduce a corresponding error in the $p_3\gamma_1$ and $p_3\gamma_2$ coefficients of the same order of magnitude.

2) Spectrum Stripping.

The $p_3\gamma_1$ and $p_3\gamma_2$ angular distributions were obtained by spectrum stripping. This involves the subtraction of one statistically uncertain spectrum shape from another which also has a statistical uncertainty. As an example consider the $\theta=0^\circ$ case (refer to Figure 15.). The number assigned

to the $\theta = 0^\circ$ point in the $p_3\gamma_1$ angular distribution table (Table 5.) is the value of the area A_1 which is the result of subtracting the area A_2 below the dashed line in the region between channels 51 and 61 from the total area under the continuous curve in this region $A_1 + A_2$. The statistical error in each point on the angular distribution curve is not $\sqrt{A_1}$ but is actually $\sqrt{A_1 + A_2}$ Here and in the following, the quantities A_b when calculating errors refer to the numerical values of A_b which correspond to the sum of the number of counts in the region defining A_b. A similar argument leads to the assignment of an error $\sqrt{A_3}$ to the error in the $\theta = 0^\circ$ $p_3\gamma_2$ angular distribution point, where A_3 is the area in Figure 15. under the continuous curve between channels 30 and 45. An additional error in the $p_3\gamma_2$ angular distribution arises from the uncertainty in the amount of $p_3\gamma_1$ spectrum (A_4 in Figure 17.) that should be subtracted from the summed $p_3\gamma_1$ and $p_3\gamma_2$ spectrum. The statistical uncertainty in A_4 is proportional to the uncertainty in the value of the $p_3\gamma_1$ angular distribution at this point ($\theta = 0^\circ$) which is $\sqrt{A_1 + A_2}$. That is, the uncertainty due to the $p_3\gamma_1$ subtraction will be equal to $A_4 \frac{\sqrt{A_1 + A_2}}{A_1 + A_2} = \frac{A_4}{\sqrt{A_1 + A_2}}$

In summary, the errors σ introduced by spectrum stripping into the $\theta = 0^\circ$ point of the $p_3\gamma_1$ and $p_3\gamma_2$ angular distributions by spectrum stripping were:

$$\sigma_{p_3\gamma_1}(\theta = 0^\circ) = \pm \left(\sqrt{A_3} + \frac{A_4}{\sqrt{A_1 + A_2}}\right)$$

$$\sigma_{p_3\gamma_2}(\theta = 0^\circ) = \pm \sqrt{A_1 + A_2}$$

Similar reasoning was used in the assignment of $\sigma_{p_3\gamma_i}(\theta)$ for the other angles θ at which the double correlations were measured.

iii.) CALCULATION OF ERRORS IN THE DOUBLE ANGULAR DISTRIBUTION COEFFICIENTS (b_n)

The measured $p_3\gamma_i$ distributions were fitted to functions of the form

$W_{\gamma_i}(\theta_i) = \sum_n b_n(\gamma_i) P_n(\cos\theta_i)$ in Chapter V. The errors in the coefficients $b_n(\gamma_i)$ were calculated using the statistical errors $\sigma_{p_3\gamma_i}(\theta)$ in each point θ as defined in ii.) (a) and (b). That is

$$\sigma_{p_3\gamma_1}(\theta) = \pm\left(\sqrt{A_3(\theta)} + \frac{A_4(\theta)}{\sqrt{A_1(\theta) + A_2(\theta)}}\right)$$

$$\sigma_{p_3\gamma_2}(\theta) = \pm\sqrt{A_1(\theta) + A_2(\theta)}$$

$$\sigma_{p_3\gamma_3}(\theta) = \pm\sqrt{N(\theta)}$$

$N(\theta)$ = number of counts at angle θ in the $p_3\gamma_3$ correlation measurements.

To the calculated errors in the $b_n(\gamma_i)$'s, based on these statistical errors (for calculation see Appendix II), were added the errors outlined in i.) (a), (b), (c) and ii.) (b) 1 which are expected to produce systematic fluctuations in the b_n's.

iv.) ERRORS IN THE TRIPLE CORRELATION MEASUREMENT

The errors outlined in i.) apply to the triple correlation as well as the double correlation measurements. The only additional error involved in this measurement result from the background count rate subtraction outlined in Appendix I. The random background amounted to about 25% of the total triple coincidence counts N(P) at each point P. The statistical uncertainty $\sigma_{N'(P)}$ in the actual number of triple coincidence counts N'(P) (i.e. with randoms subtracted) was

$$\sigma_{N'(P)} = \pm\sqrt{N(P)}$$

Typically

N(P) = 200 counts

N'(P) = 150 counts

randoms = 50 counts

and

$$\frac{\sigma_{N'(P)}}{N'(P)} \cong 10\%$$

The total error in each triple coincidence measurement was taken to be equal to this error since the errors from i.) are negligible when compared with the statistical error $\sigma_{N'(P)}$ (typically 10%).

CHAPTER V

ANALYSIS OF CORRELATION RESULTS

The double and triple correlation measurements made between protons (p_3) populating the 5.03 Mev level in B^{11} and gamma rays γ_1, γ_2 and γ_3 from the decay of this state are outlined in Chapter IV along with the results of these measurements. These results are analysed in this chapter in terms of the correlation theory developed in Chapter II.

A.) METHOD OF FITTING CORRELATION RESULTS TO THEORY

One conclusion can be drawn immediately from inspection of the $p_3\gamma_3$ angular distributions and that is that since there is a non-isotropic angular distribution from the decay of the 5.03 Mev state, therefore $J \neq \frac{1}{2}$. A more detailed analysis of the results is necessary before further statements can be made of the spins of the levels concerned.

The results of the $p_3\gamma_i$ ($i = 1$, 2 and 3) double correlation measurements $W_{E_j}(\gamma_i\theta_{ij})$ appear in Tables 4. and 5. for each angle θ_{ij} at which W_{E_j} was measured. The theoretical expression for the double correlation function, expressed in terms of the spin JJ_I, the multipole mixing ratios x_i and the tensor parameters a_n, was:

$$W_{T_j}(\gamma_i\theta_{ij}JJ_Ix_ia_n) = W_i(JJ_Ix_i\theta_{ij}) \quad \text{(Chapter II Part C.)}$$
$$= \sum_n a_nB_n(JJ_Ix_i)\,P_n(\cos\theta_{ij})$$

For the triple correlation measurements, the experimental results, and the theoretical correlation functions were (when the two gamma counters were at angles θ_{1j}, θ_{2j}, ϕ_j) $W_{E_j}(\theta_{1j}\theta_{2j}\phi_j)$ - (listed in Table 6.)

and

$$W_{T_j}(JJ_Ix_1x_2a_n\theta_{1j}\theta_{2j}\phi_j) = \sum_{kKMN} a_k A'^N_{KM}(JJ_Ix_1x_2k)X^N_{KM}(\theta_{1j}\theta_{2j}\phi_j) \text{-(See Chapter II Part D.)}$$

The Maximum Likelihood estimates ($\bar{J}$, $\bar{J}_I$, $\bar{a}_n$, $\bar{x}_i$) of the values of the

parameters J, J_I, x_i, a_n were those values which maximized the likelihood function L,

$$L(W_{E_j}\sigma_{E_j}JJ_Ia_nx_i) = \prod_{j=1}^{N} f_j(W_{E_j}\sigma_{E_j}JJ_Ia_nx_i)P(JJ_I)P(a_n)f^{w}(x_i)$$

with respect to the variables J, J_I, a_n, x_i. $f(W_{E_j}\sigma_{E_j}\bar{J}\bar{J}_I\bar{a}_n\bar{x}_i)$ is the normalized distribution function describing the probability of obtaining the measured value of W_{E_j} at the angular positions $\theta_{ij}\phi_j$(for the N different sets of angular orientations) if the true value of W was that obtained by equating the set (J, J_I, a_n, x_i) to the set $(\bar{J}, \bar{J}_I, \bar{a}_n, \bar{x}_i)$ and if the measured value of W_{E_j} had an error σ_{E_j} associated with it. If we assume that the errors are distributed in a Gaussian fashion, with variances σ_{E_j}, then

$$f_j = \frac{1}{2\pi\sigma_{E_j}} \exp\frac{-(W_{E_j} - W_{T_j})^2}{2\,\sigma_{E_j}^{\,2}}$$

The functions $P(JJ_I)$, $P(a_n)$ and $f^{w}(x_i)$ are probability functions introduced to take account of previous knowledge of the probabilities that given values of these variables should occur.

$$P(JJ_I) = 1 \qquad \left.\begin{array}{l} \frac{1}{2} \leqslant J \leqslant \frac{9}{2} \\ \frac{1}{2} \leqslant J_I \leqslant \frac{7}{2} \end{array}\right\} \text{Follows from Chapter II Part F.)}$$

$= 0$ for all other values of JJ_I

$P(a_n) = 0$ if the value of a_n predicts a negative (unphysical) diagonal density matrix element.

$= 1$ otherwise.

Two methods of dealing with the probability $f^{w}(x_i)$ have been used in this chapter. The first was to assume that all values of x_i are equally probable. (This is not consistent with the experimental evidence (Wilkinson 16.) regarding

relative probabilities for M1 and E2 transitions, but is in accord with the desire to try and make a spin assignment without recourse to arguments involving transition probabilities). Allowing x_i to take any value leads to the problem of having to solve sets of non-linear equations. The equations were linearized by assuming all the x_i's were small compared with unity (which is a physically realistic assumption) and then solved. The x_i's so obtained were in fact small enough to justify the original assumption. It turned out that this method gave rise to five sets of spins JJ_I which could not be rejected on the basis of the χ^2 test (see Part D.). However, all but one of these spin assignments require values of x_i which are considerably larger than those expected on the basis of the observed ratios of M1 and E2 transition probabilities. The second method (Part E.) uses values of $f''(x_i)$ estimated as described in Appendix IV. The result of including these probabilities in the Maximum Likelihood calculation is that only one spin assignment then remains.

The evaluation of $\overline{x_i}$ and $\overline{a_n}$ for each set of JJ_I allowed by $P(JJ_I)$ as outlined above would be an extremely tedious calculation but is in principle possible. However, the evaluation of the maximum L was simplified by factoring L into two sections, one corresponding to the frequency functions for the three double correlation measurements and the other corresponding to the frequency functions of the triple correlation measurements. (At this point it is assumed that $P(a_n) = 1$ for all a_n and $P(x_i) = 1$ for all x_i. The correct form for $P(a_n)$ will be introduced in Part D.), and for $P(x_i)$ in Part F.)

$$L = L' \cdot L''$$

where

$$L' = \prod_{j=1}^{N'} f_j(W_{E_j} \sigma_{E_j} JJ_I a_n x_i)$$

$$L'' = \prod_{j=N'}^{N} f'_j(W'_{E_j} \sigma'_{E_j} JJ_I a_n x_i)$$

$N' =$ number of double correlation measurements (W_{E_j})

$N - N' =$ number of triple correlation measurements (W'_{E_j})

The reason for factoring L in this way is that experimentally the errors in the measured distributions were much smaller for the double correlations than for the triple correlation (i.e. $\sigma_{E_j} \ll \sigma'_{E_j}$) therefore the point of maximum likelihood was to a first approximation independent of the triple correlation measurement. The procedure used in the analysis was to maximize L' (Part B.) then calculate the second order effects of W'_{E_j} (triple correlation measurements) on L (Part D.).

B.) DOUBLE CORRELATION ANALYSIS

The experimentally measured points $W_E(\theta_j)$ of the double correlation function (Chapter IV Part A.) were least square fitted to functions of the form

$$W_E(\theta) = \sum_n b_n(\gamma_i)P_n(\cos\theta) \qquad n = 0,2,4 \text{ (Chapter II)}$$

and the normalized $b_n(\gamma_i)$ coefficients and the errors in these coefficients (as calculated in Appendix II) were found to be:

$$b_0(\gamma_i) = 1 \text{ (normalization)}$$

$$b_2(\gamma_1) = 0.38 \pm 0.07 \qquad b_2(\gamma_2) = 0.00 \pm 0.06$$

$$b_4(\gamma_2) = 0.06 \pm 0.09 \qquad b_4(\gamma_2) = 0.13 \pm 0.12$$

$$b_2(\gamma_3) = -0.18 \pm 0.03$$

$$b_4(\ _3) = 0.04 \pm 0.05.$$

Figures 18., 19. and 20. show the experimental points and the least squares fitted curves for the $p_3\gamma_i$ distributions.

The theoretical correlation functions (Chapter II) have the form (for a particular choice of JJ_I)

$$W_T(\theta) = W_{\gamma_i}(\theta) = \sum_n a_n B_n(JJ_I x_i)P_n(\cos\theta)$$

The maximum L' estimate of the a_i and x_i for a given JJ_I are those

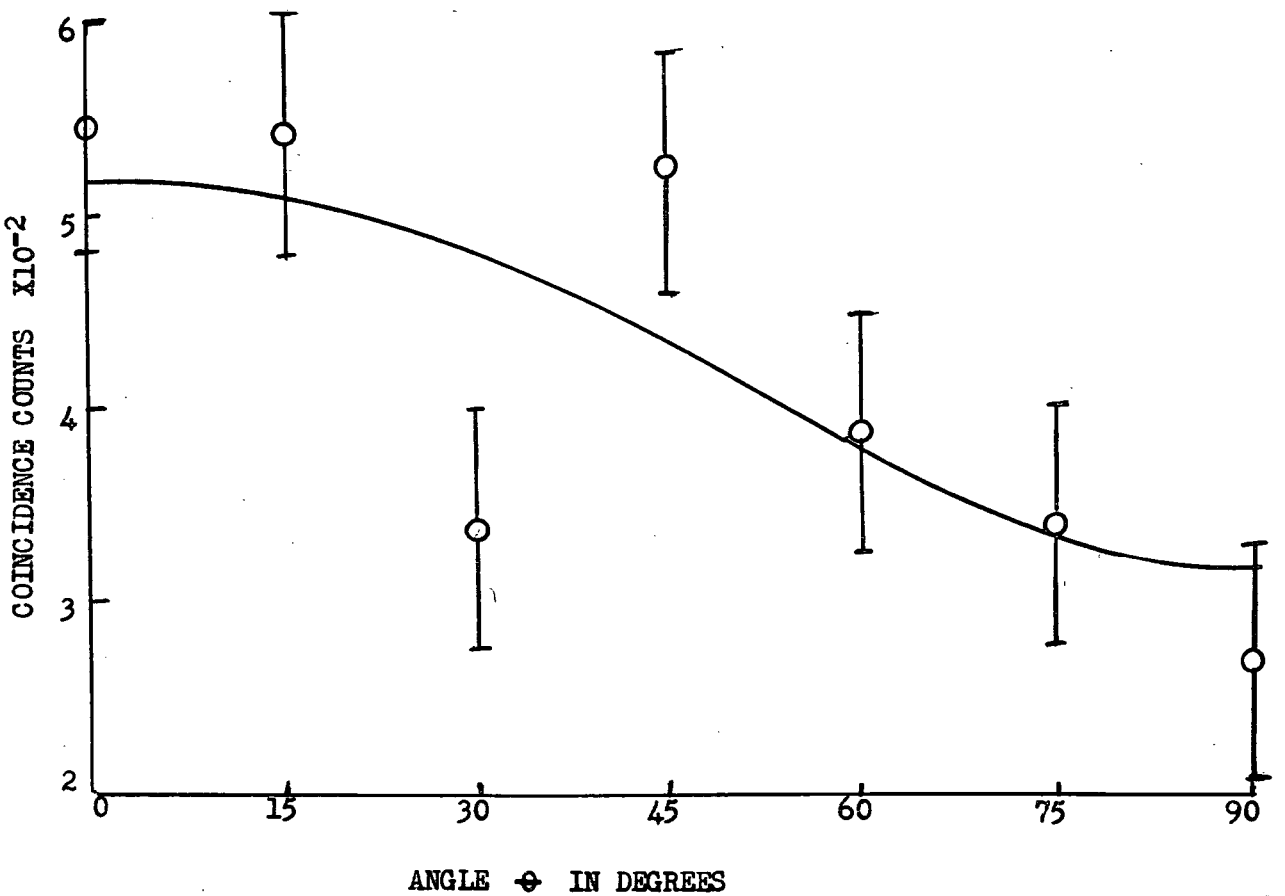

FIGURE 18. $p_3 \gamma_1$ ANGULAR DISTRIBUTION

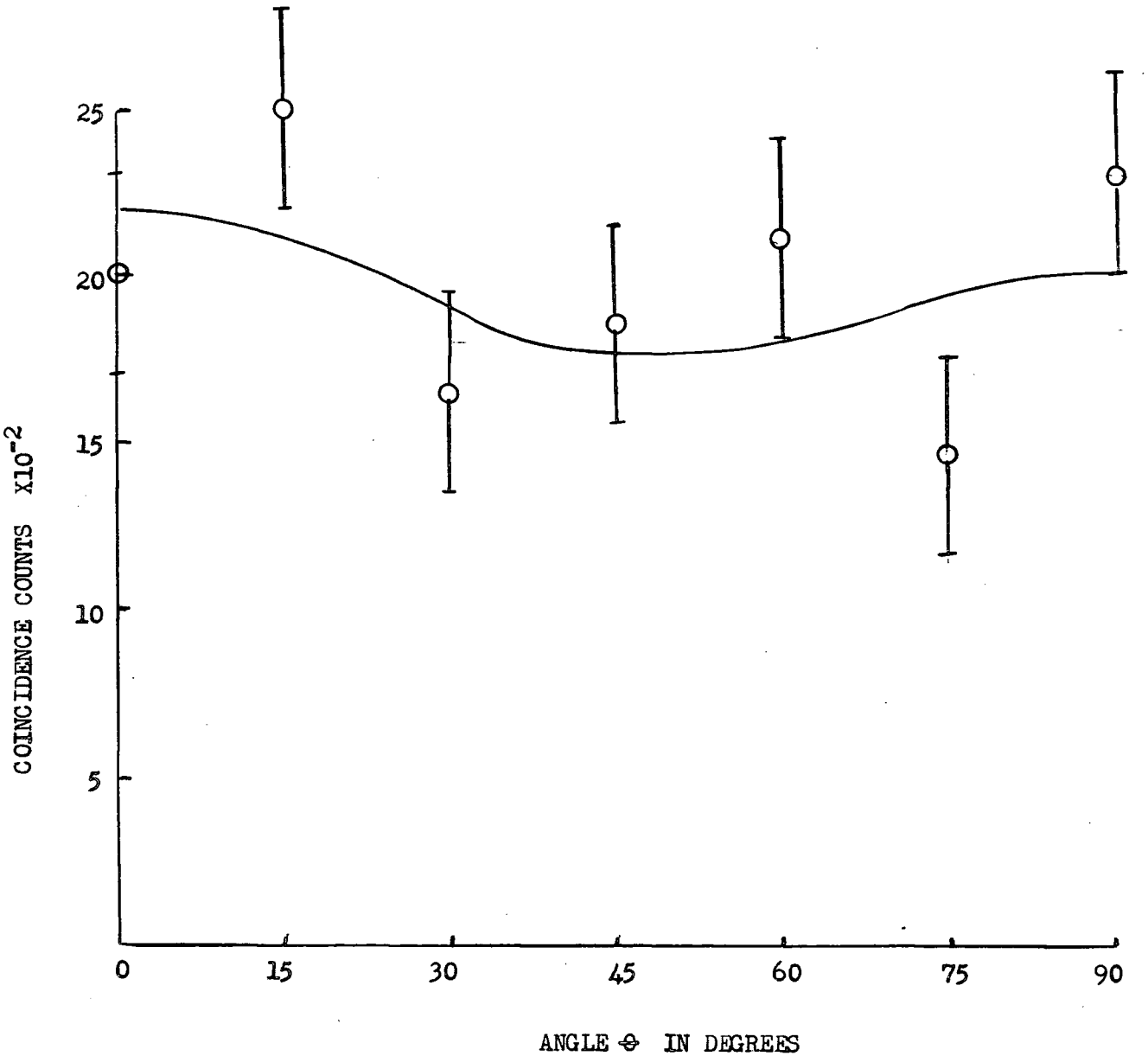

FIGURE 19. $p_3\gamma_2$ ANGULAR DISTRIBUTION

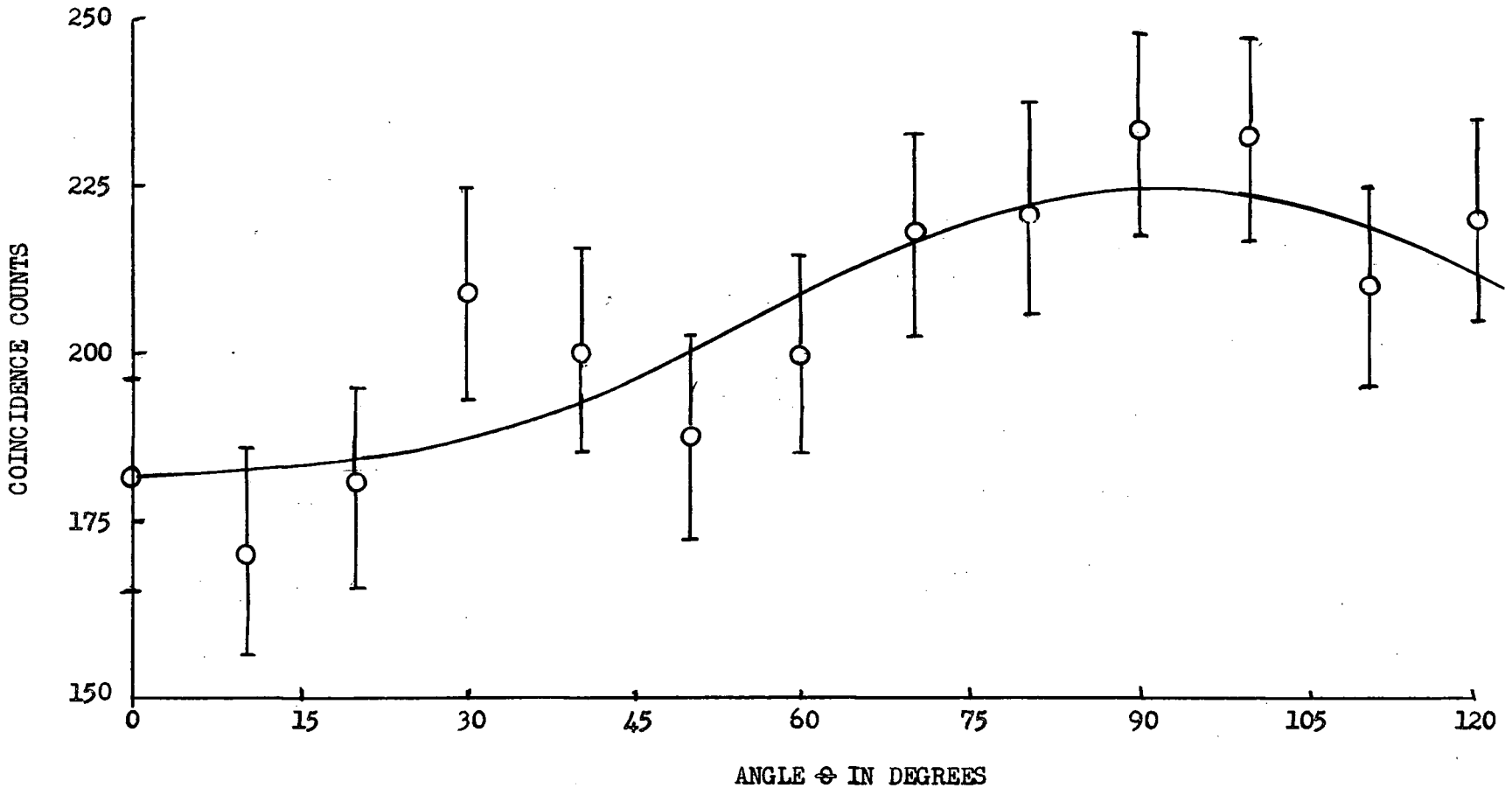

FIGURE 20. $p_3\gamma_3$ ANGULAR DISTRIBUTION

values which maximize

$$L' = \prod_{j=1}^{N'} f_j(W_{E_j} \sigma_{E_j} JJ_I a_n x_i)$$

If the form of f (described in Part A.) is substituted into L', the maximum L' estimate leads to the Least Squares estimate of the a_n and x_i. That is $\bar{a}_n$ and $\bar{x}_i$ minimize S where

$$S = \sum_{j=1}^{N'} \frac{(W_{E_j} - W_{T_j})^2}{\sigma_j^2}$$

The values of $\bar{a}_n$ and $\bar{x}_i$ were derived from the values of the b_n's for the following three cases.

a.) Those assignments of J and J_I which gave rise to a number of unknowns (a_n and x_i) which exactly equalled the number of equations available to determine them.

b.) Those assignments of J and J_I which gave rise to a number of unknowns which was more than the number of equations.

c.) Those assignments of J and J_I which gave rise to a number of unknowns which was less than the number of equations.

For the first two classes the maximum L' requirement is satisfied by the following equation:

$$\frac{a_n B_n(JJ_I x_i)}{a_0 B_0} = \frac{b_n(\chi_i)}{b_0} \qquad (1)$$

In the first case equation (1) gives a definite set of values for $\bar{a}_n$ and $\bar{x}_i$, the second case gives relations between the $\bar{a}_n$ and $\bar{x}_i$, which are used in the treatment of the triple correlation, to get values of $\bar{a}_n$ and $\bar{x}_i$.

In the third class the maximum L' values of a_n and x_i could not be derived from the system of equations (1) since the $\bar{a}_n$ and $\bar{x}_i$ values were overdetermined. In principle the values of $\bar{a}_n$ and $\bar{x}_i$ for various JJ_I assignments could be obtained by maximizing L' with respect to the a_n and

x_i, one would then accept or reject these assignments on the basis of a χ^2 test. It was possible however for these cases to reject all these assignments by dividing the sets of equations (1) into subsets (each falling into class a.) and then checking for consistency (to within experimental error) between the various values of $\bar{a}_n$ and $\bar{x}_i$ derived from these subsets. Each subset of equations represented on independent determination of the unknowns a_n and x_i, therefore as an example if the results of calculating a_n from subset 1 was $\bar{a}_{n1} \pm \sigma(a1)$ and subset 2 was $\bar{a}_{n2} \pm \sigma(a2)$, the assignment was rejected if $|a_{n2} - a_{n1}| \geqslant 2\left[\sigma(a2) + \sigma(n1)\right]$

It was found that five values of JJ_I fell into class a.) and only the assignment $JJ_I = \frac{3}{2}\frac{1}{2}$ fell into class b.); these assignments are listed in Table 7. along with the maximum L' estimate of $x_2(\bar{x}_2)$. In some cases two values of $\bar{x}_2$ were allowed and in these cases the smallest value of $\bar{x}_2$ was chosen. The reason for choosing this value is outlined in Section D.) of this chapter.

The values of the maximum L' for the six JJ_I's listed in Table 7. are all equal, therefore any further differentiation between the JJ_I's as to which is the best assignment must come from the inclusion of the triple correlation measurements into the likelihood function.

C.) TRIPLE CORRELATION ANALYSIS

The values of $\bar{x}_i$ and $\frac{\bar{a}_n}{a_0}$, which maximized L' for each of the six remaining possible values of JJ_I were related to $\frac{a_2}{a_0}$ by equations of the form:

$$\bar{x}_i = \bar{x}_i\left(\frac{\bar{a}_2}{a_0}\right)$$

$$\frac{\bar{a}_4}{a_0} = \frac{\bar{a}_4}{a_0}\left(\frac{\bar{a}_2}{a_0}\right)$$

These equations were substituted into L" then L" was maximized with respect to $\frac{\bar{a}_2}{a_0}$

TABLE 7.

DOUBLE CORRELATION

$J\ J_I$	$\bar{x}_2$
$\frac{3}{2}\ \frac{1}{2}$	N.I.*
$\frac{3}{2}\ \frac{3}{2}$	0.26 ± 0.18
$\frac{3}{2}\ \frac{5}{2}$	-0.20 ± 0.05
$\frac{5}{2}\ \frac{1}{2}$	N.I.
$\frac{5}{2}\ \frac{3}{2}$	0.26 ± 0.05
$\frac{5}{2}\ \frac{5}{2}$	0.20 ± 0.05

*N.I. means no information was gained from the experiment on these parameters.

$$L'' = \prod_{j=N'}^{N} f'_j(W'_{E_j} \sigma'_{E_i} JJ_I \frac{\bar{a}_2}{\bar{a}_0})$$

and
$$\frac{\partial L''}{\partial \frac{a_2}{a_0}} = 0$$

Then with the resulting values of $\frac{\bar{a}_2}{\bar{a}_0}$ the values of $\bar{x}_i$ were determined. Table 8. lists the parameter estimates $\frac{\bar{a}_n}{\bar{a}_0}$ and $\bar{x}_i$ opposite each of the six remaining choices of JJ_I.

D.) DISCUSSION OF RESULTS

On the basis of the three double correlation measurements $(p_3 \gamma_i)$ and the assumptions outlined in Chapter II, it has been possible in the previous sections of this chapter to limit the spin assignments for the 5.03 (J) and 2.14 (J_I) Mev states to the six values listed in Table 8. The χ^2's (Hoel 29.) for the fit of the experimental results to the theoretical triple correlation functions W_T(Triple) obtained for each set of parameters $(J, J_I, \bar{a}_n, \bar{x}_i)$ were calculated and are listed in Table 8. opposite the six possible choices of JJ_I. The only assignment which might be rejected on the basis of its χ^2 value is $\frac{3}{2}\frac{5}{2}$ ($\chi^2 = 10$). The probability of this value of χ^2 or larger occuring is approximately 0.03 if $\frac{3}{2}\frac{5}{2}$ is the correct assignment. The remaining possible values of JJ_I have a χ^2 assignment of three which corresponds to the most probably value (the probability of a value of $\chi^2 = 3$ or larger occuring is 0.60).

The values of the parameters $\frac{a_n}{a_0}$ which were also determined in the experiment have not as yet been discussed and, without referring to any reaction theory, there is no way of knowing if the values found are reasonable. However, there is one requirement on the values of $\frac{a_n}{a_0}$ and that is that they must predict a density matrix which has positive values for all diagonal elements (i.e. population parameters). The tensor parameters for

TABLE 8.

SUMMARY OF CORRELATION ANALYSIS

J	J_I	$\bar{x}_1$	$P(\bar{x}_1)$	$\bar{x}_2$	$P(\bar{x}_2)$	$\bar{x}_3$	$P(\bar{x}_3)$	$\frac{\bar{a}_2}{a_0}$	$\frac{\bar{a}_4}{a_0}$	χ^2	$\frac{P(\chi^2)}{P(\chi^2)_{max}}$	$P'(JJ_I)$	$\frac{P'(JJ_I)}{P'(\frac{3}{2}\frac{1}{2})}$
$\frac{3}{2}$	$\frac{1}{2}$	N.I.	0.60	N.I.	0.85	N.I.	0.75	N.I.		3	1	0.38	1
$\frac{3}{2}$	$\frac{3}{2}$	0.00	0.30	0.26	0.02	0.37	0.05	-1.0		3	1	$3\ 10^{-4}$	10^{-3}
$\frac{3}{2}$	$\frac{5}{2}$	-0.21	0.10	-0.20	0.03	0.21	0.08	-1.5		10	0.15	$3.6\ 10^{-5}$	10^{-4}
$\frac{5}{2}$	$\frac{1}{2}$			N.I.	0.85	-0.19	0.10	-7.1	-0.1	3	1		
$\frac{5}{2}$	$\frac{3}{2}$	-0.16	0.20	0.26	0.02	0.18	0.13	0.5	0.0	3	1	$5.2\ 10^{-4}$	$1.3\ 10^{-3}$
$\frac{5}{2}$	$\frac{5}{2}$	0.00	0.30	-0.20	0.03	0.28	0.07	-0.9	0.0	3	1	$6.3\ 10^{-4}$	$1.5\ 10^{-3}$

N.I. means that no information on the absolute values of these parameters was gained from these experiments. $P(\bar{x}_i)$ in this case is chosen as the value corresponding to the most probable value of x_i.

The places which are left blank in the table correspond to instances where the parameter is not present in the formalism.

$JJ_I = \frac{5}{2}\frac{1}{2}$ were corrected for the finite solid angle of the gamma counters (refer to Appendix III) and found to be

$$\frac{\bar{a}_2}{a_0} = -7.6$$

$$\frac{\bar{a}_4}{a_0} = -0.15$$

These values were then substituted into the equation relating the density matrix and statistical tensors (Chapter II Part B.) and it was found that the population parameter for the $m = \frac{5}{2}$ magnetic substate was negative. Since this does not correspond to any realistic physical situation, this assignment was rejected, that is $P(\frac{a_2}{a_0} = -7.6) = 0$. No similar inconsistences were found for the remaining five assignments.

On the basis of the expermental evidence presented so far the possible values of JJ_I have been reduced from sixteen to a maximum of five possible assignments with one assignment $(\frac{3}{2}\frac{5}{2})$ being approximately seven times less probable than the other four. To determine which of the JJ_I's is the most probable assignment further experimental information must be introduced. In Part F.) suggestions are made as to further experimental investigations which can be made to absolutely determine JJ_I and in Part E.) arguments based on previous measurements of transition probabilities and lifetimes are introduced to weight the possible JJ_I assignments by the known probabilities of getting values of x_i as large as those needed to maximize L (refer to Table 8.).

E.) CONCLUSIONS ON SPIN ASSIGNMENT BASED ON MULTIPOLE MIXTURE PROBABILITIES

Wilkinson 16.) has compiled the experimental data on the lifetimes τ and radiation widths Γ of M1 and E2 transitions in light nuclei ($A < 20$) and has compared this data with the theoretical estimates as calculated using the Weisskopf extreme single particle model. From this data the frequency functions of $\Gamma M1$, $\Gamma E2$ and x_i^2 (where $x_i^2 = \frac{\Gamma_i\ M1}{\Gamma_i\ E2}$) were estimated using the

method outlined in Appendix IV. The probabilities of particular values of x_i arising were incorporated into the Likelihood estimates of $\bar{a}_n$ and $\bar{x}_i$ in Part A.).

$$L = L'''(W_{E_j}\sigma_{E_j} JJ_I a_n x_i) f''(x_i)$$

where

$$L''' = \prod_{j=1}^{N} f_j(W_{E_j}\sigma_{E_j} JJ_I a_n x_i) P(JJ_I) P(a_n)$$

In the preceeding sections L''' was maximized under the assumption $f''(x_i) = 1$ for all values of x_i. However, the effect of $f''(x_i)$ on the maximum L must be considered if $f''(x_i)$ is not equal to a constant. The maximum of L under this condition is more easily determined by evaluating the maximum in W where W = ln L

$$W = \ln L = \ln f''(x_i) + \ln L'''$$

Only the equations maximizing W with respect to the x_i's will change from those used to maximize L''';

$$\frac{\partial W}{\partial x_i} = 0 = f(x_i)^{-1} \frac{\partial f''(x_i)}{\partial x_i} + \frac{\partial L'''}{\partial x_i}$$

The remaining equations were unaffected by the inclusion of $f''(x_i)$ since

$$\frac{\partial f'(x_i)}{\partial a_n} = 0$$

The new term $\left[f''(x_i)\right]^{-1} \frac{\partial f''(x_i)}{\partial x_i}$ introduced into the above equations was small compared to the second term $\left[\text{since } L''' = C \exp{-W(a_n x_i)}\right]$ as long as $\frac{\partial f''}{\partial x_i}$ was small. The condition was satisfied by the particular form of $f''(x_i)$ derived in Appendix IV. The other condition in which the new term became large was when $f''(x_i)$ was small, but this corresponded to a minimum in L and this solution was ignored.

We were then justified in ignoring the effect of $f''(x_i)$ on the estimates of the maximum likelihood values $\bar{a}_n$ and $\bar{x}_i$. This means that the esti-

mates derived in the previous section are unchanged to any extent by the inclusion of $f''(x_i)$ in the Likel hood function. Of course, $f''(x_i)$ does have a very important effect in estimating the relative probabilities to be associated with each spin assignment JJ_I. These probabilities now become

$$P'(JJ_I) = \frac{P(\chi^2)\ JJ_I}{P(\chi^2)\ max} \prod_i P(x_i)$$

where $\frac{P(\chi^2)\ JJ_I}{P(\chi^2)\ max}$ = the ratio of (the probability of getting this value χ^2) to (the probability of getting the most probable value of χ^2)

$P(x_i)$ = probability of getting a value of $|x_i|$ in the range $|x_i \pm \Delta x_i|$ the magnitude of Δx_i is chosen small (0.05) compared with 1; its actual magnitude is not significant sincethe quantities of interest in Table 8. are ratios of probabilities $\frac{P'(J\ J_I)}{P'(\frac{3}{2}\ \frac{1}{2})}$

The probabilities $P(x_i)$ for each value of JJ_I, calculated as outlined in Appendix IV, are listed in Table 8. along with $\frac{P(\chi^2)\ JJ_I}{P(\chi^2)\ max}$ and $P(JJ_I)$.

The assignment of $JJ_I = \frac{3}{2}\frac{1}{2}$ was found to have a value of $P'(JJ_I)$ a factor of 1000 larger than any other assignment, and is therefore at least one thousand times more probable than any of the other four possibilities.

The tensor parameter ratio $\frac{a_2}{a_0}$ for the 5.03 Mev level was not determined for the spin assignment $JJ_I = \frac{3}{2}\frac{1}{2}$ if any arbitrary value of multipole mixing was allowed (any value of x_i's). However on the basis of previous experiments it is apparent that the value of the mixing parameters (See Appendix IV for most probable values of x_i) should be quite small and in

creasing both the efficiency of the counting system and the experimental running time. With the system as it is it would require approximately 10^3 hours of running time to acquire sufficient statistics on the triple correlation function to differentiate between the five possible spin assignments. If the size of the NaI crystals used were increased from the present 2" X 2" to 5" X 4", the improvement in counting efficiency of each gamma counter could be increased by a factor of seven producing a total rise in efficiency of approximately fifty. Under these conditions the required statistics could be gathered in approximately twenty running hours.

ii.) EXPERIMENT TO DETERMINE MULTIPOLE MIXING

G.J. McCallum 20.) describes a technique for measuring the linear polarization of the gamma rays from which the multipole mixing ratio can be determined. As he points out this method is particularly applicable to the situation outlined in this thesis. A rough calculation of the counting rate expected for such a measurement using the same experimental arrangement as McCallum's and reaction rates similar to those encountered in this experiment indicates a running time of ten hours to get statistics good enough to determine the multipole mixing ratios. When used in conjunction with the data from the correlation measurements outlined in this thesis, the multipole mixing ratio should determine the values of J and J_I absolutely.

CHAPTER VI

COMPARISON OF RESULTS WITH THEORY

In this chapter the spin assignments made in Chapter V are compared with those predicted by the Independent Particle Model (Part A.). The present assignments agree with those made by previous workers. In Part B.) the relative populations of the magnetic substates of the 5.03 Mev level as measured in Chapter V are compared with those calculated assuming the Butler Plane Wave (B.P.W.) stripping mechanism and Distorted Wave Born approximation (D.W.B.).

A.) COMPARISON OF SPIN ASSIGNMENTS WITH THE INDEPENDENT PARTICLE MODEL PREDICTIONS

The experimentally determined level scheme for the ground and first three excited states of B^{11}, including the results in this thesis, has the following appearance. (For the spin assignment to the ground and second excited state see Lauritsen et al 21.)

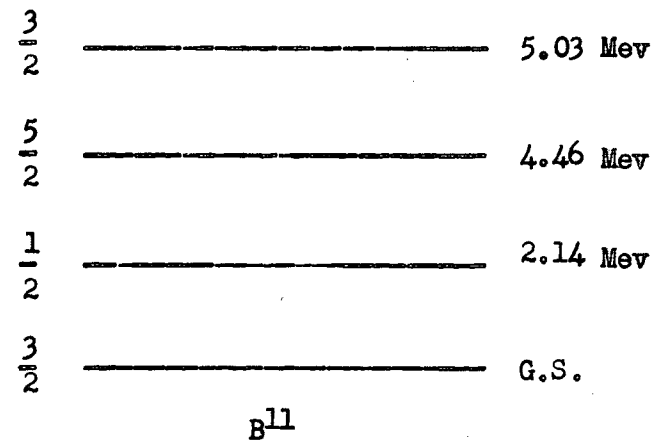

Using the Independent Particle Model Cohen and Kurath 22.) have calculated the level scheme for B^{11} using firstly the Intermediate Coupling Model (Inglis 23.) and secondly the many parameter Two-Body Matrix Element Model. Cohen and Kurath show that both models give good agreement between the experimental level scheme and theory.

B.) CALCULATION OF THE DENSITY MATRIX FOR THE 5.03 Mev LEVEL AND COMPARISON WITH STRIPPING THEORY

The ratio of the tensor parameters for the 5.03 Mev level in B^{11} populated by the $B^{10}(dp)B^{11}$ reaction was determined in Chapter V Part F.) on the basis of the reasonable assumption that the $|x_1|$'s were less than 0.05. The value of the ratio (of the attenuated tensor parameters, see Appendix III) was found to be:

$$\frac{a_2}{a_0} = 0.53 \pm 0.07$$

The solid angle corrected ratio of tensor parameters $\frac{R_{20}}{R_{00}}$ is calculated in Appendix III to be:

$$\frac{R_{20}}{R_{00}} = 0.59 \pm 0.07$$

The equation relating these tensor parameters to the density matrix ρ was shown in Chapter II to have the form:

$$\rho^{m\,m'}_{J\,J} = \sum_{Kk} (-1)^{J-m'} (JJm-m' | Kk) R_{Kk}(JJ)$$

Using this equation the density matrix corresponding to the observed ratio of the tensor parameters $\frac{R_{20}}{R_{00}}$ may be calculated. Since only the R_{Kk}, $k=0$ and K even are non-zero (Refer to Chapter II) ρ is diagonal and symmetric and there are only two independent non-zero matrix elements.

$$\rho^{\frac{1}{2}\,\frac{1}{2}}_{\frac{3}{2}\,\frac{3}{2}} = \rho^{-\frac{1}{2}\,-\frac{1}{2}}_{\frac{3}{2}\,\frac{3}{2}} = (-1)\left[-\frac{1}{2}+\frac{1}{2}(0.59)\right] R_{00} = 0.21\, R_{00}.$$

$$\rho^{\frac{3}{2}\,\frac{3}{2}}_{\frac{3}{2}\,\frac{3}{2}} = \rho^{-\frac{3}{2}\,-\frac{3}{2}}_{\frac{3}{2}\,\frac{3}{2}} = \left[\frac{1}{2}+\frac{1}{2}(0.59)\right] R_{00} = 0.79\, R_{00}.$$

The normalization of the wavefunction describing this state requires

TRACE $\rho = 1$ (Sharp 24.) which when applied to this density matrix gives $R_{00} = \frac{1}{2}$. The density matrix then takes the form:

$$\rho^{m\,m'}_{\frac{3}{2}\,\frac{3}{2}} = \begin{pmatrix} 0.40 & & & 0 \\ & 0.10 & & \\ & & 0.10 & \\ 0 & & & 0.40 \end{pmatrix}$$

The diagonal elements of the density matrix $\rho^{m\,m}_{J\,J}$ (Refer to Chapter II Part B.) represent the probability of finding the state ψ_J in the particular magnetic substate ψ_{Jm} (m = projection of J on the quantization axis which in this case corresponds to the incident deuteron beam direction.). It is seen then that in the $B^{10}(dp)B^{11}$ reaction leading to the 5.03 Mev level the $m = \frac{3}{2}$ states are more favourably populated than the $m = \frac{1}{2}$ states by a factor of four.

It is now of interest to enquire how the states would be populated if some particular nuclear reaction mechanism is postulated. The $B^{10}(dp)B^{11}$ reaction has been studied at a deuteron bombarding energy of 2 Mev (Marion et al 25.) and the protons (p_3) populating the 5.03 Mev level were found to exhibit a very well developed stripping peak, that is, the proton angular distribution with respect to the deuteron beam showed a strong peak at 25°. It is reasonable to expect that the application of stripping theory to this reaction should predict a density matrix similar to the one found experimentally. The simplest version of stripping theory and one which can be solved analytically is the Plane Wave Butler (P.W.B.) theory.

To apply P.W.B. stripping theory to the dp reaction, the deuteron is considered as a very loosely bound proton - neutron system. When the deuteron is incident on the target nucleus X the neutron is captured into the target nucleus producing the resultant nucleus Y and the proton continues on past without reacting strongly with either X or Y. These assumptions are

formulated specifically by first writing the complete Schroedinger equation for the system as:

$$(H_x + T_p + T_n + V_{xp} + V_{xn} + V_{np})\psi(r_n\, r_p\, \vec{\xi}) = \psi\, E$$

and then introducing the P.W.B. approximation by deleting various terms from the Hamiltonian.

In this equation:

H_x = Hamiltonian for the target nucleus in the laboratory system.

T_a = Kinetic energy of nucleon (a) in the laboratory system.

V_{ij} = interaction potential between particles i and j.

ξ = internal coordinates of the target.

r_p = proton spatial coordinates.

r_n = neutron spatial coordinates.

The first approximation used for plane wave Butler stripping is to set $V_{xp} = 0$ (the proton does not interact with the target nucleus). Secondly $V_{np} = 0$ when neutron n is within the boundary of the target nucleus. The final major assumption and approximation is that the only part of the total wavefunction ψ which is considered to contribute significantly to the matrix element is the incident plane wave deuteron wavefunction. A more complete description of the assumptions made in P.W.B. calculations may be found in Butler 26.)

Satchler 27.) has calculated the theoretical statistical tensors $R'_{Kk}(JJ)$ assuming P.W.B. stripping theory. Quantities proportional to the statistical tensors appear in this article labeled η_K (See equation 2 Reference 27.) In this article he showed that using P.W.B. stripping assumptions the capture process in dp stripping is formally the same as that of a plane wave neutron captured along the target nucleus recoil axis which in this

experiment corresponds to the -Z direction (i.e. the protons are detected in the Z direction and the target nuclei recoil in the -Z direction). The tensor parameters describing the state formed by this reaction are shown in Reference 27.) to be:

$R'_{Kk}(JJ) = 0 \qquad k \neq 0$

$R'_{K0}(JJ) \propto \eta_K(jjJ_iJ)$ where the constant of proportionality independent of K and k.

$j =$ total angular momentum of captured neutron

i.e. $\vec{j} = \vec{\ell} + \vec{s}_n = \frac{3}{2}$

$J_i =$ spin of initial nucleus

$=$ spin of $B^{10} = 3$

$J =$ spin of 5.03 Mev level $= \frac{3}{2}$

From Table 4 a.) Reference 27.)

$$\frac{R'_{20}(\frac{3}{2}\,\frac{3}{2})}{R'_{00}(\frac{3}{2}\,\frac{3}{2})} = \frac{\eta_2(\frac{3}{2}\,\frac{3}{2}\,3\,\frac{3}{2})}{\eta_0} = -0.200.$$

If now the actual experimental conditions are considered where the protons are detected in a finite solid angle ($\theta \leq 5^\circ$) instead of just at $\theta = 0^\circ$ and an average of the tensor parameters due to protons emitted at angles $0^a \leq \theta \leq 5^\circ$ is taken symmetrically about $\theta = 0^\circ$, it is expected that the cylindrical symmetry conditions on the resultant average R_{Kk}'s will be applicable and only two R_{k0}'s need be defined. This averaging process should cause the alignment to tend toward istropy but only by a small amount since the average is taken over only 5°. This tendancy toward isotropy when referred to the tensor parameter R_{20} means that R_{20} should tend toward zero, that is to be reduced in magnitude by a small amount. It will be assumed in the following that the tensor parameters resulting from protons being emitted at $\theta = 0^\circ$ are a good approximation to those that would result if an

average over θ up to 5° were taken and that this certainly is a good estimate of the upper limit of the R_{k0}'s resulting from this theoretical (P.W.B.) reaction.

Following the same procedure as with the experimental tensor parameters, the theoretical density matrix ρ' (P.W.B.) calculated from the Plane Wave Butler assumptions is found to take the form:

$$\rho'(\text{P.W.B.})^{m\,m'}_{\frac{3}{2}\,\frac{3}{2}} = \begin{pmatrix} 0.2 & & & 0 \\ & 0.3 & & \\ & & 0.3 & \\ 0 & & & 0.2 \end{pmatrix}$$

That is, plane wave stripping theory predicts that the $m = \frac{1}{2}$ states should be more favourably populated than the $m = \frac{3}{2}$ states. This result may be interpreted from a semi-classical viewpoint by considering only those neutrons which are captured into the B^{10} nucleus with orbital angular momentum $\ell = 1$ and with their linear momentum in the -Z direction. This situation is arranged by selecting only those protons which come from dp reaction in the $+Z(\theta = 0^{\circ})$ direction (i.e. along the deuteron beam axis.). Using the definition of orbital angular momentum and the Law of Conservation of angular momentum, we now show that only $m = \frac{1}{2}$ states can be populated.

The law of the conservation of angular momentum states that:

$$\vec{J} = \vec{J}_i + \vec{\ell} + \vec{S}$$

Since $J = \frac{3}{2}$ and $J_i = 3$ the only way angular momentum can be conserved is for both $\vec{\ell}$ and $\vec{S}$ to be antiparallel to $\vec{J}_i$ (since $\vec{\ell} = 1$). But by definition ($\vec{\ell} \propto \vec{V} \times \vec{r}$), $\vec{\ell}$ is perpendicular to the direction of motion ($\vec{V}$) of the captured neutron and therefore $m_{\ell} = 0$, where m_{ℓ} is the projection of $\vec{\ell}$ on the Z axis. Also as was just pointed out only those nuclei with angular momentum $\vec{J}_i$ oriented antiparallel to $\vec{\ell}$ contribute to this reaction, therefore the projection of $\vec{J}_i$ on the Z axis must also be zero ($M_{J_i} = 0$). Only

the intrinsic spin of the neutron (S) may have a non-zero projection on the Z axis, and must take the values $m_s = \pm\frac{1}{2}$. The only magnetic substates of the 5.03 Mev level (spin J) which are populated have values

$$m = M_{J_i} + m_\ell + m_s = m_s = \pm\tfrac{1}{2}.$$

Based on this very restricted semiclassical model the density matrix for the 5.03 Mev level takes the form:

$$\rho(\text{semiclassical})\,{}^{m\ m'}_{\frac{3}{2}\ \frac{3}{2}} = \begin{pmatrix} 0 & & & 0 \\ & 0.5 & & \\ & & 0.5 & \\ 0 & & & 0 \end{pmatrix}$$

In quantum mechanical terms the question of which of the magnetic substates can be populated by the coupling scheme:

$$\vec{\ell} + \vec{S} = \vec{j}$$
$$\vec{j} + \vec{J}_i \quad \vec{J}$$

is equivalent to asking for what value of m is the product of the rector coupling coefficients:

$$(\ell S 0 m_s | j m_s)(j J_i m_s M_{J_i} | J m) - \text{non zero}$$

In this case we have

$$\ell = 1 \qquad J_i = 3$$
$$S = \frac{1}{2} \qquad J = \frac{3}{2}$$
$$j = \frac{3}{2}$$

By referring to my table of Clebsh-Gordon coefficients it can be seen that no value of m (final state magnetic quantum number) is excluded by this coupling scheme, however from the previous semiclassical argument one would expect that the $m = \frac{1}{2}$ states would be more favourably populated. This effect indeed occurs in the plane wave stripping calculation. It can be seen that the P.W.B. calculation of the alignment resulting from the dp reaction and that found experimentally do not agree either in magnitude or in sign, hence,

the need for a more accurate theory to describe this reaction is indicated. Such a theory has been developed and is referred to as the Distorted Wave Born Approximation. (D.W.B.)

The D.W.B. uses optical model elastic scattering wavefunctions in place of plane waves to represent the relative motion of the incident and target nuclei and of the outgoing residual nuclei, thereby approximating the effect of both the coulomb and nuclear forces on the incoming deuteron and outgoing proton. Also a spin-orbit interaction is sometimes introduced when calculations of the polarization of the resultant protons is made. (Newns and Refai 28.). Goldfarb 29.) has calculated, using the D.W.B., the tensor parameters of the state formed by the dp reaction where the protons are detected at zero degrees to the incident deuteron beam. He shows that the calculated tensor parameters are independent of the form of the optical potentials used and depend only on the spin orbit distorting potential in the following manner:

$$\frac{R_{k0}(\text{D.W.B.})}{R_{00}(\text{D.W.B.})} = \frac{R'_{k0}}{R'_{00}}\left[1 - \frac{4k(k+1)}{(2j-1)(2j+3)}\;\frac{\xi}{1+\xi}\right]$$

where R'_{k0} = Plane Wave Butler statistical tensors calculated previously

and where ξ is referred to as the spin distortion parameter and is positive and real. This factor arises from the D.W.B. formalism when a spin dependent effect is included in the distorting potential and is a measure of the ratio of the populations of the $m_h = \frac{3}{2}$ to $m_h = \frac{1}{2}$ spin states of the transferred neutron, which takes into the nucleus a total angular momentum j with magnetic quantum number m_h (m_h refers to the projection of j on the quantization axis which in this case corresponds to the deuteron beam direction.)
If no spin dependent distortion is included Goldfarb 29.) shows that

$$\xi = 0$$

By choosing values of ξ between zero and infinity (i.e. allowing any magnitude of spin distortion) the predicted value of the tensor parameter varies over the range

$$-\frac{R'_{k0}}{R'_{00}} \leqslant \frac{R_{k0}(\text{D.W.B.})}{R_{00}(\text{D.W.B.})} \leqslant \frac{R'_{k0}}{R'_{00}}$$

or, using the value of $\frac{R'_{k0}}{R'_{00}} = -0.20$ derived earlier.

$$-0.20 \leqslant \frac{R_{k0}\ (\text{D.W.B.})}{R_{00}\ (\text{D.W.B.})} \leqslant 0.20$$

Apparently the introduction of a spin dependence in the potential can change the sign of the tensor parameter ratio but no amount of distortion of the deuteron wave function, as introduced by D.W.B., can produce the required agreement between experiment and theory.

The inability of the D.W.B. to predict the correct tensor parameters is usually attributed to the interference of such reaction mechanisms as compound nucleus formation, heavy particle stripping and stripping associated with coulomb excitation.

APPENDIX 1

ANALYSIS OF THE RANDOM TRIPLE COINCIDENCE COUNT RATE

The random triple coincidence monitor (Slow Coincidence Circuit - See Chapter III, Part F.) was operated in parallel with the fast coincidence circuit to record the random coincidence and triple coincidence rates simultaneously. In order to measure the random coincidence rates with adequate precision, the resolving time in the random coincidence monitoring circuit was made larger, by a factor of ten, than the resolving time in the main coincidence circuit. This resulted in the random monitor counting many more random coincidences than those detected by the main coincidence circuit. There are three processes by which a triple coincidence event occurs in either coincidence circuit signifying a time overlap of the coincidence pulses. These occur when there is an :

1.) Overlap due to three uncorrelated events.

2.) Overlap due to two correlated ("true") and one uncorrelated event.

3.) Overlap due to a "true" triple coincidence.

The number of events occuring in time T from 1.) is:

$$N_{rand\ 1.)} = 3N_1N_2N_3T^2$$

where T = resolving time of circuit, N_i = Count rate in i^{th} channel

The contribution of 2.) will be:

$$N_{rand\ 2.)} = \underset{(a)}{N_{12}N_3T} + \underset{(b)}{N_{23}N_1T} + \underset{(c)}{N_{13}N_2T}$$

N_{ij} = number of "true" double coincidences between channels i and j

The contribution of 3.) to the coincidence count rate recorded in the T 15ns circuit is the quantity required for the triple correlation measurement.

Typical measured count rates during the experiment were:

$N_1 = 2.1 \ 10^3$ protons/sec

$N_2 = N_3 = 3 \ 10^4$ gamma rays/sec

$N_{12} = 4 \ sec^{-1}$

$N_{13} = N_{12}$

$N_{23} = 10 \ sec^{-1}$

In a time t the total numbers of counts recorded in the slow $N_{rand(tot.)}$ and fast N_{coinc} coincidence circuit were typically:

$t = 2.4 \ 10^3$ sec

$N_{rand(tot.)} = 511$

$N_{coinc} = 26$

The theoretical number of counts in the random (slow) coincidence circuit ($T = 1.5 \ 10^{-7} \mu sec$) is:

$$N(\text{slow})_{\text{rand 1.)}} = 3(2.1 \ 10^3)(3 \ 10^4)^2(1.5 \ 10^7)^2$$

$$= 14.1 \ 10^2 \ sec^{-1}$$

$$N(\text{slow})_{\text{rand 2.)}} = 2(4)(3 \ 10^4)(1.5 \ 10^{-7}) \quad 10(2.1 \ 10^3)(1.5 \ 10^{-7})$$

$$= 4 \ 10^{-2} \ sec^{-1}$$

$N(\text{slow})_{\text{rand 3.)}} = 2 \ N_{coinc}$ (The factor of 2 arises from the 50% efficiency of the fast coincidence circuit)

therefore $$N(\text{slow})_{\text{rand(tot.)}} = \left[N(\text{slow})_{\text{rand 1.)}} + N(\text{slow})_{\text{rand 2.)}} \right] t + 2 \ N_{coinc}$$

$$= (338 + 91 + 5) + 52$$

$$= 486 \text{ counts (theoretical)}$$

- which is in reasonably good agreement with the experimental value of 511.

When taking a random reading to determine the relation between the two coincidence circuits, the timing on the proton counter was changed by about 300 n sec. thereby destroying all the "true" triple coincidences in both

circuits. This also destroyed all the "true" double coincidences produced in parts (a) and (c) in $N_{rand\ 2.)}$. Therefore the reading for the same beam conditions when the circuit is off coincidence should be:

$$N'_{rand}(slow) = N_{rand}(slow) - N_{true} - N_{rand\ 1.)}\ (a) \text{ and } (c)$$

That is:

$$N'_{rand}(slow) = 486 - 91 - 52 = 343.$$

The actual experimental reading off coincidence was 366 which one again is good agreement between theory and experiment.

The number of random triple coincidences in the fast coincidence was recorded at the same time as $N'_{rand}(slow)$ and this rate was found to be:

$N'_{rand}(fast) = 5$ counts (this is an average over 5 readings taken with constant beam conditions)

The theoretical estimate of $N'_{rand}(fast)$ is -

$$N'_{rand}(fast) = \left[N_{rand\ 1.)}(fast) + N_{rand\ 2.)}(fast)\ \text{part (b)}\right] t$$

Substituting in the appropriate values:

$$N'_{rand}(fast) = (13\ 10^{-4} + 3\ 10^{-4})\ 2.4\ 10^{3}$$

$$\cong 4 \text{ counts}$$

- which compares quite favourably with the measured value of 5 counts in $2.4\ 10^{3}$ sec.

The theoretical ratio of:

$$\frac{N'_{rand\ 1.)}(slow)}{N'_{rand\ 1.)}(fast)} = \left[\frac{T(slow)}{T(fast)}\right]^2 = \left(\frac{150ns}{15ns}\right)^2 = 100$$

and it was found that (experimentally)

$$N_{rand\ 1.)}(slow) = 336$$

$$N_{rand\ 1.)}(fast) = 3$$

which gave good agreement between the theoretical and experimental performance of

this system. With this internal consistency it was possible to convert the random count rate as measured by the slow coincidence circuit to the equivalent random rate in the fast coincidence circuit. In this way it was possible to monitor the random triple coincidence count rate as the triple coincidence measurement was made.

The method used to calculate the random count rate $N_{rand}(fast)$ was:

1.) Subtract from the measured $N_{rand}(slow)$ the calculated effects of $N_{rand}(slow)$ 2.) and 3.) leaving $N_{rand}(slow)$ 1.)

2.) Calculate $N_{rand}(fast)$ 1.) from the known relation

$$\frac{N_{rand}(slow)\ 1.)}{N_{rand}(fast)\ 1.)} = 100$$

3.) Add to this the calculated smaller effect $N_{rand}(fast)$ 2.) and 3.) to get the total number of random events. This number was then subtracted from the measured triple coincidence to give the corrected number of coincidences.

APPENDIX II

DERIVATION OF ESTIMATE OF FITTED PARAMETERS AND ERRORS IN PARAMETERS

The results of fitting the angular distribution measurement $p_3\gamma_1$ to functions of the form:

$$W_{\gamma_i}(\theta_i) = \sum_n b_n(\gamma_i)\ P_n(\cos\theta_i)$$

are reported in Chapter V along with an estimate of the accuracy of the determination of the b_n's. The method known as Maximum Likelihood (Cramer 30.) was used to estimate the b_n's and their associated errors.

Let x_a be the experimentally measured value of $W(\theta)$ at $\theta = \theta_a$. If x_a is a reasonably large number (larger than 50) it can be shown (Cramer 30.) that the Maximum Likelyhood estimate of the b_n's leads to the commonly used least squares estimate, that is the best estimate of the b_n's is one which maximizes the function $F(b_n x_a)$ where

$$F(b_n x_a) = \sum_{a=1}^{N} \frac{\left[x_a - W(\theta_a)\right]^2}{\sigma_a} \qquad (1)$$

and σ_a = estimate of the error in x_a.

N = number of samples of $W(\theta)$.

Cramer also shows that the Maximum Likelihood technique also gives the estimate of the error in the determination of the b_n's as:

$$\sigma(b_n) = \left[\sum_a \frac{x_a}{W(\theta_a)^2}\ P_n^2(\cos\theta_a)\right]^{-\frac{1}{2}}$$

Using:

$x_a = W(\theta_a)$ (satisfied to a good approximation for all x_a)

and $\sigma_a^2 = W(\theta_a)$ (Cramer)

it is found

$$\sigma(b_n) = \left[\sum_a \frac{P_n^2(\cos\theta_a)}{\sigma_a^2}\right]^{-\frac{1}{2}} \qquad (2)$$

In summary the procedure used to estimate the b_n's and the associated errors in these estimates $\sigma(b_n)$, was to least squares fit the data to functions of the form of $W(\theta)$ following the same format outlined in Cramer 30.) to determine the b_n's, then calculate the $\sigma(b_n)$ using (2).

APPENDIX III

SOLID ANGLE CORRECTION FACTOR FOR GAMMA COUNTERS

The theoretical angular correlation functions $W(\theta)$ (See Chapter II) describe the expected flux of gamma rays from the source (B^{10} target) through an element of solid angle $d\Omega$ at an angle θ. Measurements of $W(\theta)$ (Chapter IV) were made using 2" x 2" NaI crystals which subtended a large solid angle at the target and which were not 100% efficient. The effect of the finite solid angle of these counters on the measured distribution is outlined in the following.

The gamma counters in the experiment were right circular cylinders whose base was oriented toward the origin. The source at the origin was on the intersection of the axis of the cylinders and the z axis (deuteron beam axis)

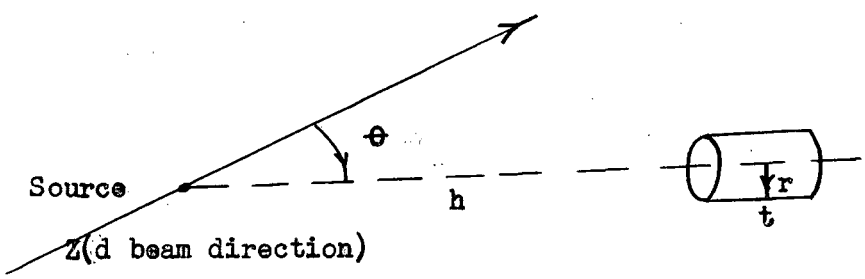

Rose 31.) shows that the measured angular correlation function $\overline{W}(\theta)$ is obtained from the theoretical correlation function $W(\theta)$ where

$$W(\theta) = \sum_k C_k P_k(\cos\theta)$$

by multiplying each coefficient C_k by calculable correction factors Q_k, so that

$$\overline{W(\theta)} = \sum_k C_k Q_k P_k(\cos\theta)$$

The factors Q_k are functions of the counter geometry. (See above)

$$Q_k = Q_k(h,t,r,T) \qquad T = \text{gamma ray absorption coefficient}$$

In Chapter IV the statement was made that the spin assignments based on the double correlation measurements were independent of this solid angle correction factor Q_k. In that chapter, the theoretical $W(\theta)$ were shown to have the form:

$$W_{\gamma_i}(\Theta) = \sum_k R_{k0}(JJ)A_k P_k(\cos\Theta)$$

A_k = known function of the angular momenta involved.

R_{k0} = the tensor parameters for the initial state of the decay.

If now the solid angle correction is added, the experimental correlation function is obtained.

$$\overline{W}_{\gamma_i}(\Theta) = \sum_k Q_k R_{k0} A_k R_k(\cos\Theta)$$

and if the substitution $Q_k R_{k0} = a_k$ is made all the double correlation equations listed in Chapter II are obtained. The a_k referred to in Chapter II, IV and V as tensor parameters should more correctly be called attenuated tensor parameters.

The attenuated tensor parameters contribute no more undetermined parameters than the tensor parameters themselves (other than the finite experimentally limited accuracy of calculation of the quantities Q_k), so that no additional indeterminacy is introduced into the spin assignments by the geometrical corrections to the double correlation measurements.

The solid angle correction to the triple correlation measurement is a little more complicated with the function $W(\Theta_1\Theta_2\phi)$ (refer to Chapter II Part D) taking the corrected form:

$$\overline{W(\Theta_1\Theta_2\phi)} = \sum_{KMNk} R_{k0} A^N_{KM} Q_K Q_M P^N_K(\cos\Theta_1) P^N_M(\cos\Theta_2)\cos N\phi$$

(See Kaye et al 32)

The determination of this function required the calculation of the R_{k0}'s from the a_k derived from the double correlation measurement. The function $\overline{W}(\Theta_1\Theta_2\phi)$ was then calculated using the Q_K's derived in Rose 31.) for the dimensions used experimentally:

r = 1 in.

h = 3.5 in.

t = 2 in.

T was assumed to have the same value for each of the three gamma ray energies measured. The effect of ignoring the change in Q_L due to the change in T over the gamma ray energy range considered was to introduce a possible error in Q_L of less than ½%. Using these values the correction factors Q_L, when Q_0 is normalized to unity (since the geometry makes no difference for isotropic radiation), were found to be:

$$Q_0 = 1$$

$$Q_2 = 0.96$$

$$Q_4 = 0.91$$

The spin assignments of the first and third excited states of B^{11} were made in Chapter V and the ratio of the attenuated tensor parameters $\frac{a_2}{a_0}$ were determined for the spin assignment $J = \frac{3}{2}$ $J_I = \frac{1}{2}$ as

$$\frac{a_2}{a_0} = 0.53 \pm 0.07^*$$

The corrected ratios $\frac{R_{20}}{R_{00}}$ used in Chapter VI are:

$$\frac{R_{20}}{R_{00}} = \frac{\frac{a_2}{a_0}}{\frac{Q_2}{Q_0}} = 0.59 \pm 0.07$$

* The estimate of the value of $\frac{a_2}{a_0}$ and error in this estimate was determined from the two independent estimates of $\frac{a_2}{a_0}$ derived directly from the ratios $\frac{b_2(\gamma_i)}{b_0(\gamma_i)}$ (for i = 1 and 3) using the assumption that $x_i = 0$ (see table 1).

APPENDIX IV

CALCULATION OF PROBABILITIES OF MULTIPOLE MIXING

In the analysis of the correlation results in Chapter V the probabilities of obtaining particular values of x_i, the multipole mixing ratio were introduced. These probabilities were estimated from the experimental data compiled by Wilkinson 16.) on the probability distribution describing the transition probabilities for M1(ΓM1) and E2(ΓE2) transitions. The frequency distribution of the data is shown in the figures below as the crosshatched portion and the heavy dark line outlines the shape assumed for simplicity in the probability calculations.

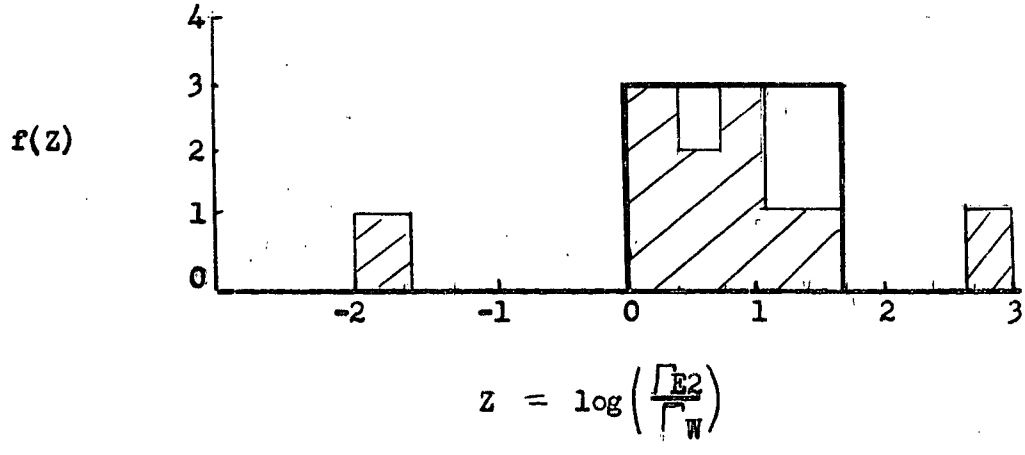

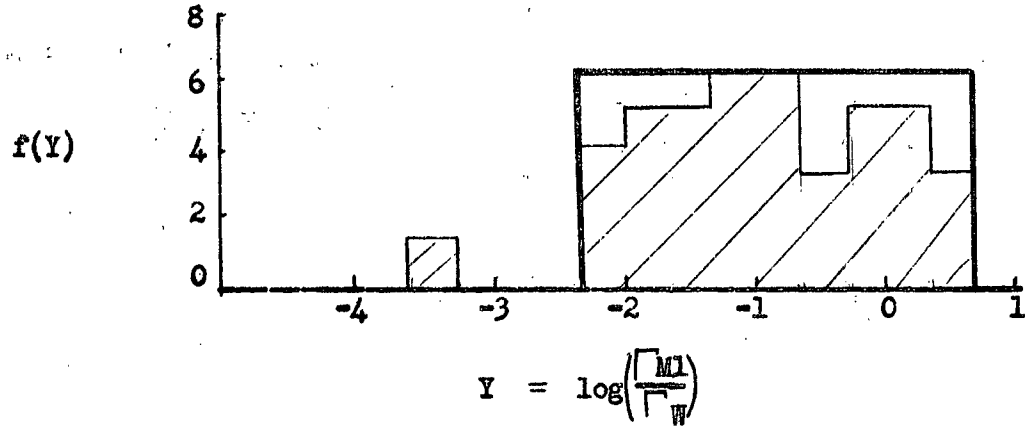

In both figures the symbol Γ_W refers to the Weisskopf width estimate (16.)

The assumed frequency function can be seen to have the form:

$$f\left(\ln\frac{\Gamma_{E2}}{\Gamma_W}\right) = a \qquad 1 \leq \frac{\Gamma_{E2}}{\Gamma_W} \leq 50$$
$$= 0 \qquad \text{elsewhere}$$

$$f'\left(\ln\frac{\Gamma_{M1}}{\Gamma_W}\right) = b \qquad 5\ 10^{-3} \leq \frac{\Gamma_{M1}}{\Gamma_W} \leq 5$$
$$= 0 \qquad \text{elsewhere}$$

Converting these to linear functions of the Γ's and using the requirement that:

$$\int_0^\infty f(\Gamma)d\Gamma = 1 \qquad \text{(normalized probability)}$$

it was found that the frequency functions for Γ_{E2} and Γ_{M1} have the form:

$$f(\Gamma_{E2}) = \frac{1}{3.91\ \frac{\Gamma_{E2}}{\Gamma_W}} \qquad 1 \leq \frac{\Gamma_{E2}}{\Gamma_W} \leq 50 \qquad (1)$$
$$= 0 \qquad \text{elsewhere}$$

$$f'(\Gamma_{M1}) = \frac{1}{6.91\ \frac{\Gamma_{M1}}{\Gamma_W}} \qquad 5\ 10^{-3} \leq \frac{\Gamma_{M1}}{\Gamma_W} \leq 5$$
$$= 0 \qquad \text{elsewhere}$$

The fact that these approximate distributions are identically zero outside certain intervals of Γ does not affect our arguments, since the values of Γ_{E2} and Γ_{M1} we wish to discuss always lie inside those intervals.

The probability of getting a particular value of Γ_{E2} between $\Gamma_{0}E2$ and $\Gamma_{0}E2$ $d\Gamma_{E2}$ is simply:

$$P(\Gamma_{0}E2) = f(\Gamma_{0}E2)d\,\Gamma_{E2} \qquad (3)$$

The values of $P(x_2)$ were calculated (Chapter V Part E.) using equations (1) and (3). To evaluate $P(x_1)$ and $P(x_3)$ the frequency function of $x^2 = \frac{E2}{M1}$ had to be calculated.

If it is assumed that the measurements of Γ_{E2} and Γ_{M1} are uncorrelated, the frequency function $f''(E2, M1)$ will be:

$$f''(\Gamma_{E2},\Gamma_{M1}) = f(\Gamma_{E2})f'(\Gamma_{M1}).$$

The frequency function $f(\Gamma_{E2},\Gamma_{M1})$ such that $\frac{\Gamma_{E2}}{\Gamma_{M1}} = x^2$ is:

$$f''(x^2\Gamma M1, \Gamma M1) = f(x^2\Gamma M1)f'(\Gamma M1)$$

The total frequency function $f(x^2)$ will be this function summed over all the allowed values of $\Gamma M1$ i.e.:

$$f''(x^2) = \int_0^\infty f(x^2\Gamma M1)f'(\Gamma M1)d\Gamma M1 \qquad (4)$$

The frequency function $f''(x^2)$ were evaluated numerically using equations (1), (2) and (4) for the values of x_1^2 and x_3^2 which appear in Chapter V Table 8. From this, the probability of these values of x_i $[P(x_i)]$ were calculated using:

$$P(x_i) = f(x_i)d(x_i)$$

where the $d(x_i)$ was determined by the range of x_i allowed in Chapter V Part E.) The interval $d(x_i)$ was treated as a constant factor occuring in the calculation of all the $P(x_i)$, so that its value does not affect the values of the ratios of the $P(x_i)$'s which are the important quantities.

REFERENCES

1.) S. Cohen and D. Kurath. Argonne National Laboratory, to be published.

2.) D. Evans. Proc. Phys. Soc. A67, 684 (1954).

3.) J. Gorodetsky. Compt. Rend. 242, 2545 (1956).

4.) F.R. Metzger, C.P. Swann and V.K. Rasmussen. Phys. Rev. 110, 906 (1958).

5.) P.F. Donovan, J.V. Kane, R. E. Pixley and D.H. Wilkinson. Phys. Rev. 123, 589 (1961).

6.) D.H. Wilkinson. Phys. Rev. 105, 666 (1957).

7.) A.S. Rupaal. Ph.D. Thesis U.B.C. (1964).

8.) H.E. Gove, J.A. Kuehner, A.E. Litherland, E. Almqvist and D.A. Bromley. Bull Am. Phys. Soc. 2 No. 1, 51 RA^2 (1957).

9.) J.K. Blair, J.D. Kington and J.B. Willard. Phys. Rev. 100, 21 (1955).

11.) A.E. Litherland and A.J. Ferguson. Can. and Phys. 39, 788 (1962).

12.) U. Fano. Rev. Mod. Phys. 29, 74 (1957).

13.) L.C. Biedenharn and M.E. Rose. Rev. Mod. Phys. 25, 729 (1953).

14.) J.M. Blatt and L. C. Biedenharn. Rev. Mod. Phys. 24, 258 (1952).

15.) M.J. Steenland and H.A. Tolhoek. Prog. in Low Temp. Phys. Vol. 2.

16.) D.H. Wilkinson. "Analysis of Gamma Decay Data. Nuclear. Spectroscory Part B.

17.) S.H. Vegors, L.L. Marsden and R.L. Heath. Calculated Efficiencies of Cylindrical Radiation Detectors. A.E.C. Report. I.D.O. - 16370.

18.) Harshaw Chemical Company Catalogue.

19.) P. G. Hoel. Introduc tion to Mathematical Statistics.

20.) G.J. McCallum. Phys. Rev. 123, 568 (1961).

21.) T. Lauritsen and F. Ajzenberg-Selove. Energy Levels of Light Nuclei (1962

22.) S. Cohen and D. Kurath. Effective Interactions for the 1p Shell. (To be published).

23.) D. R. Inglis. Rev. Mod. Phys. 25, 390 (1953).

24.) W.T. Sharp. The Quantum Theory of Angular Momentum. A.E.C.L. Ltd. C.R.L. - 43.

25.) J.B. Marion and G. Weber. Phys. Rev. 103, 1408 (1956).

26.) S.T. Butler. "Nuclear Stripping Reactions".

27.) G.R. Satchler. Proc. Phys. Soc. 66A, 1081 (1953).

28.) H.C. Newns and M.Y. Refai. Proc. Phys. Soc. A71, 627 (1958)

29.) L.J.B. Goldfarb. Nuc. Phys. 57, 4 (1964).

30.) H. Cramer. "Mathematical Methods of Statistics.".

31.) M.E. Rose. Phys. Rev. 91, 510 (1953)

32.) G. Kaye, E.J.C. Read and J.C. Willmott. "Table of Coefficients for Analysis of Triple Angular Correlations from Aligned Nuclei" (Chadwick Laboratory 1963).

33.) T.K. Alexander. Private Communication.

34.) G. Jones. Private Communication.

35.) G. Dearnaly and D.C. Northrop. "Semiconductor Counters for Nuclear Radiation" (Wiley).

36.) E.U. Condon and G.H. Shortley. "Theory of Atomic Spectra" (Rambridge 1951).

37.) W.T. Sharp , J.M. Kennedy, B.J. Sears and H.G. Hoyle. "Tables of Coefficients for Angular Distribution Analysis" C.R.T. - 556.

38.) A.J. Ferguson and A.R. Rutledge. "Coefficients for Triple Angular Correlation Analysis in Nuclear Bombardment Experiments" C.R.P. - 615.

39.) J.L. Leigh. M.Sc. Thesis "The Efficiency of Scintillation Counters for Gamma Ray Detection" (1964).